JAERI-M
83-090

EVALUATION REPORT ON CCTF CORE-I REFLOOD TESTS C1-2 (RUN 11) AND C1-3 (RUN 12)

—EFFECTS OF INITIAL SUPERHEAT OF THE DOWNCOMER WALL

June 1983

Hajime AKIMOTO and Yoshio MURAO

日本原子力研究所
Japan Atomic Energy Research Institute

JAERI-Mレポートは，日本原子力研究所が不定期に公刊している研究報告書です。
入手の問合わせは，日本原子力研究所技術情報部情報資料課（〒319-11茨城県那珂郡東海村）あて，お申しこしください。なお，このほかに財団法人原子力弘済会資料センター（〒319-11 茨城県那珂郡東海村日本原子力研究所内）で複写による実費頒布をおこなっております。

JAERI-M reports are issued irregularly.
Inquiries about availability of the reports should be addressed to Information Section, Division of Technical Information, Japan Atomic Energy Research Institute, Tokai-mura, Naka-gun, Ibaraki-ken 319-11, Japan.

編集兼発行　日本原子力研究所
印　　刷　いばらき印刷㈱

JAERI-M 83-090

Evaluation Report on CCTF Core-I Reflood Tests C1-2 (Run 11) and C1-3 (Run 12)

— Effects of Initial Superheat of the Downcomer Wall —

Hajime AKIMOTO and Yoshio MURAO

Department of Nuclear Safety Research
Tokai Research Establishment, JAERI

(Received May 28, 1983)

In order to clarify the effect of the initial superheat of the downcomer wall on the system and the core cooling behaviors during the reflood phase of a PWR-LOCA, two tests were performed with the Cylindrical Core Test Facility (CCTF). One is the superheated wall test (test C1-2) with the initial superheat of 79K, as in the actual PWR, and the other is the saturated wall test (test C1-3) without any initial superheat. Through the comparisons of the test results from these two tests, the following conclusions were obtained.

(1) The initial superheat of the downcomer wall resulted in the lower downcomer water head as observed in our separate-effect tests for the downcomer water head.
(2) The superheat also caused the core inlet subcooling to be decreased, and led to the lower core water head.
(3) The mass flow rate through the intact loop was reduced only by 4% by the initial superheat of the downcomer wall because the core water head was reduced as well as the downcomer water head. Whereas the mass flow rate through the broken loop was increased because of the increased pressure drop through the broken cold leg.
(4) The difference of the core inlet mass flow rate was small between the superheated and the saturated wall tests. It can be considered

---

The work was performed under contract with the Atomic Energy Bureau of Science and Technology Agency of Japan.

that small difference of the core inlet mass flow rate results from the compensation of the decreased mass flow rate through the intact loops by the increased mass flow rate through the broken loop.

(5) The main discrepancies of the core cooling and the carry-over behaviors between two CCTF tests, were consistent with those observed in the parametric tests for the core inlet subcooling of the FLECHT LOW FLOODING TEST series.

Keywords: PWR, LOCA, Reflood, Heat Transfer, Two Phase Flow, ECC Bypass, Hot Wall Effect, System Behavior.

JAERI－M 83－090

大型再冠水円筒第1次炉心試験C1－2（Run 11）及びC1－3（Run 12）評価報告書

―― ダウンカマ壁初期過熱度の影響 ――

日本原子力研究所東海研究所安全工学部
秋本　肇・村尾　良夫

（1983年5月28日受理）

加圧水型原子炉の冷却材喪失事故再冠水期におけるシステム挙動と炉心冷却挙動に対するダウンカマ壁初期過熱度の影響を調べるために，円筒炉心試験装置を用いて二回の試験を行なった。一方の試験は，実炉と同様の初期過熱度79Kの過熱壁試験（試験名C1－2）で，他方の試験は初期過熱のない飽和壁試験（試験名C1－3）である。両試験結果の比較検討により以下の結論が得られた。

(1) ダウンカマ壁過熱により，個別効果試験と同様に，ダウンカマ水頭の低下が観察された。

(2) ダウンカマ壁過熱により，炉心入口サブクーリングは低下し，炉心水頭も低くなることがわかった。

(3) ダウンカマ水頭とともに炉心水頭も減少したので，健全ループからの流出量の減少は4％にすぎなかった。他方破断ループからの流出量は，破断コールドレグでの圧力損失が大きくなったことで増加した。

(4) 両試験での炉心入口流量の差は小さかった。炉心入口流量の差が小さかったのは，健全ループからの流出流量の減少分が破断ループからの流出量の増加分により打消されたためと考えられる。

(5) 両試験間にみられる炉心内冷却挙動・キャリーオーバ特性の相異点は，FLECHT LOW FLOODING試験の炉心入口サブクーリングに関するパラメータ効果でみられた相異点と類似であった。

本報告書は，電源開発促進対策特別会計法に基づき，科学技術庁からの受託により行なわれた研究の成果である。

Contents

List of tables

List of figures

Fig. 14 Comparison of the carry-over rate fraction between the superheated and the saturated downcomer wall tests

1. INTRODUCTION

During the reflood phase in a large cold-leg-break loss-of-coolant-accident (LOCA) of a pressurized water reactor (PWR), only the static water head in the downcomer is the driving force to supply the emergency core coolant into the core. The saturation temperature of fluid in the primary system falls rapidly during the blowdown phase prior to the reflood phase. The walls of downcomer are superheated during the reflood phase and much heat is still released into fluid in the downcomer. This causes the downcomer water head to be decreased because two-phase mixture is established in the downcomer.

The effect of the superheated wall on the downcomer water head was studied by Sudo, et al. with the test facility modeling the downcomer part of the actual PWR system.[(1)∿(5)] They confirmed experimentally that the static water head was decreased because of the steam generation due to the heat release from the superheated slab. They developed a correlation to evaluate the void fraction in the downcomer and studied the effect of the scaling factor and the applicability of the correlation for the prediction of the static water head. They concluded that the correlation gave a good agreement in case when the static water head changed slowly.

However it is still necessary to study the effect of the superheat of the downcomer wall on the system behavior during the reflood phase of a PWR-LOCA. Because the privious experiment by Sudo, et al. is the separate-effect test, it is uncertain how the superheated wall affects the flow behavior in the other components of the primary system of the PWR. For example, the core inlet mass flow rate can be related to the downcomer water head as follows:[(6)]

$$\dot{m}_F = \dot{m}_C + \dot{m}_U + \sum_{i=1}^{3} \dot{m}_{Ii} + \dot{m}_B \quad , \tag{1}$$

$$\dot{m}_I = \sqrt{2\Delta P_I \rho_I / K_I} \quad , \tag{2}$$

$$\dot{m}_B = \sqrt{2\Delta P_B \rho_B / K_B} \quad , \tag{3}$$

$$\Delta P_I = \Delta P_D - \Delta P_C - \Delta P_U \quad , \tag{4}$$

$$\Delta P_B = \Delta P_I + \Delta P_{BCN} \quad , \tag{5}$$

where $\dot{m}$ is the mass accumulation rate or the mass flow rate, ΔP is the differential pressure, ρ is the fluid density, K is the so-called K factor and subscripts C, U, I, B, D and BCN denote the core, the upper plenum, the intact loop, the broken loop, the downcomer and the broken cold leg nozzle and its connecting pipe, respectively. Eqs.(1) through (5) show that the reduction of the downcomer water head ΔP_D results in the reduction of the core inlet mass flow rate m_F if the other properties in Eqs.(1) through (5) are constant. If the core inlet mass flow rate is reduced, the thermal-hydraulic behavior in the core would be changed and cause the change of the thermal-hydraulic behavior in the upper plenum and the primary loops too.

To study the effect of the initial superheat of the downcomer wall on the system behavior experimentally, two tests were performed using the Cylindrical Core Test Facility (CCTF). One test was performed with the initially-superheated downcomer wall as in the actual PWR. The other test was performed with the saturated downcomer wall as a reference test.

The objectives of this report are to present the test results from these two tests and to discuss the effect of the initial superheat of the downcomer wall on the system behavior and the core cooling behavior.

The test results from these two CCTF tests are shown in Appendixes A through C. Appendix A shows the measuring location of the referred data and the definition of the evaluated data shown in the Appendixes B and C. The main test results from these two tests are shown in the Appendixes B and C.

2. TEST FACILITY AND TEST CONDITIONS

2.1 Test Facility

The CCTF was designed to reasonably simulate the flow conditions in the primary system of a 4-loop PWR during the refill and reflood phases of a LOCA. The reference reactors are the Trojan reactor and, in certain aspects, the Ohi reactor in Japan. The vertical dimensions and the flow pathes of the system components in the CCTF are kept as close to the reference reactor as possible. The flow area of each system component is scaled down in proportion to the scaling factor of the core flow area,

where $\dot{m}$ is the mass accumulation rate or the mass flow rate, ΔP is the differential pressure, ρ is the fluid density, K is the so-called K factor and subscripts C, U, I, B, D and BCN denote the core, the upper plenum, the intact loop, the broken loop, the downcomer and the broken cold leg nozzle and its connecting pipe, respectively. Eqs.(1) through (5) show that the reduction of the downcomer water head ΔP_D results in the reduction of the core inlet mass flow rate m_F if the other properties in Eqs.(1) through (5) are constant. If the core inlet mass flow rate is reduced, the thermal-hydraulic behavior in the core would be changed and cause the change of the thermal-hydraulic behavior in the upper plenum and the primary loops too.

To study the effect of the initial superheat of the downcomer wall on the system behavior experimentally, two tests were performed using the Cylindrical Core Test Facility (CCTF). One test was performed with the initially-superheated downcomer wall as in the actual PWR. The other test was performed with the saturated downcomer wall as a reference test.

The objectives of this report are to present the test results from these two tests and to discuss the effect of the initial superheat of the downcomer wall on the system behavior and the core cooling behavior.

The test results from these two CCTF tests are shown in Appendixes A through C. Appendix A shows the measuring location of the referred data and the definition of the evaluated data shown in the Appendixes B and C. The main test results from these two tests are shown in the Appendixes B and C.

2. TEST FACILITY AND TEST CONDITIONS

2.1 Test Facility

The CCTF was designed to reasonably simulate the flow conditions in the primary system of a 4-loop PWR during the refill and reflood phases of a LOCA. The reference reactors are the Trojan reactor and, in certain aspects, the Ohi reactor in Japan. The vertical dimensions and the flow pathes of the system components in the CCTF are kept as close to the reference reactor as possible. The flow area of each system component is scaled down in proportion to the scaling factor of the core flow area,

that is, 1/21.4. The assumed break location is the cold leg piping corresponding to the outer surface of the biological shield of the reference reactor.

Figure 1 shows the schematic of the CCTF. The facility is equipped with four primary loops which are composed of three intact loops and a broken loop. Each loop has a hot-leg-piping section, an active steam generator, a loop-seal-piping section, a pump simulator, an ECC injection port and a cold-leg-piping section.

The steam generator is of U-tube and shell type. The tube length is about 15 m and it is shorter by about 5 m than that of the reference reactor. However, it is long enough to simulate the heat transfer characteristics between the primary and secondary sides. The secondary side is filled with the saturated water at high pressure.

Each pump simulator is equipped with an orifice plate to simulate the flow resistance and with vanes to simulate the counter-current flow limiting characteristics of the pump in the reference reactor.

The emergency core cooling system (ECCS) of the CCTF consists of the accumulator (Acc) and low pressure coolant injection (LPCI) systems. Each system is connected to the emergency core cooling (ECC) water injection ports attached at the cold legs and the lower plenum of the pressure vessel.

The containment vessel is simulated with two tanks, the containment tanks 1 and 2 in Fig. 1. The containment tank 1 is equipped with a steam-water separator to collect the water flowing through the broken cold leg. It is also equipped with a liquid level meter to measure the level of the collected water inside the tank. The steam separated in the containment tank 1 can flow into the containment tank 2 through the connecting piping between the tanks. The total volume of the two tanks is smaller than that of the containment vessel in the reference reactor system. The pressure in the containment tank 2 is kept constant by means of a pressure control system. The steam in the containment tank 2 is exhausted to the atmosphere through the pressure regulation valve.

Figure 2 shows the schematic of the pressure vessel of the CCTF.

The core consists of 32 bundles arranged in a cylindrical configuration. Each bundle consists of 8×8 heater rods and it contains 57 heater rods and 7 non-heated rods. The 57 heater rods consists of 12 high, 17 medium and 28 low power rods. The power ratios of the high, medium and low power rods to the bundle-average power are 1.1, 1.0 and

0.95, respectively. The axial peaking factor of each rod is 1.49. The power supply to the bundles is subdivided into three-radial regions as shown in Fig. 2. The power supply to each region can be controlled independently, then the radial power distribution can be controlled in the CCTF.

The design of the upper plenum internals is based on that for the Westinghouse 17×17 array fuel assemblies. The radial dimension of each internal is scaled down by factor of 8/15 from that of the reference reactor because the heater rods of the CCTF simulates the 15×15 array fuel assembly. The quantities of internals in the CCTF are in proportion with those in the reference reactor. The CCTF has 12 control rod guide tubes, 4 support columns, 8 stub mixers, 2 orifice plates and 6 open holes.

The downcomer is an annulus with 61.5 mm gap in the CCTF. In the scaling of the CCTF downcomer, the volume of the baffle region in the reference reactor was added to the volume of the downcomer. The CCTF has a wider downcomer gap. However, the wider downcomer provides more conservatisms in the downcomer water accumulation rate.[6] The outside wall of the downcomer is constructed of carbon steel cladded with 5 mm stainless steel. The thickness of carbon steel is 85 mm. The wall is preheated to a certain temperature before the test. The inside wall of the downcomer is preheated to the saturation temperature by steam flow.

The main dimensions of the CCTF are summarized in Table 1.

2.2 Test Procedure

The test procedure was as follows: After establishing the initial conditions of the test, the lower plenum was filled with saturated water to a specified level of 0.9 m for these tests. Electric power was supplied to the heater rods of the core. The ratios of the power supplied to a rod of three radially divided zones to the core average linear power were 1.15, 1.10 and 0.89, respectively. When the maximum temperature of heater rods reached the specified temperature (775 K), the water injection from the accumulator into the lower plenum was initiated. When the estimated water level in the pressure vessel reached the bottom of the core, decay of the heating power was started. Heating power was changed at a programmed rate, simulating the reactor decay heat. After the assumed time, the injection location of the water was changed from the lower plenum to the ECC ports of the three intact cold legs. The

ECC water was still supplied from the accumulator and this period is defined as the accumulator mode. After a specified time, the water injection mode was transferred from the accumulator mode (Acc mode) to the low pressure coolant injection mode (LPCI mode).

2.3 Test Conditions

The test conditions of the tests C1-2 and C1-3 are summarized in Table 2. The test conditions of the test C1-2 were determined based on the safety analysis for the actual PWRs with the evaluation model (EM) codes.[6] The core power was decayed following the decay curve type of the ANS × 1.2 + Actinide × 1.1 (30 s after the shutdown) from the initial linear power of 1.40 kW/m. The containment pressure was kept at about 0.2 MPa during the test. The initial superheat of the downcomer wall was adjusted to simulate the heat release from the wall to the unit volume of the downcomer. Using the DONTAQ2 code developed by Sudo,[2] it was found that the best fit initial temperature for the simulation of a PWR was considered to be 443 K in the case of the system pressure of 0.2 MPa. In the test C1-2, the initial downcomer wall temperature was set at slightly higher temperature (471 K) than the best fit initial temperature for the conservativeness. The primary piping was kept at the saturation temperature (391 K) at the initiation of the test. The secondary side of the steam generator was filled with the water by the level of 7.3 m. The water temperature was 536 K and the pressure of the secondary side was about 5 MPa. The ECC flow rate in the tests are about 75% of that estimated with EM codes. Lower ECC flow rate was selected to preserve the conservativeness of the tests.

The test conditions of the test C1-3 are almost the same as those of the test C1-2 except the initial downcomer wall temperature. The saturation temperature (391 K) was selected to minimize the heat transfer between the downcomer wall and the fluid in the downcomer.

In the following sections, the test C1-2 and C1-3 will be briefly called *the superheated wall test* and *the saturated downcomer wall test*, respectively.

3. RESULTS AND DISCUSSION

Figure 3 shows the differential pressure between the bottom and the top of the downcomer, that is, the downcomer water head. Because the water and the steam velocities are relatively small in the downcomer, the friction loss is negligibly small comparing to the static water head in the downcomer. The increasing rate of the downcomer water head is reduced at 12 s after flood because the ECC water injection mode was switched from the Acc mode to the LPCI mode, and the injection rate of the ECC water was reduced about one ninth of the injection rate in the Acc mode. The downcomer water head increases until about 200 s in each test and remains nearly constant after 200 s.

The static water head can be 64.3 kPa if the downcomer is filled with the solid water from the bottom to the level of the broken cold leg nozzle. The saturated values of the downcomer water head after 200 seconds are 62 and 57 kPa in the saturated and the superheated wall tests, respectively. The saturated value of the downcomer water head is lower by 5 kPa in the superheated wall test than that in the saturated wall test. It can be considered that this difference arises from the steam generation on the superheated wall as observed in the experiments by Sudo, et al.[(1)∿(5)] The difference of the downcomer water head between both tests remains by the end of the tests. This suggests that the steam generation continues by the end of the tests.

Figure 4 shows the comparison of the void fractions at the various vertical sections of the downcomer. The void fraction was evaluated from the measured differential pressure, assuming that the differential pressure consists of only the static water head. At 40 s in the saturated wall test, the void fraction between 2.683 and 4.483 m becomes zero and the void fraction between 4.483 and 6.383 m starts to decrease at the same time. This indicates that the top of the solid water reaches to the elevation of 4.483 m. The same behavior of the void fraction can be observed at 155 s in the saturated wall test. These results shows that the ECC water is accumulated as the solid water in the lower portion of the downcomer and that no steam was generated on the downcomer wall in the saturated wall test.

In the superheated wall test, the void fraction start to decrease earlier than that in the saturated wall test, even though the injection rate of the ECC water is almost identical with that of the saturated

wall test. The void fraction between 4.483 and 6.383 m does not become zero when the void fraction between 6.383 and 6.950 m starts to decrease at 150 s. The superheated wall causes the swelling of the fluid and results in the faster increase of the mixture level in the downcomer.

The void fraction below 4.483 m remains zero after 75 s in the superheated wall test. This result shows that the lower portion of the downcomer is almost filled with the solid water even in the superheated wall test. This is caused by the subcooling of the fluid and by the buoyancy force acting to the generated steam.

The two-phase mixture through the broken cold leg was separated into steam and water in the containment tank I. Only the steam flowed through the connecting pipe between the containment tanks I and II. Therefore the differential pressure between the containment tanks I and II can be considered to be a measure of the steam mass flow rate through the broken cold leg. Figure 5 shows the comparison of the differential pressure between the containment tanks. The differential pressure in the superheated wall test is higher than that in the saturated wall test during the tests. And the steam mass flow rate from the intact cold legs was nearly the same between both tests. These results also prove the steam generation on the superheated downcomer wall in the superheated wall test. The differential pressure is about 16% higher at 200 s in the superheated wall test than in the saturated wall test. This means that the steam mass flow rate through the broken cold leg in the superheated wall test is 1.08 times of that in the saturated wall test. Additional 8% of the steam mass flow rate in the superheated wall test is attributed to the steam generation in the downcomer. The steam mass flow rate from the intact cold legs was estimated to be about 1.5 kg/s and the steam generation rate in the downcomer was estimated to be about 0.12 kg/s.

Figure 6 shows the comparison of the water mass collected in the containment tank I. More water is exhaused through the broken cold leg in the superheated wall test than that in the saturated wall test. The slope of the water mass curve means the water mass flow rate through the broken cold leg. The slope changes at about 200 s. The turning point is consistent with the time when the saturated behavior of the downcomer water head starts. Hence, it is concluded that the increase of the water mass flow rate at that time is cuased by the arrival of the downcomer mixture level to the elevation of the broken cold leg

nozzle. In other words, the water mass flow rate increases because the spill-over of the downcomer fluid is initiated.

The other finding from Fig. 6 is that the water flow through the broken cold leg can be established before the downcomer mixture level reaches to the level of the broken cold leg. This phenomenon can be considered to be a sort of the ECC water bypass. It is generally agreed that the ECC water bypass is caused by the upward steam flow in the downcomer. In the saturated wall test, no steam was generated in the downcomer and no steam flow from the core to the downcomer was observed because the lower part of the downcomer was filled with the solid water. However, the bypass of the ECC water was observed in the saturated wall test. The CCTF result from the saturated wall test suggests another mechanism of the ECC water bypass.

The bypass of the ECC water became noticable at about 70 s in the saturated wall test. The downcomer mixture level was 5.5 m from the bottom of the pressure vessel at 70 s in the saturated wall test. The ECC injection mode was switched from the Acc mode to the LPCI mode at 12 s. During the LPCI mode, 2.78 kg/s of the ECC water with the temperature of 311 K was injected into each intact cold leg. The subcooled ECC water can condense 0.42 kg/s of steam due to the direct contact with flowing steam in the cold leg at 0.2 MPa if the complete mixing of the ECC water with the steam is attained in the cold leg. The steam mass flow rate through the pump simulator to the cold leg was estimated to be about 0.8 kg/s using the measured differential pressure through the orifice plates in the pump simulator. During the LPCI mode, the ECC water can not condense steam completely. A dispersed flow was observed near the cold leg nozzle during the LPCI mode and the measured fluid temperature showed the saturation temperature at the cold leg nozzle during the LPCI mode. It is concluded that the residual steam and the saturated water flowed into the downcomer from the intact cold leg during the LPCI mode.

It is considered that the steam from the three intact cold legs flows in the azimuthal direction along the downcomer wall and it is exhausted to the containment tank through the broken cold leg. The ECC water bypass in the saturated wall test is caused probably by the azimuthal steam flow due to the steam from the three intact cold legs. The CCTF result from the saturated wall test show that the bypass of the ECC water is triggered not only by the upward flow in the downcomer but

also by the azimuthal flow induced by the steam from the intact cold legs.

Figure 7 show the comparison of the water mass flow rate through the broken cold leg. The water mass flow rate was evaluated by the differentiation of the collected water mass in the containment tank I.

Before 200 s, in other words, before the initiation of the spill-over of the downcomer fluid, the water mass flow rate increases with time in both tests. It seems that the water mass flow rate increases as the downcomer mixture level approaches to the level of the broken cold leg nozzle. The water mass flow rate is higher in the superheated wall test. Probably, this is caused by both the higher steam mass flow rate because of the steam generation on the superheated wall and the earilier increase of the downcomer fluid level due to the swelling of the fluid in the superheated wall test.

The bypass of the ECC water results in the slower water accumulation in the downcomer and acts to reduce the core inlet mass flow rate. More detailed study of the ECC bypass phenomena is recommended for the conservative evaluation in the safety analysis of the PWRs.

After 300 s, that is, in the period of the spill-over of the downcomer fluid, the water mass flow rate is almost the same between both tests. From the mass balance relation for the downcomer, the spilled-over water mass flow rate $\dot{m}_o$ is given by

$$\dot{m}_o = \Sigma\dot{m}_{DL} - \dot{m}_D - \dot{m}_g - \dot{m}_F + \dot{m}_{ECC/LP} \quad , \tag{6}$$

where
- $\dot{m}_{DL}$: Water mass flow rate from each intact loop [kg/s],
- $\dot{m}_D$: Water accumulation rate in the downcomer [kg/s],
- $\dot{m}_g$: Steam generation rate in the downcomer [kg/s],
- $\dot{m}_F$: Core inlet water mass flow rate [kg/s], and
- $\dot{m}_{ECC/LP}$: ECC water injection rate from the lower plenum.

In the period of the spill-over, no ECC water was injected from the lower plenum in both tests (that is, $\dot{m}_{ECC/LP} = 0$), and the water accumulation rate $\dot{m}_D$ can be considered to be zero approximately as shown in Fig. 3. The steam generation rate $\dot{m}_g$ in the superheated wall test was evaluated to be about 0.12 kg/s. This rate is negligibly small relative to the spilled-over mass flow rate. The water mass flow rate from the cold legs $\Sigma\dot{m}_{DL}$ was almost the same between both tests because the ECC injection rate, ECC water temperature and the steam mass flow rate from the steam generator to the cold leg were almost the same between both

tests. The core inlet mass flow rate $\dot{m}_F$ in the superheated wall test was identical with that in the saturated wall test, as will be discussed later. Therefore, the spilled-over water mass flow rate was almost the same between both tests.

Figure 8 shows the comparison of the fluid temperature in the downcomer at the elevation of 0.983 m from the bottom of the pressure vessel. In the early period of the saturated wall test ($t < 120$ s), the fluid is subcooled, probably because the water injected during the Acc mode fills near the elevation of 0.983 m. The downcomer water level was about 3.2 m from the bottom of the pressure vessel when the ECC water injection mode was switched from the Acc mode to the LPCI mode at 12 s in the saturated wall test. During the LPCI mode, the saturated water flowed into the downcomer from the cold legs because the subcooled ECC water was heated to the saturation temperature due to the energy transfer from the condensed steam on the ECC water. It can be considered that the saturated water is accumulated above the fluid accumulated during the Acc mode. Because the water flows into the lower plenum, the boundary between the subcooled water and the saturated water travels downward in the downcomer with time. The water mass accumulated between 0.983 and 3.2 m from the bottom of the downcomer was estimated to be 415 kg assuming that the density of the water is 950 kg/m^3. The water mass flow rate to the lower plenum was estimated to be about 5 kg/s in the saturated wall test based on the mass balance calculation (see Appendix D). If no mixing of the saturated water with the subcooled water through the boundary can be assumed and if the fluid behaves one-dimensionally in the downcomer, the boundary between the subcooled water and the saturated water arrives at the elevation of 0.983 m at 83 s after the initiation of the LPCI mode, that is, 95 s after flood. By the arrival of the boundary between the subcooled water and the saturated water, the fluid temperature should become higher. It can be considered that the fluid temperature rise at 120 s in the saturated wall test is caused by the arrival of the boundary between the subcooled water and the saturated water.

In the superheated wall test, the downcomer mixture level was about 3.2 m from the bottom of the pressure vessel when the ECC water injection mode was switched from the Acc mode to the LPCI mode. The estimated mass flow rate to the lower plenum was also about 5 kg/s in the superheated wall test. Then, it can be expected that the fluid temperature

rise due to the arrival of the boundary between the subcooled water and the saturated water occurs at about 120 s as observed in the saturated wall test if the superheated wall has little effect on the fluid temperature. However, the fluid temperature rise in the superheated wall test occurs at about 25 s. Hence, the temperature rise in the superheated wall test is attributed to the heat release from the superheated downcomer wall. If it can be assumed that the fluid in the vicinity of the elevation is heated uniformly by the heat release from the superheated wall, the heating rate of 0.4 k/s is equivalent to the heat flux of 9.3×10^4 W/m^2 on the downcomer wall surface.

Figure 9 shows the comparison of the core inlet subcooling between both tests. The subcooling in the superheated wall test is lower than that in the saturated wall test. The heated water by the superheated downcomer wall flows into the lower plenum. Because the mixing behavior of the fluid in the lower plenum is still uncertain, it is difficult to evaluate the effect of the incoming fluid temperature from the downcomer on the core inlet subcooling quantitatively. However, it is reasonable that the higher fluid temperature from the downcomer results in the lower subcooling of the fluid at the core inlet.

Figure 10 shows the comparison of the core inlet mass flow rate between both tests. The mass flow rate was evaluated by the mass balance calculation for the pressure vessel. The details of the calculation are shown in the appendix D. The error of the evaluated core inlet mass flow rate was estimated to be about 15% at most. The difference of the core inlet mass flow rate between both test is small and it is in the range of the estimation error of the core inlet mass flow rate.

Based on Eqs. (1) through (5), the core inlet mass flow rate is affected by $\dot{m}_C$, $\dot{m}_U$, ρ_I, K_I, ρ_B, K_B, ΔP_I and ΔP_B. In Eq. (1), the water accumulation rates in the core and the upper plenum, $\dot{m}_C$ and $\dot{m}_U$, were negligibly small relative to the mass flow rates through the intact and the broken loops, $\dot{m}_{Ii}$ and $\dot{m}_B$. Because both tests were performed under the same loop configulation and system pressure, it can be expected that ρ_I, ρ_B, K_B and K_I in Eqs. (1) through (5) are nearly the same between both tests. Under these conditions, as described by Eqs. (2) and (3), $\dot{m}_{Ii}$ and $\dot{m}_B$ are proportional to the square root of the pressure drop through the intact and the broken loops, ΔP_I and ΔP_B, respectively.

Figure 11(a) shows the comparisons of ΔP_I and ΔP_B between both tests. After 200 s in the saturated wall test, the pressure drop through the

intact loop is about 26 kPa. The downcomer water head in the superheated wall test was lower by 5 kPa than that in the saturated wall test as previous mentioned. Based on Eq. (4), the expected pressure drop through the intact loop is 21 kPa in the superheated wall test if the core and upper plenum water head were not affected by the initial superheat of the downcomer wall. In such an idealized situation, 5 kPa reduction of the pressure drop through the intact loop leads to about 10% lower mass flow rate through the intact loops. This corresponds to the reduction of about 0.3 kg/s of the mass flow rate through the three intact loops.

However, the measured pressure drop through the intact loop was about 24 kPa after 200 s in the superheated wall test. 2 kPa reduction corresponds to the reduction of 0.1 kg/s of the mass flow rate through the three intact loops. The smaller difference of the measured pressure drop through the intact loop than that in the idealized situation, that is, no reduction of the core and upper plenum water head, was caused by the lower core water head in the superheated wall test as shown in Fig. 11(b). The effect of the decreased downcomer water head on the mass flow rate through the intact loop was compensated by the effect of the decreased core water head in the superheated wall tests.

The lower core water head in the superheated wall test arises from the lower core inlet subcooling. The lower subcooling results in the lower elevation of the incipient point of boiling and leads to the lower core water head.

The pressure drop through the broken loop is higher in the superheated wall test than in the saturated wall test in Fig. 11(a). This is attributed to the higher pressure drop through the broken cold leg because of the higher steam mass flow rate and nearly the same water mass flow rate through the broken cold leg in the superheated wall test. The pressure drop through the broken loop is about 10% higher in the superheated wall test than in the saturated wall test at 200 s. This difference of the pressure drop is equivalent to that the difference of the mass flow rate through the broken loop is about 0.07 kg/s.

The reduction of the mass flow rate through the intact loops because of the reduced downcomer water head was suppressed by the effect of the reduced core water head. The effect of the reduced mass flow rate through the intact loop was compensated by the increase of the mass flow rate through the broken loop resulting from the increased pressure drop through the broken cold leg. Finally, the difference of the core inlet

mass flow rate between both tests became small.

Figure 12 shows the comparison of the clad surface temperature histories at various elevations along an average power rod. Each elevation shows the distance from the bottom of the heated section. Below 1.015 m, no significant difference was observed for the clad surface temperature histories between both tests. Above 1.83 m, the turnaround time and temperature are nearly the same between both tests. Whereas the quench times in the superheated wall test are longer than those in the saturated wall tests. The effect of the initial superheat of the downcomer wall on the core cooling becomes significant in the later period of the reflood phase.

Because the main difference of the flow behavior at the core inlet was the core inlet subcooling between the superheated and the saturated wall test, the test results from these CCTF tests are compared with the test results from the parametric tests for the core inlet subcooling in the FLECHT LOW FLOODING TEST series.[8] Figure 13 shows the comparisons of the temperature rise and the quench time at the midplane of the core. The CCTF results show the data from the superheated and the saturated wall tests. Because the core inlet subcooling changed with time in these tests as shown in Fig. 9, the time-averaged subcooling between the reflood initiation and the quench time was used to plot the CCTF results. Both the FLECHT and the CCTF results show that the temperature rise is nearly constant regardless of the core inlet subcooling and they show that the quench time decreases with the core inlet subcooling. The CCTF results from the superheated and the saturated wall tests show the same qualitative tendency of the turnaround and quench behaviors of the heater rods as observed in the parametric study for the core inlet subcooling in the FLECHT LOW FLOODING TEST series. It can be concluded that the difference of the core cooling behavior between both CCTF tests results mainly from the descrepancy of the core inlet subcooling.

Figure 14 shows the comparison of the carry-over rate fraction between the superheated and the saturated wall tests. The carry-over rate fraction CRF is defined by

$$CRF = \frac{\dot{m}_{UP} + \dot{m}_L}{\dot{m}_{CR} + \dot{m}_{UP} + \dot{m}_L} \qquad (6)$$

where $\dot{m}_{CR}$: Water accumulation rate in the core (kg/s),

$\dot{m}_{UP}$: Water accumulation rate in the upper plenum (kg/s), and

$\dot{m}_L$: Mass flow rate vented through four primary loops from the upper plenum (kg/s).

The superheated wall test shows the higher carry-over rate fraction than that in the saturated wall test. The lower core subcooling resulted in the higher carry-over rate fraction in the tests. The same tendency of the carry-over rate fraction for the core inlet subcooling was reported in the FLECHT LOW FLOODING TEST. It can be considered that the lower core inlet subcooling results in the more steam generation in the core and lead to the more carry-over from the core as reported in the reference.[8]

4. CONCLUSIONS

In order to clarify the effect of the initial superheat of the downcomer wall on the system and the core cooling behaviors during the reflood phase of a PWR-LOCA, two tests were performed with the Cylindrical Core Test Facility. One is the superheated wall test (test C1-2) with the initial superheat of 79 K, as in the actual PWR. And the other test is the saturated wall test (test C1-3). Through the comparisons of the test results from these tests, the following conclusions were obtained.

(1) The initial superheat of the downcomer wall resulted in the lower downcomer water head as observed in our separate effect tests for the downcomer water head.

(2) The superheat also caused the core inlet subcooling to be decreased, and led to the lower core water head.

(3) The mass flow rate through the intact loop was reduced only 4% by the initial superheat of the downcomer wall because the core water head was reduced as well as the downcomer water head. Whereas the mass flow rate through the broken loop was increased because of the increased pressure drop through the broken cold leg.

(4) The difference of the core inlet mass flow rate was small between the superheated and the saturated wall test. It can be considered that small difference of the core inlet mass flow rate results from the compensation of the decreased mass flow rate through the intact loops by the increased mass flow rate through the broken loop.

$\dot{m}_L$: Mass flow rate vented through four primary loops from the upper plenum (kg/s).

The superheated wall test shows the higher carry-over rate fraction than that in the saturated wall test. The lower core subcooling resulted in the higher carry-over rate fraction in the tests. The same tendency of the carry-over rate fraction for the core inlet subcooling was reported in the FLECHT LOW FLOODING TEST. It can be considered that the lower core inlet subcooling results in the more steam generation in the core and lead to the more carry-over from the core as reported in the reference.[8]

4. CONCLUSIONS

In order to clarify the effect of the initial superheat of the downcomer wall on the system and the core cooling behaviors during the reflood phase of a PWR-LOCA, two tests were performed with the Cylindrical Core Test Facility. One is the superheated wall test (test C1-2) with the initial superheat of 79 K, as in the actual PWR. And the other test is the saturated wall test (test C1-3). Through the comparisons of the test results from these tests, the following conclusions were obtained.

(1) The initial superheat of the downcomer wall resulted in the lower downcomer water head as observed in our separate effect tests for the downcomer water head.

(2) The superheat also caused the core inlet subcooling to be decreased, and led to the lower core water head.

(3) The mass flow rate through the intact loop was reduced only 4% by the initial superheat of the downcomer wall because the core water head was reduced as well as the downcomer water head. Whereas the mass flow rate through the broken loop was increased because of the increased pressure drop through the broken cold leg.

(4) The difference of the core inlet mass flow rate was small between the superheated and the saturated wall test. It can be considered that small difference of the core inlet mass flow rate results from the compensation of the decreased mass flow rate through the intact loops by the increased mass flow rate through the broken loop.

(5) The main discrepancies of the core cooling and the carry-over behaviors between two CCTF tests, were consistent with those observed in the parametric tests for the core inlet subcooling of the FLECHT LOW FLOODING TEST series.

ACKNOWLEDGEMENT

The authors are much indebted to Dr. M. Nozawa, deputy director general of the Tokai Research Establishment of JAERI, Dr. S. Katsuragi, director of Reactor Safety Research Center of JAERI, and Dr. K. Hirano, deputy director of department of Reactor Safety Research, for their guidance and encouragement for this program.

The authors also appreciate to the members of the CCTF analysis group, Messrs. T. Iguchi, T. Sudoh, J. Sugimoto and T. Okubo for valuable discussions. And and authors appreciate to the members of the SCTF analysis group, especially Mr. H. Adachi and Dr. Y. Sudo for valuable suggestions.

REFERENCES

1. SUDO, Y. and MURAO, Y. : JAERI-M 7490, (1978).
2. SUDO, Y. and MURAO, Y. : JAERI-M 7978, (1978).
3. SUDO, Y. MURAO, Y. and AKIMOTO, H. : JAERI-M 8978, (1980).
4. SUDO, Y. : J. Nucl. Sci. Technol., 17 [1], 1 (1980).
5. SUDO, Y. and AKIMOTO, H. : J. Nucl. Sci. Technol., 19 [1], 34 (1982).
6. MURAO, Y. et al. : J. Nucl. Sci. Technol., 19 [9], 705 (1982).
7. LILLY, G.P., et al. : WCAP 8838, (1977).

(5) The main discrepancies of the core cooling and the carry-over behaviors between two CCTF tests, were consistent with those observed in the parametric tests for the core inlet subcooling of the FLECHT LOW FLOODING TEST series.

ACKNOWLEDGEMENT

The authors are much indebted to Dr. M. Nozawa, deputy director general of the Tokai Research Establishment of JAERI, Dr. S. Katsuragi, director of Reactor Safety Research Center of JAERI, and Dr. K. Hirano, deputy director of department of Reactor Safety Research, for their guidance and encouragement for this program.

The authors also appreciate to the members of the CCTF analysis group, Messrs. T. Iguchi, T. Sudoh, J. Sugimoto and T. Okubo for valuable discussions. And and authors appreciate to the members of the SCTF analysis group, especially Mr. H. Adachi and Dr. Y. Sudo for valuable suggestions.

REFERENCES

1. SUDO, Y. and MURAO, Y. : JAERI-M 7490, (1978).
2. SUDO, Y. and MURAO, Y. : JAERI-M 7978, (1978).
3. SUDO, Y. MURAO, Y. and AKIMOTO, H. : JAERI-M 8978, (1980).
4. SUDO, Y. : J. Nucl. Sci. Technol., 17 [1], 1 (1980).
5. SUDO, Y. and AKIMOTO, H. : J. Nucl. Sci. Technol., 19 [1], 34 (1982).
6. MURAO, Y. et al. : J. Nucl. Sci. Technol., 19 [9], 705 (1982).
7. LILLY, G.P., et al. : WCAP 8838, (1977).

(5) The main discrepancies of the core cooling and the carry-over behaviors between two CCTF tests, were consistent with those observed in the parametric tests for the core inlet subcooling of the FLECHT LOW FLOODING TEST series.

ACKNOWLEDGEMENT

The authors are much indebted to Dr. M. Nozawa, deputy director general of the Tokai Research Establishment of JAERI, Dr. S. Katsuragi, director of Reactor Safety Research Center of JAERI, and Dr. K. Hirano, deputy director of department of Reactor Safety Research, for their guidance and encouragement for this program.

The authors also appreciate to the members of the CCTF analysis group, Messrs. T. Iguchi, T. Sudoh, J. Sugimoto and T. Okubo for valuable discussions. And and authors appreciate to the members of the SCTF analysis group, especially Mr. H. Adachi and Dr. Y. Sudo for valuable suggestions.

REFERENCES

1. SUDO, Y. and MURAO, Y. : JAERI-M 7490, (1978).
2. SUDO, Y. and MURAO, Y. : JAERI-M 7978, (1978).
3. SUDO, Y. MURAO, Y. and AKIMOTO, H. : JAERI-M 8978, (1980).
4. SUDO, Y. : J. Nucl. Sci. Technol., 17 [1], 1 (1980).
5. SUDO, Y. and AKIMOTO, H. : J. Nucl. Sci. Technol., 19 [1], 34 (1982).
6. MURAO, Y. et al. : J. Nucl. Sci. Technol., 19 [9], 705 (1982).
7. LILLY, G.P., et al. : WCAP 8838, (1977).

Table 1 Main dimensions of CCTF and a typical PWR

	PWR[1]	CCTF	Ratio
< Length (m) >			
Heated length	3.66	3.66	1/1
Diameter of heated rod	10.7×10^{-3}	10.7×10^{-3}	1/1
Diameter of non-heated rod	13.8×10^{-3}	13.8×10^{-3}	1/1
Rod pitch	14.3×10^{-3}	14.3×10^{-3}	1/1
Distance from the bottom of cold leg nozzle to the bottom of the heated core	4.849	4.849	1/1
Distance from the top of the heated core to the top of the core support plate	0.357	0.357	1/1
Downcomer length	6.066	6.066	1/1
Distance from the bottom of the vessel to the bottom of the heated core	-	2.1	
< Flow area (m^2)>			
Core	5.29	0.260	1/20.3
Downcomer	2.47	0.197	1/21.4
Core baffle	1.76		
Upper plenum	11.10	0.678	1/16.4
Containment tank 1	-	4.906	
Primary loop	0.487~0.383	0.019	1/25.8~1/20.3
<Volume (m^3)>			
Lower plenum*	29.6	1.38	1/21.44
Upper plenum	43.6	2.04	1/21.44

* included the downcomer region below the bottom of core.

Table 2 Test conditions of the superheated (CCTF test C1-2) and the saturated (CCTF test C1-3) downcomer wall tests.

Item	The saturated wall test (Test C1-3)	The superheated wall test (Test C1-2)
Total power (MW)	9.35	9.36
Average linear power (kW/m)	1.40	1.40
Radial power distribution	1.158 : 1.080 : 0.885	1.158 : 1.080 : 0.885
System pressure (MPa)	0.208	0.211
Initial downcomer wall temperature (K)	388	460
Primary piping wall temperature (K)	383	391
SG secondary side temperature (K)	537	536
Peak clad temperature		
at ECC initiation (K)	775	775
at BOCREC (K)	890	890
Lower plenum fluid temperature (K)	379	386
ECC water temperature (K)	311	312
Lower plenum water level (m)	0.85	0.86
SG secondary side water level (m)	7.4	7.3
Acc injection rate (m^3/s)	7.00×10^{-2}	6.72×10^{-2}
LPCI injection rate (m^3/s)	8.56×10^{-3}	8.58×10^{-3}

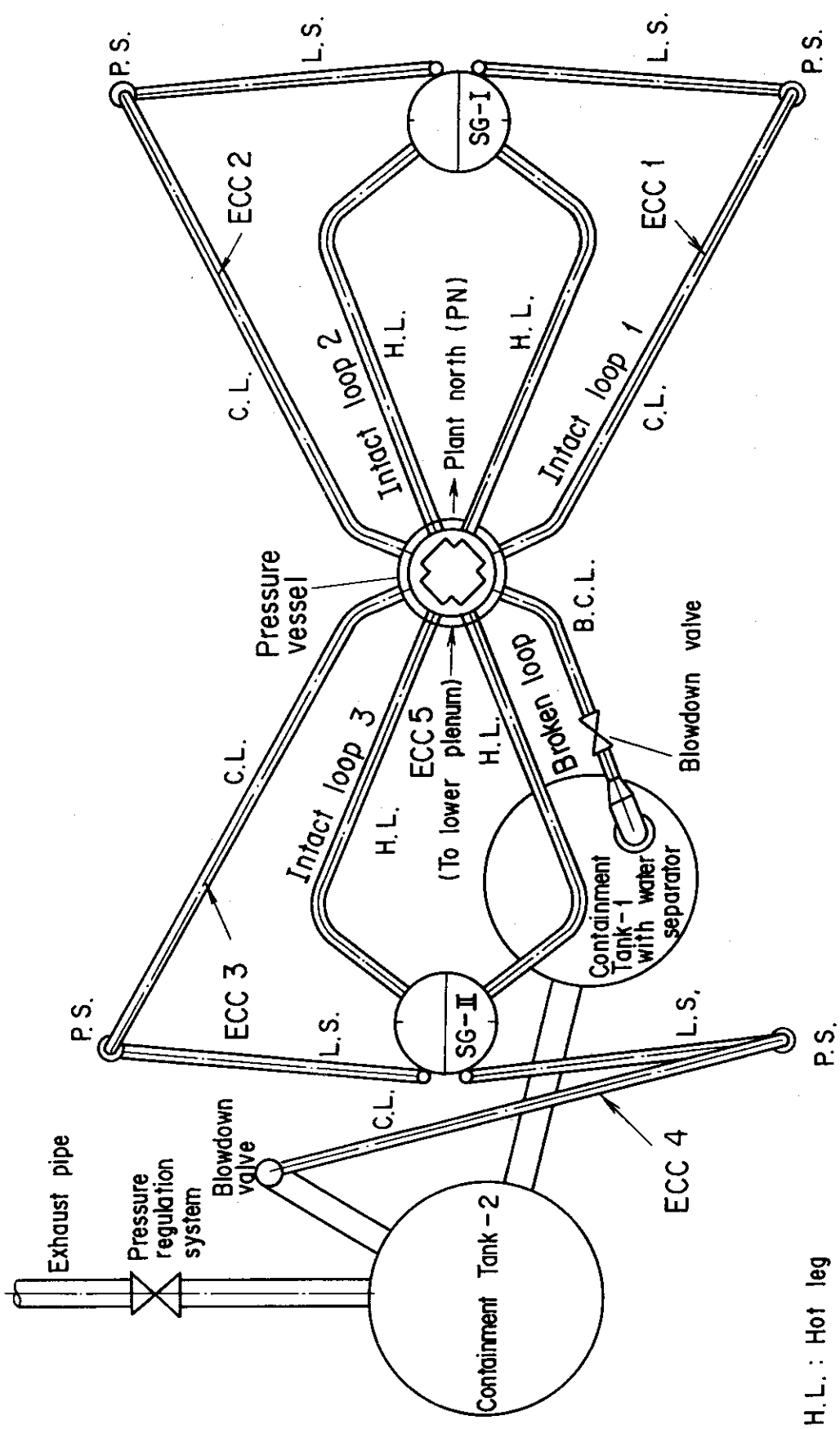

H.L. : Hot leg
S.G. : Steam generator
L.S. : Loop seal
P.S. : Pump simulator
C.L. : Cold leg

Fig. 1 Schematic of the Cylindrical Core Test Facility

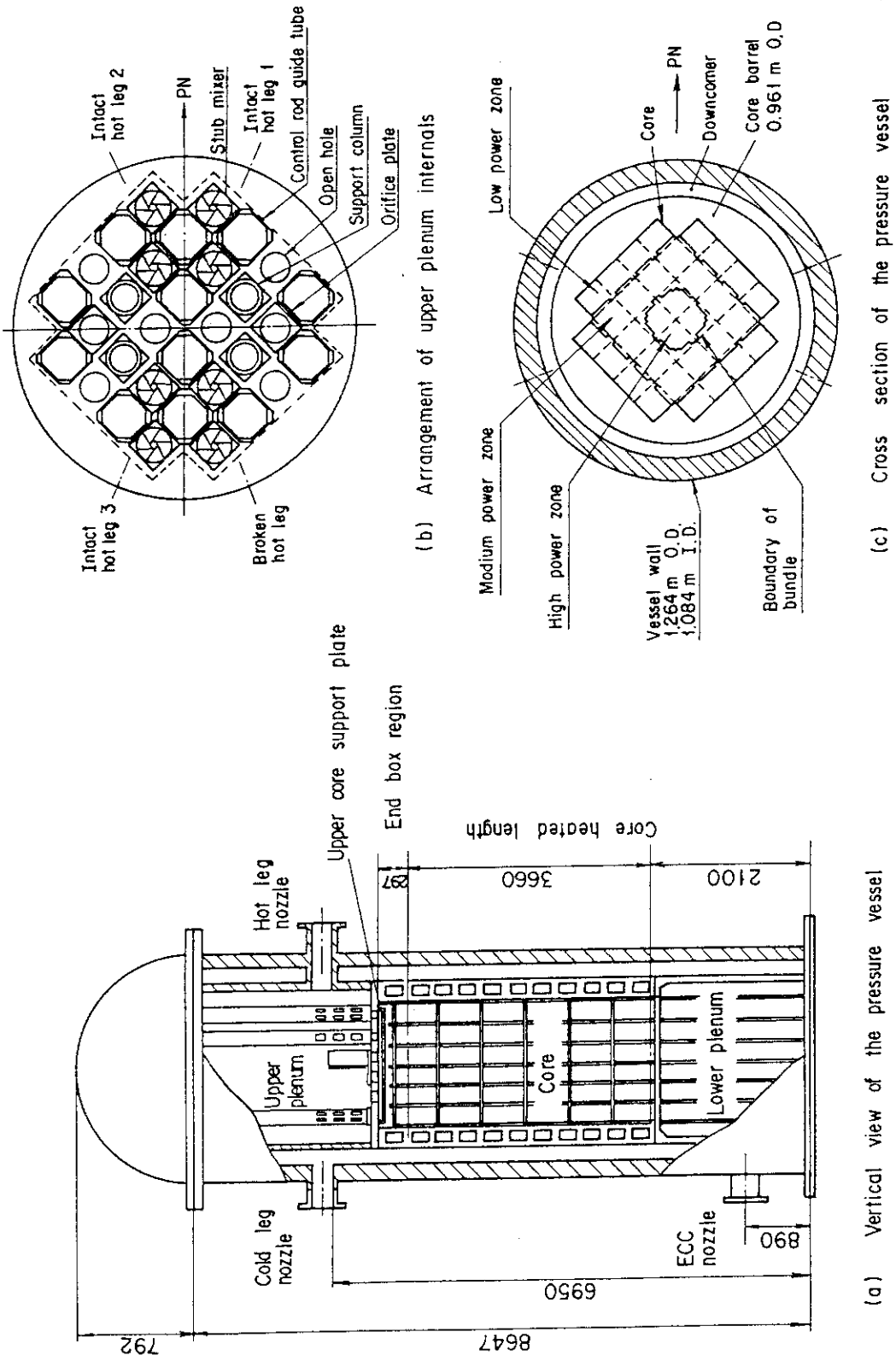

Fig. 2 Schematic of the pressure vessel of the Cylindrical Core Test Facility (CCTF)

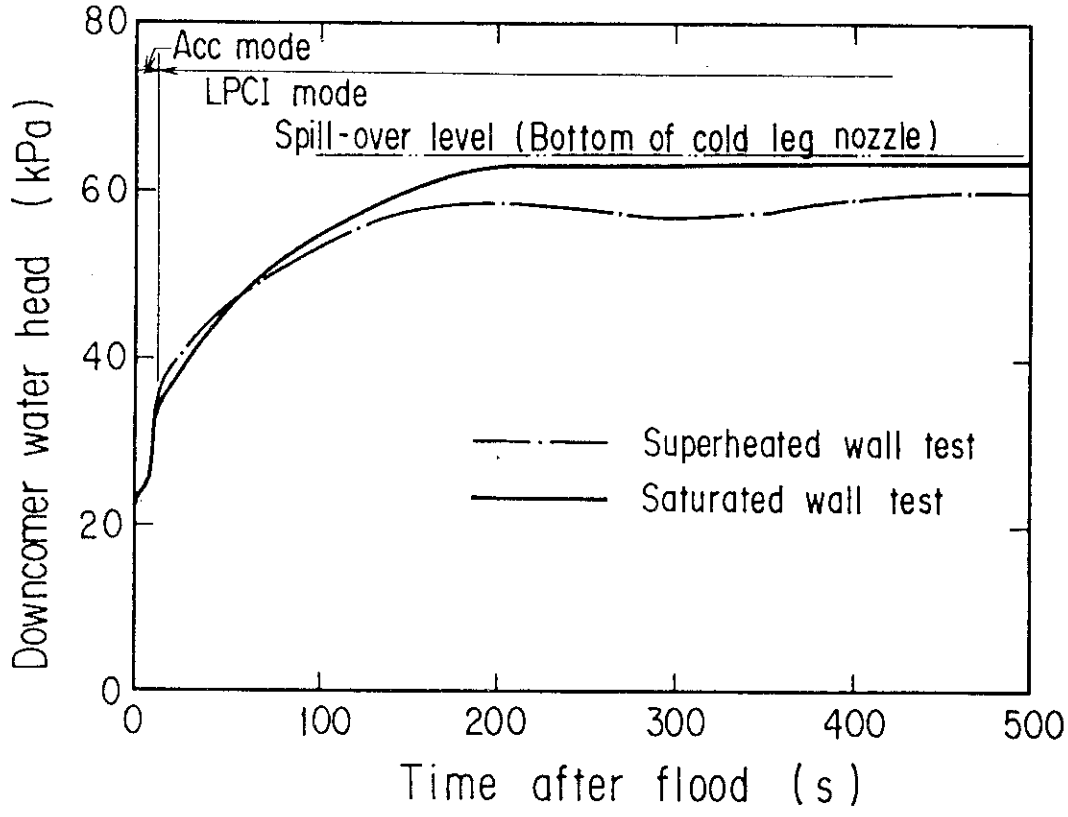

Fig. 3 Comparison of the downcomer water head between the superheated and the saturated downcomer wall tests

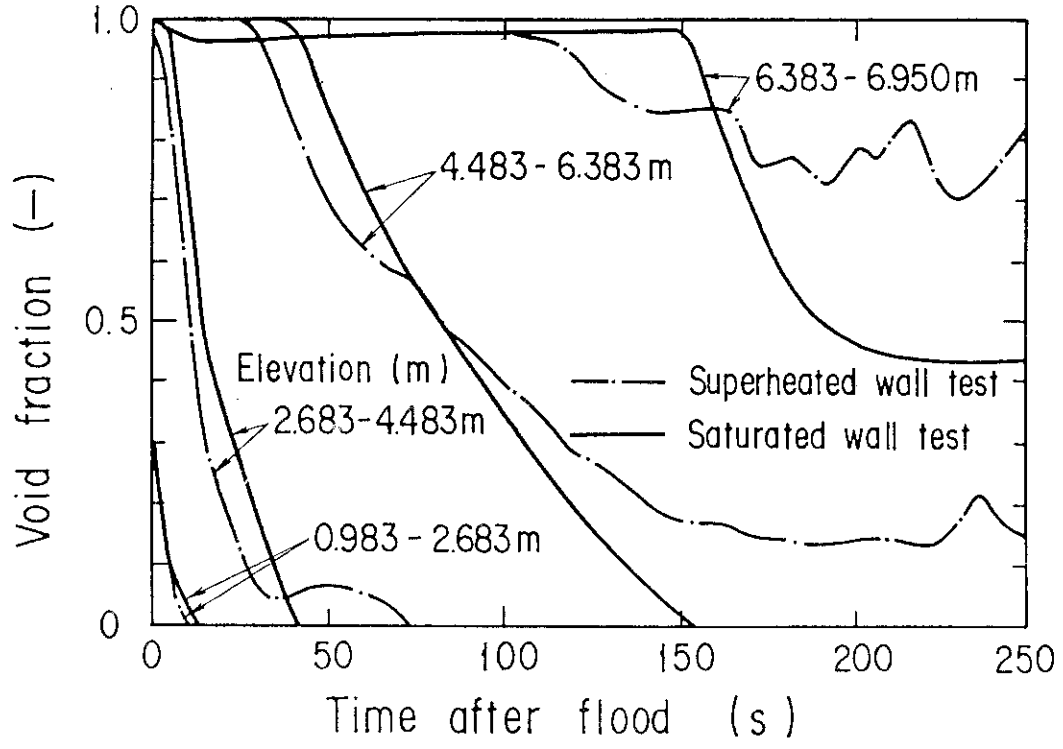

Fig. 4 Comparison of the void fraction at various elevation of the downcomer between the superheated and the saturated downcomer wall tests

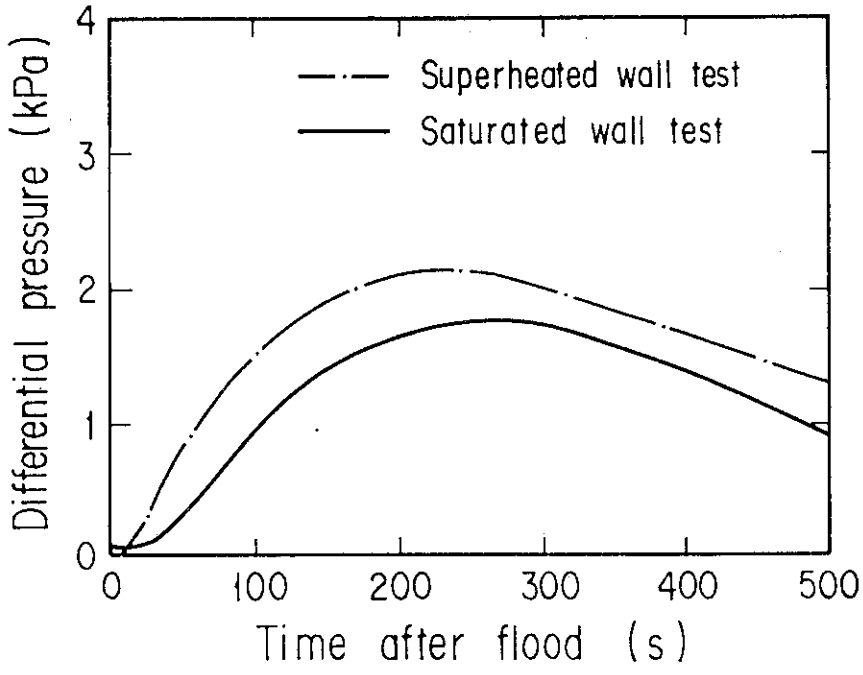

Fig. 5 Comparison of the differential pressure between the containment tank I and the containment tank II

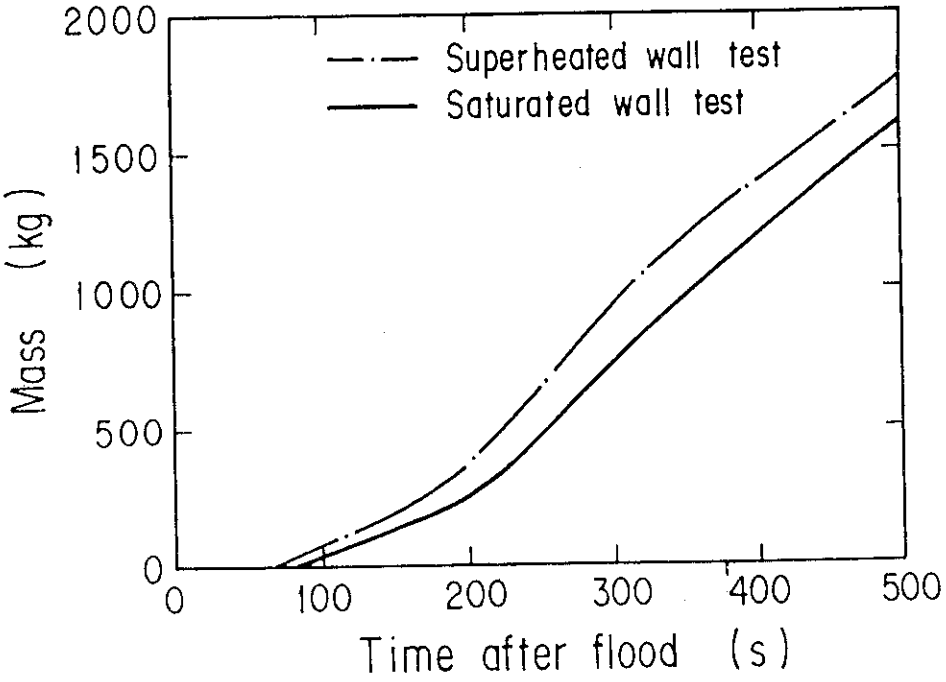

Fig. 6 Comparison of the water mass collected in the containment I between the superheated and saturated downcomer wall tests

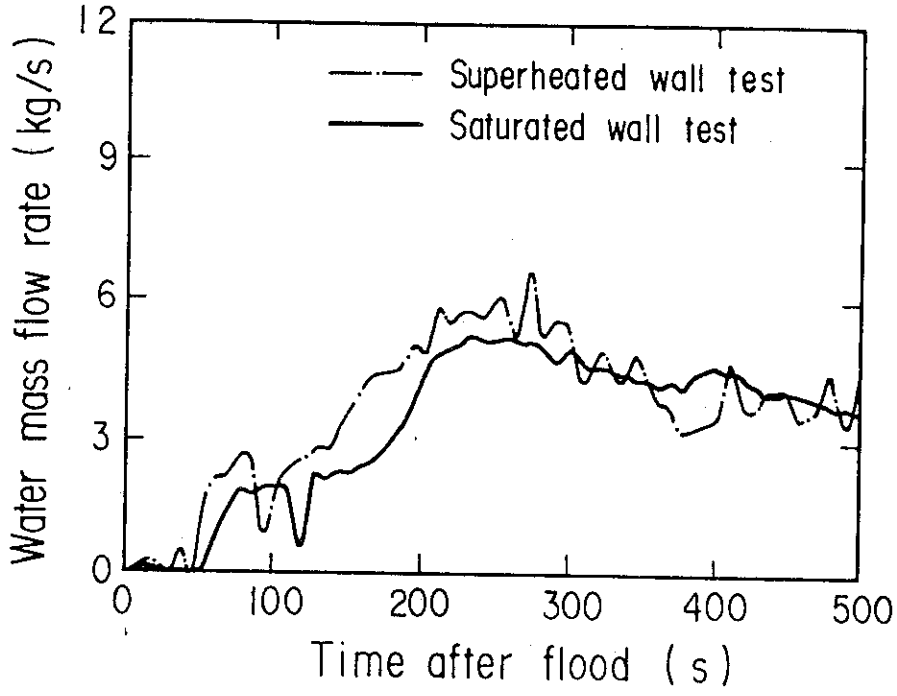

Fig. 7 Comparison of the water mass flow rate through the broken cold leg between the superheated and the saturated downcomer wall tests

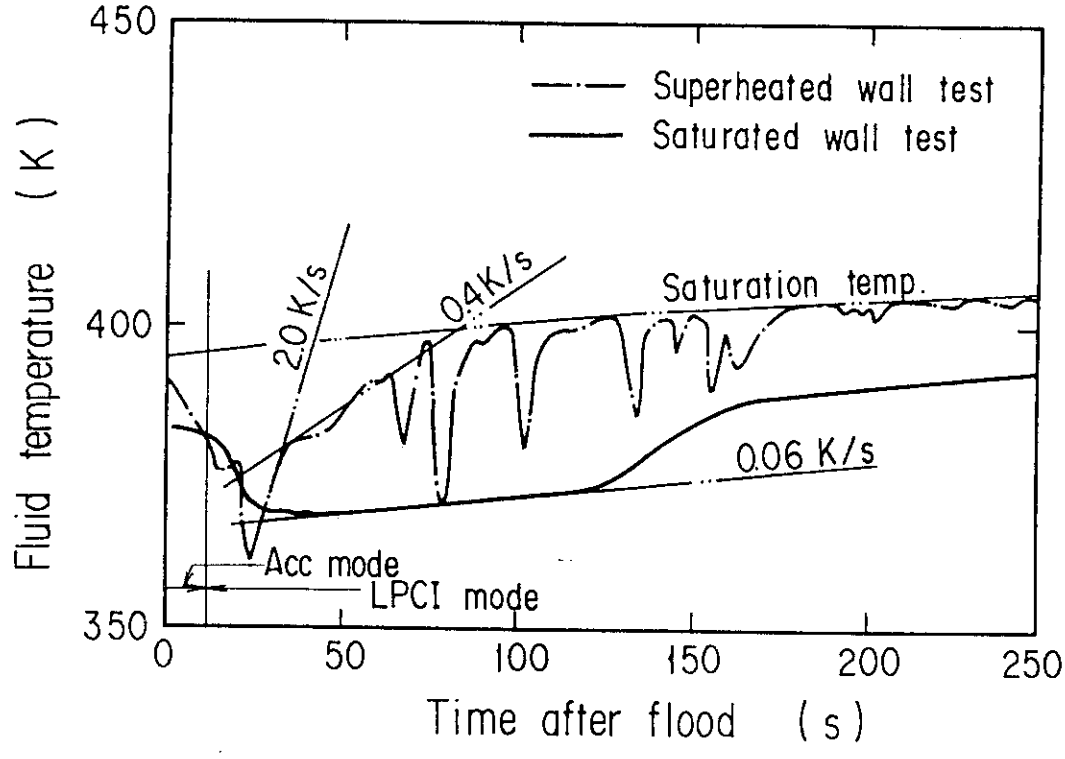

Fig. 8 Comparison of the fluid temperature in the downcomer at the elevation of 0.983 m from the bottom of the pressure vessel between the superheated and the saturated downcomer wall tests

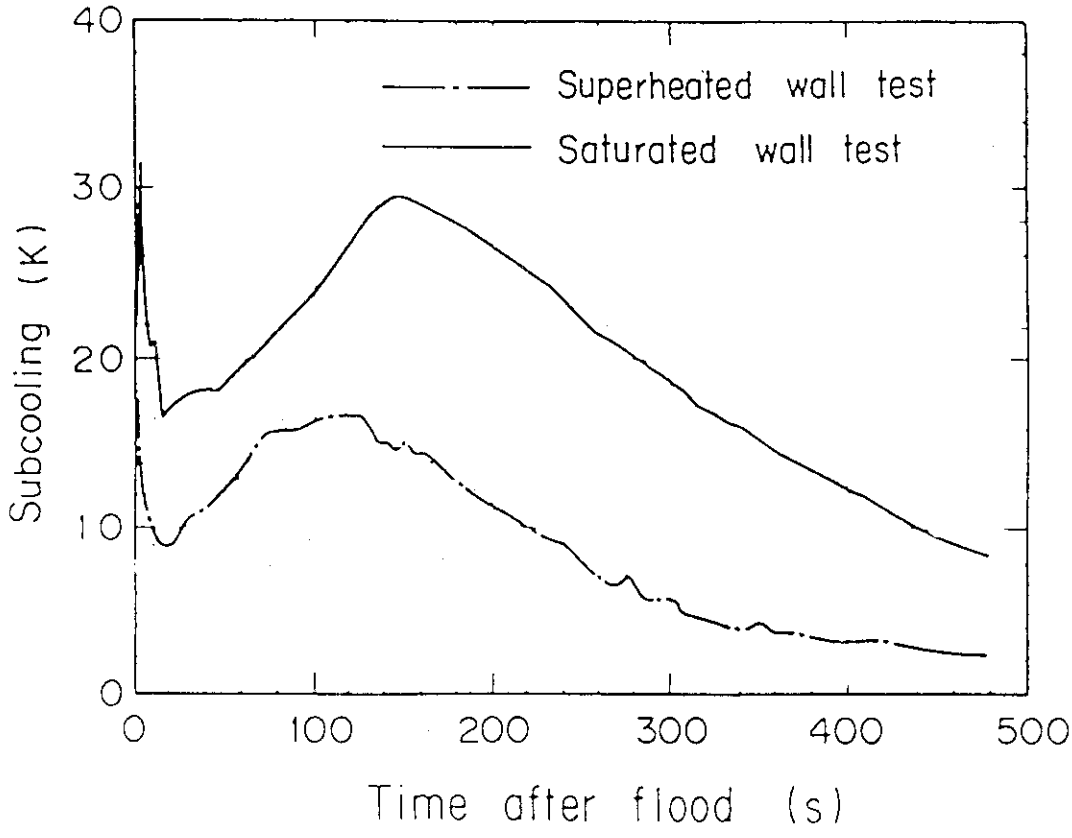

Fig. 9 Comparison of the core inlet subcooling between the superheated and the saturated downcomer wall tests

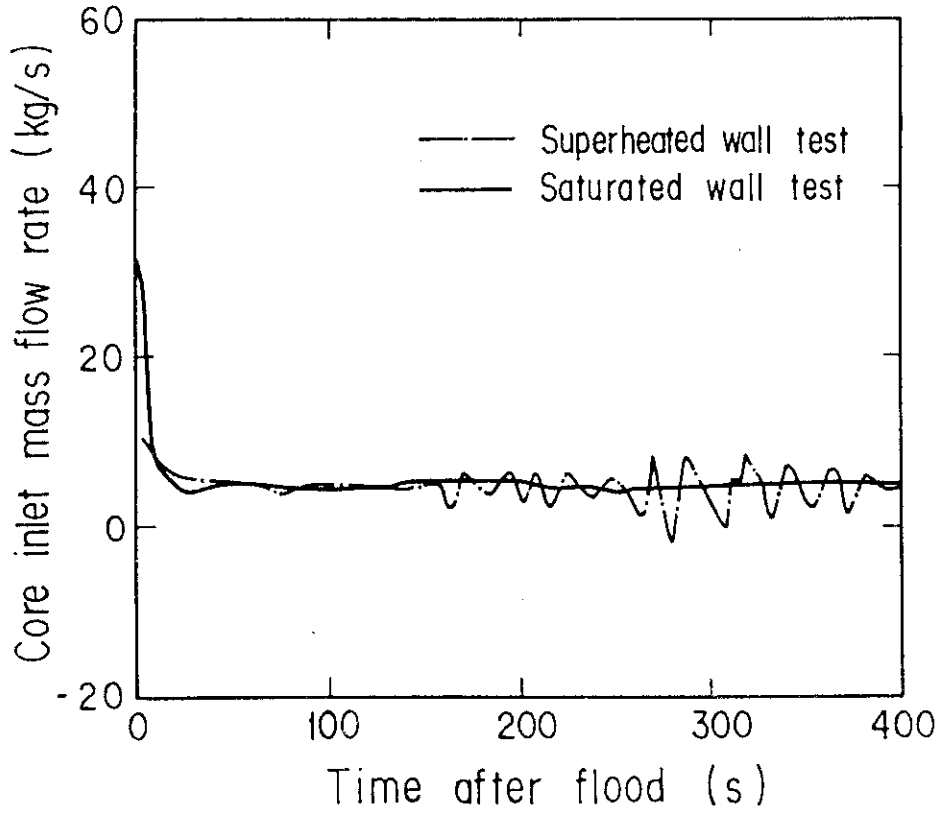

Fig. 10 Comparison of the core inlet mass flow rate between the superheated and the saturated downcomer wall tests

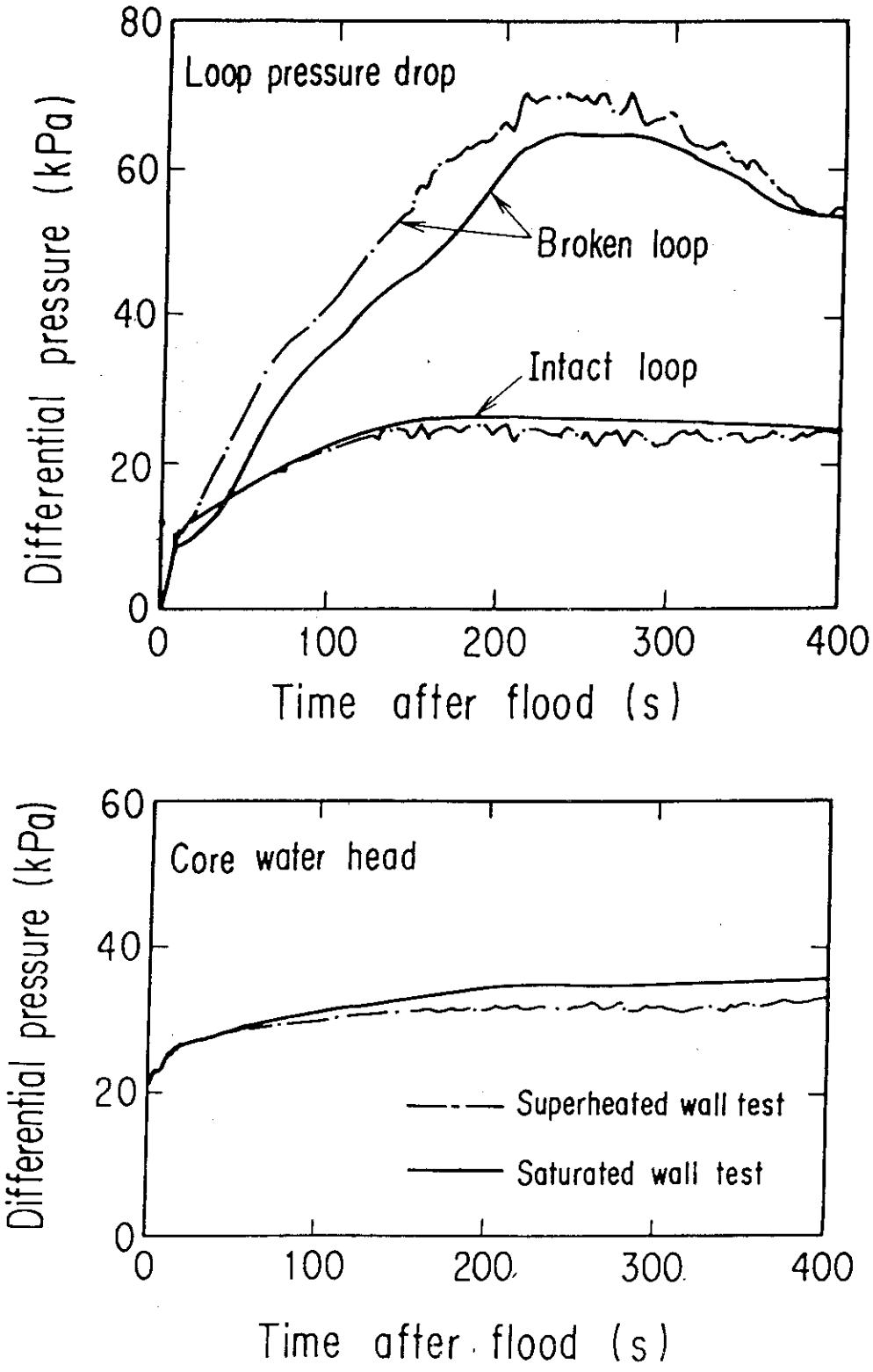

Fig. 11 Comparison of the pressure drop through the intact and the broken loops and the core water head

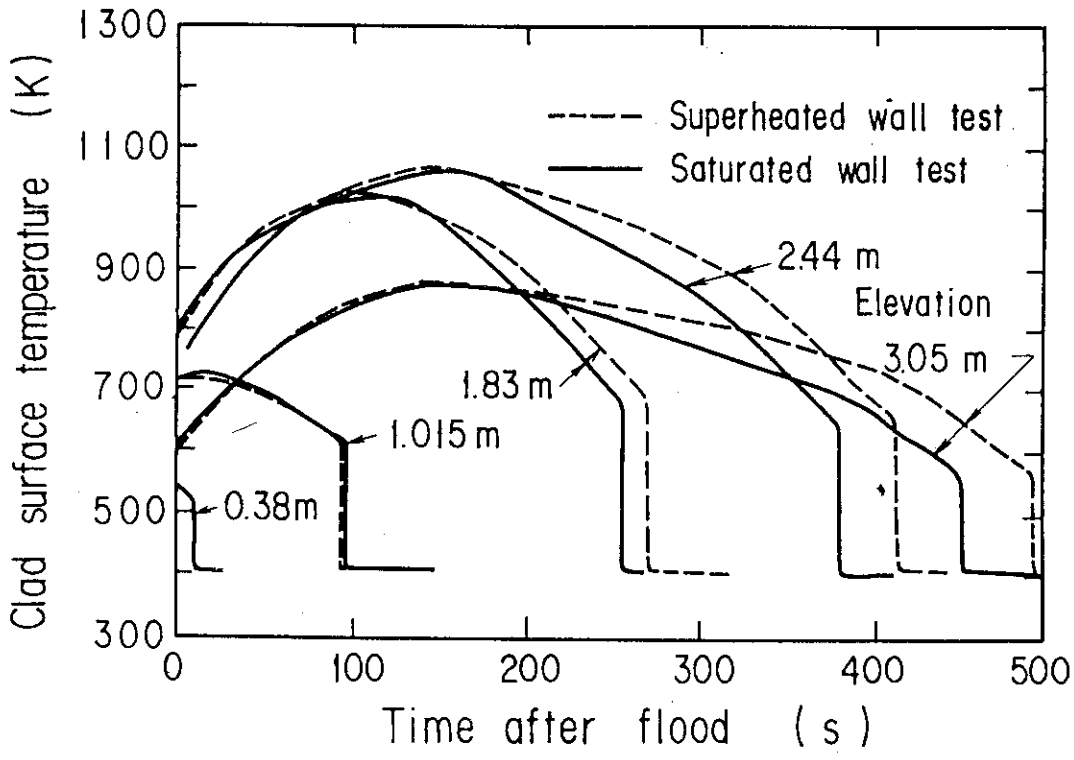

Fig. 12 Comparison of the clad surface temperature along an average power rod between the superheated and the saturated downcomer wall tests

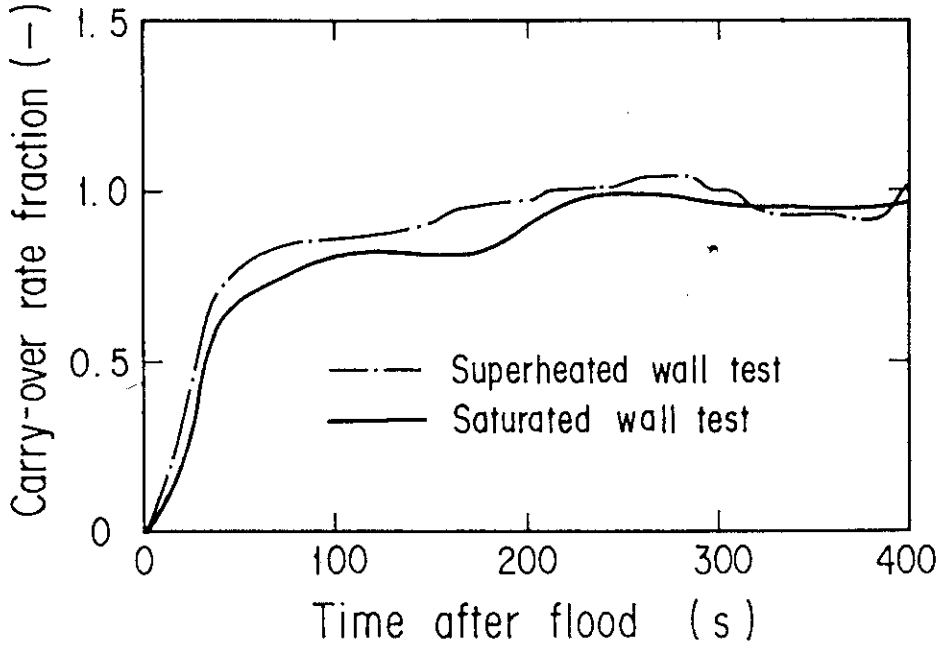

Fig. 14 Comparison of the carry-over rate fraction between the superheated and the saturated downcomer wall tests

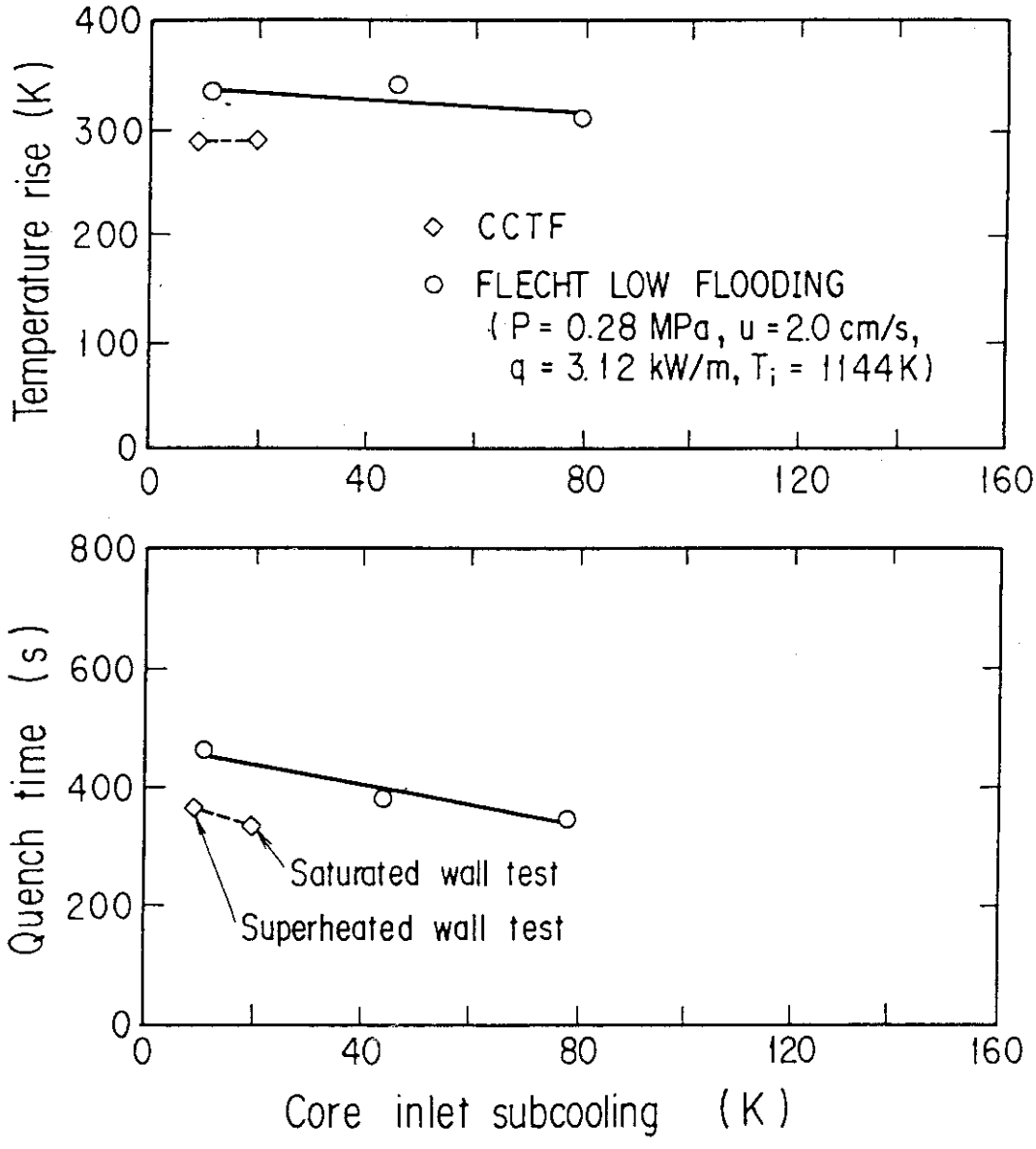

Fig. 13 Effect of core inlet subcooling on temperature rise and quench time in the FLECHT LOW FLOODING TEST and the CCTF test

Appendix A

Explanation of measuring location of referred data and definition of the evaluated data

Figure list

1. Definition of Tag.ID for clad surface temperatures

Notation : TENNWAM

NN : Bundle number

WA : Power zone

WA = X1, X2 : High power (Local power factor 1.1)

WA = Y1, Y2 : Medium power (Local power factor 1.0)

WA = Z1, Z2 : Low power (Local power factor 0.95)

M : Elevation

	Elevation (m)	Axial power factor
1	0.38	0.568
2	1.015	1.176
3	1.83	1.492
4	2.44	1.312
5	3.05	0.815

2. Definition of power zone and bundle number

See Fig. A-1

3. Definition of Tag.ID for void fraction

See Fig. A-2

4. Definition of Tag.ID for average linear power of heater rod in each power unit zone

See Fig. A-3

5. Definition of carry-over rate fraction (CRF)

$$CRF = \frac{\dot{m}_{UP} + \dot{m}_{L}}{\dot{m}_{CR} + \dot{m}_{UP} + \dot{m}_{L}}$$

The calculated data within ±25 s are averaged:

$$(CRF)_i = \frac{1}{101} \sum_{k=i-50}^{i+50} (CRF)_k$$

where

ΔP_{UP} : Average of measured data at four orientations

ΔP_{CR} : Same as above

$$\dot{m}_{UP} = A_{up} \frac{d}{dt} (\Delta P_{UP})$$

$$\dot{m}_{CR} = A_{CR} \frac{d}{dt} (\Delta P_{CR})$$

$$\dot{m}_L = \sum_{k=1}^{4} \dot{m}_{pk}$$

$\dot{m}$: mass flow rate or mass accumulation rate

ΔP: differential pressure

suffix

UP: upper plenum

CR: core

L : loop

p : primary pump

6. Definition of Tag.ID for differential pressure through downcomer, upper plenum, core and lower plenum

See Fig. A-4

7. Definition of Tag.ID for differential pressure through intact and broken loop and broken cold leg nozzle

See Fig. A-5

8. Definition of Tag.ID for fluid temperature in inlet and outlet plenum and secondary of steam generator

See Fig. A-6

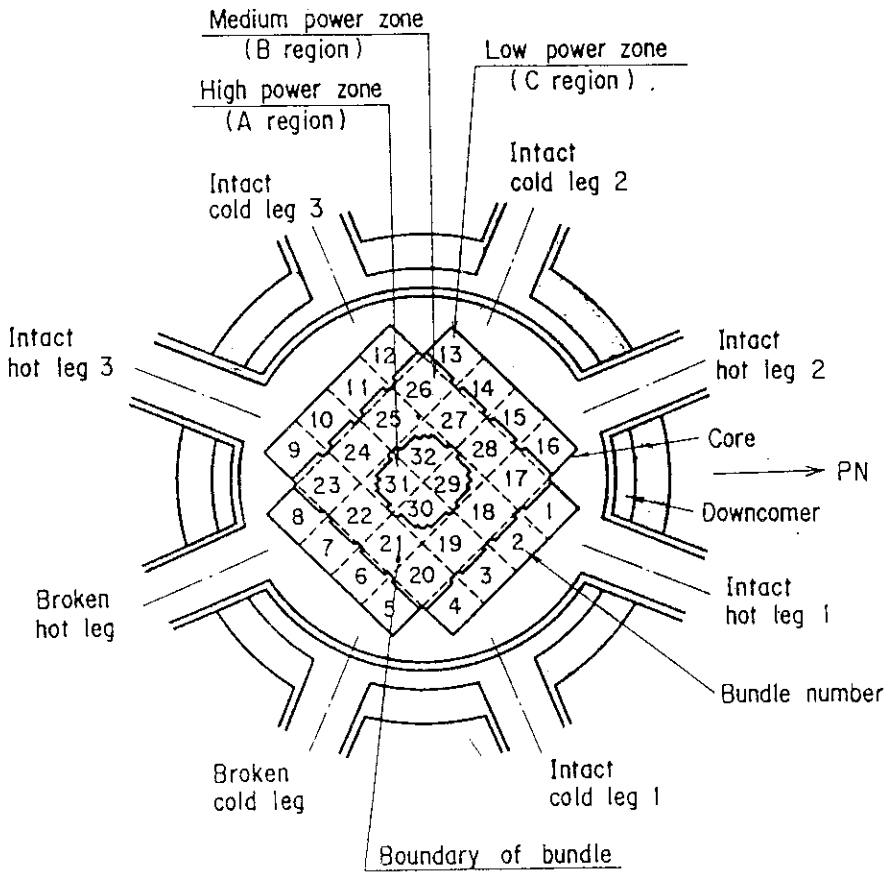

Fig.A-1 Definition of power zones and bundle numbers

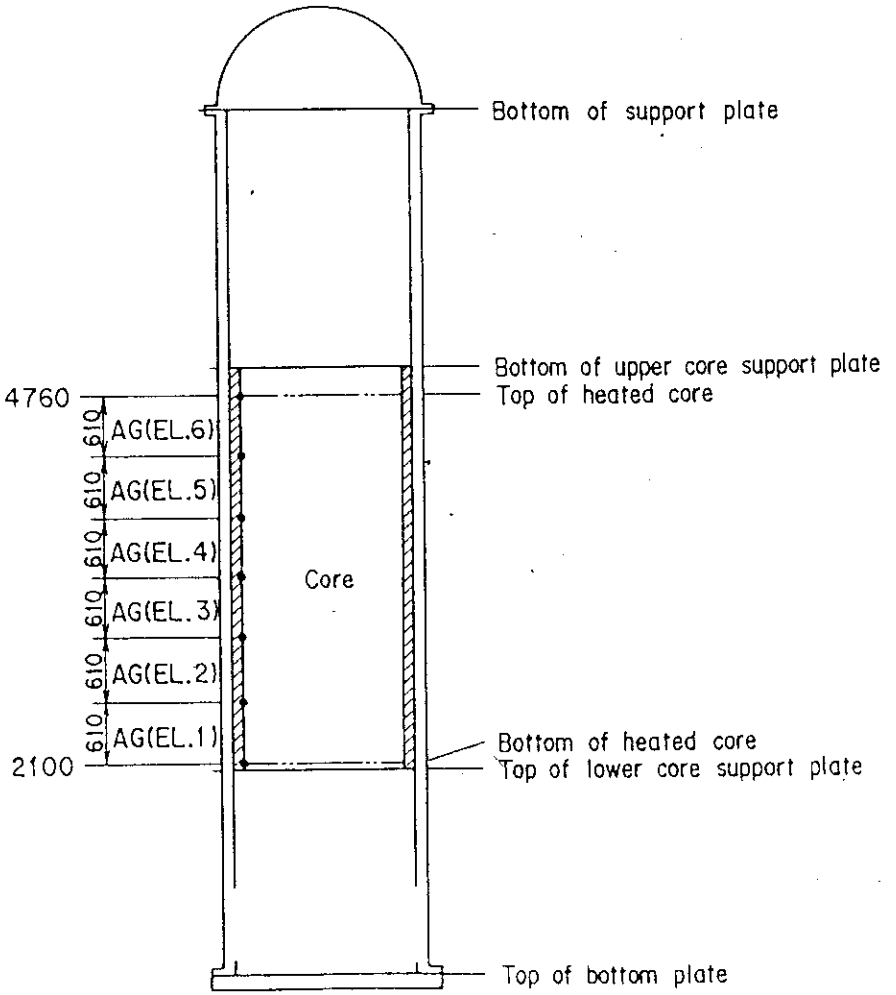

Fig.A-2 Definition of Tag.ID for void fraction (AG(EL.1)～AG(EL.6))

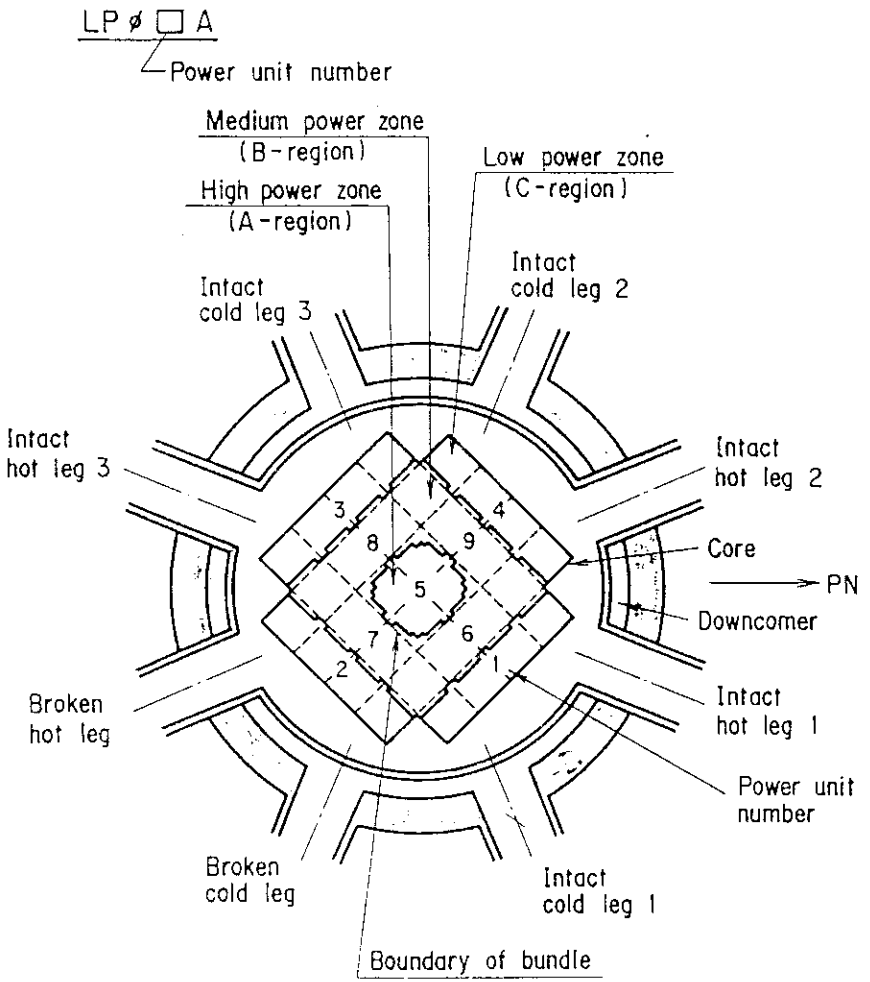

Fig. A-3 Definition of Tag. ID for average linear power of heater rod in each power unit zone (LP01A ~ LP09A)

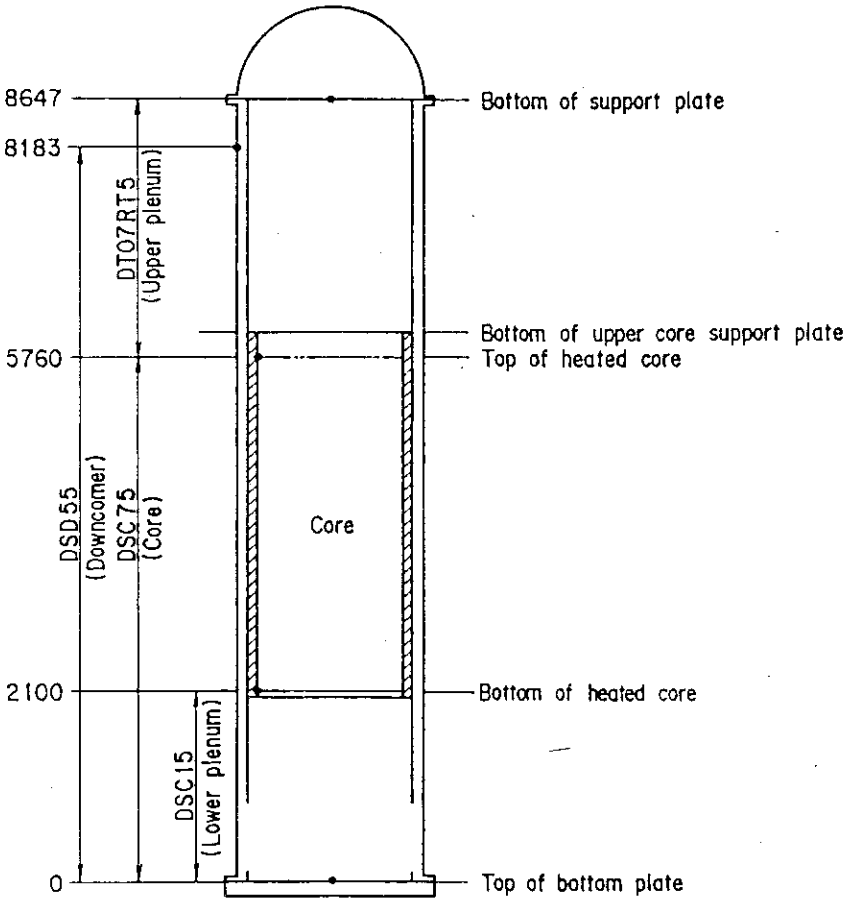

Fig. A-4 Definition of Tag. ID for differential pressure through downcomer, upper plenum, core, and lower plenum (DSD55, DTO7RT5, DSC75, DSC15)

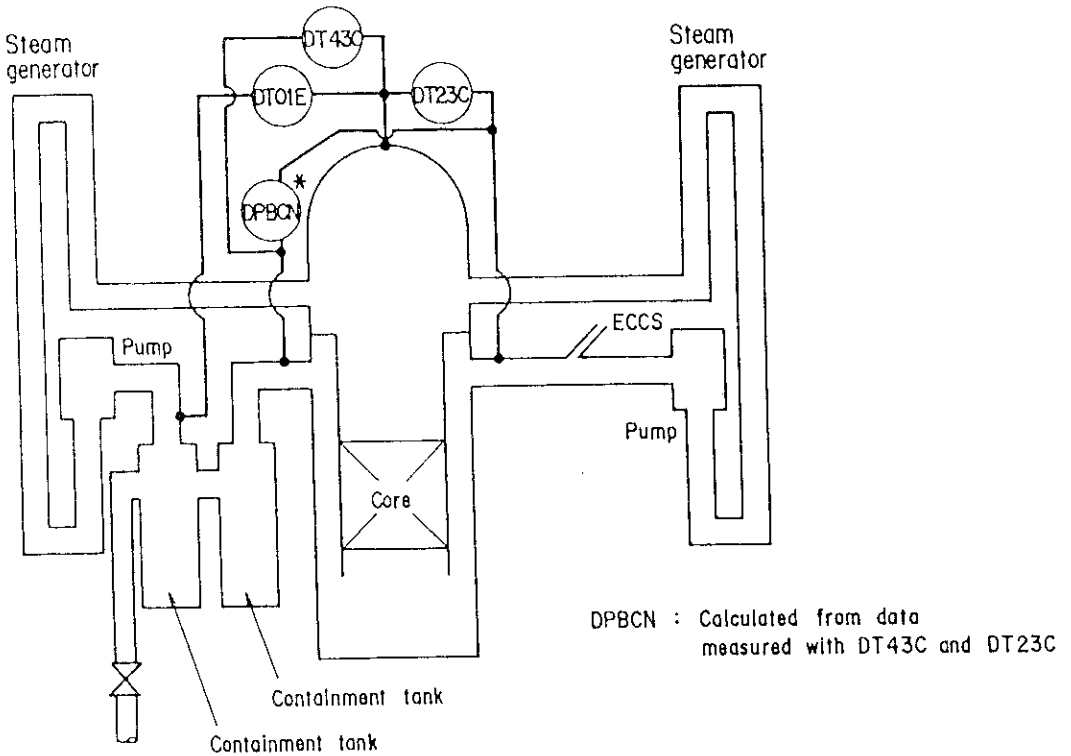

Fig. A-5 Definition of Tag. ID for differential pressure through intact and broken loop and broken cold leg nozzle (DT23C, DT01B, DPBCN)

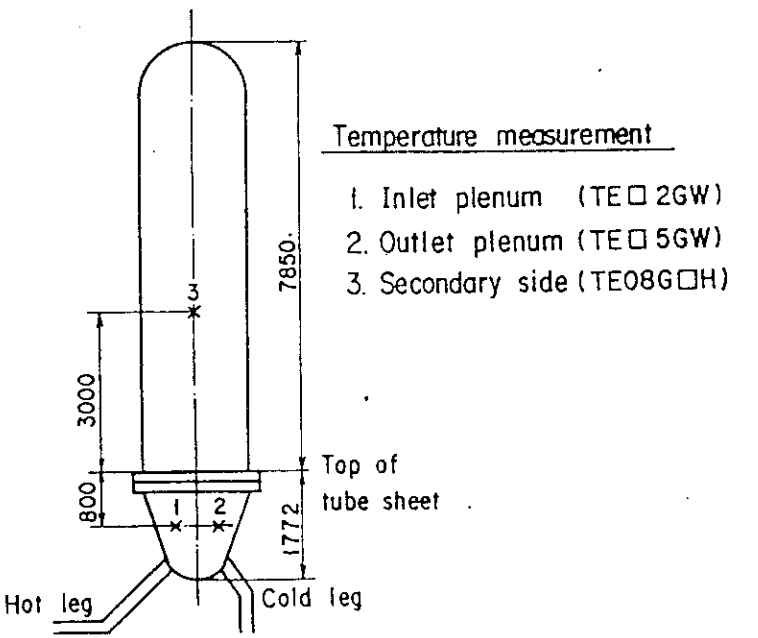

Fig. A-6 Definition of Tag. ID for fluid temperature in inlet and outlet plenum and secondary of steam generator (TE□2GW, TE□5GW, TE08G□H)

Appendix B

Main results of the test C1-2

Table and Figure List

Table B-1 Summary of test conditions

1. TEST TYPE : TEST C1-2 (CCTF MAIN TEST NO.2)
2. TEST NUMBER : RUN 011 3. DATE : July 4, 1979
4. POWER : A: TOTAL: 9.36 MW; B:LINEAR: 1.4 KW/M
5. RELATIVE RADIAL POWER SHAPE :

   A: ZONE: A B C

   B: RATIO: 1.07 : 1.0 : 0.82
6. AXIAL POWER SHAPE : CHOPPED COSINE
7. PRESSURE (KG/CM^2A) :

   A: SYSTEM: 2.07, B: CONTAINMENT 2.06,

   C: STEAM GENERATOR SECONDARY: 50
8. TEMPERATURE (DEG.C) :

   A: DOWNCOMER WALLS 187, B: VESSEL INTERNALS 120

   C: PRIMARY PIPING WALLS 118, D: LOWER PLENUM LIQUID 113

   E: ECC LIQUID 39, F: STEAM GENERATOR SECONDARY 263

   G: CORE TEMPERATURE AT ECC INITIATION 506
9. ECC INJECTION TYPE: C

   A: COLD LEG, B: LOWER PLENUM, C: LOWER PLENUM + COLD LEG
10. PUMP K-FACTOR : ~15 (UNCERTAIN)
11. ECC FLOW RATES AND DURATION :

    A: ACCUMULATOR 264 M^3/HR FROM 0 TO 25 SECONDS

    B: LPCI 30.9 M^3/HR FROM 25 TO 674 SECONDS

    C: ECC INJECTION TO LOWER PLENUM : FROM 0 TO 16 SECONDS

    (VALVE OPENING AND CLOSING TIMES ARE INCLUDED IN THE INJECTION DURATION)
12. INITIAL WATER LEVEL IN LOWER PLENUM : 0.86 M.
13. POWER CONTROL : ANS x 1.2 + ACTINIDE (30 SEC AFTER SCRAM)
14. EXPECTED BOCREC TIME FROM ECC INITIATION 12 SEC
15. EXPECTED PEAK TEMPERATURE AT BOCREC 600 C

Table B-2 Chronology of events

EVENT	TIME (sec)
Test C1-2 initiated (Heater rods power on) (Data recording initiated)	0.0
Accumulator injection initiated	53
Power decay initiated (Beginning of core recovery)	67
Accumulator injection switched from lower plenum to cold leg	69
Accumulator injection ended and LPCI injection initiated	78
All heater rods quenched	588
Power off	625
LPCI injection ended	727
Test C1-2 ended (Data recording ended)	1074

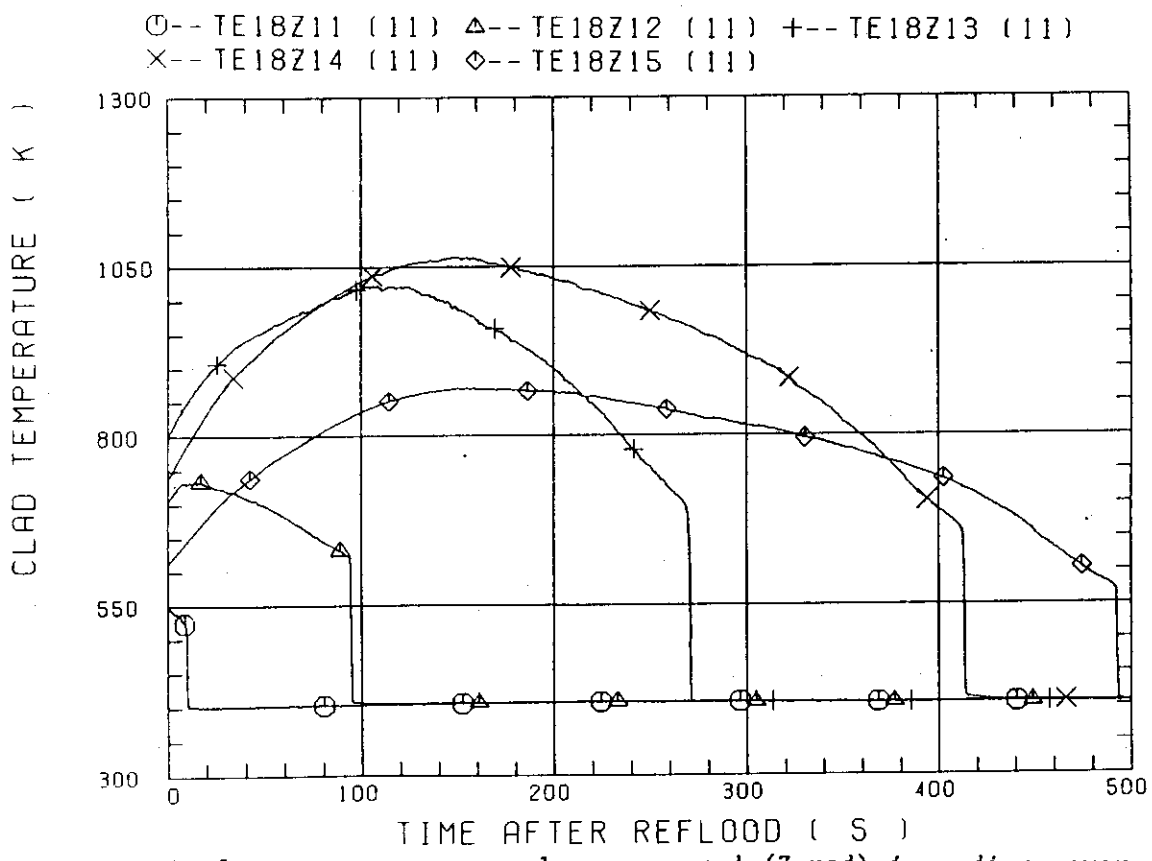

Fig. B-1 Surface temperature on low power rod (Z-rod) in medium power region (B region) (average power rod)

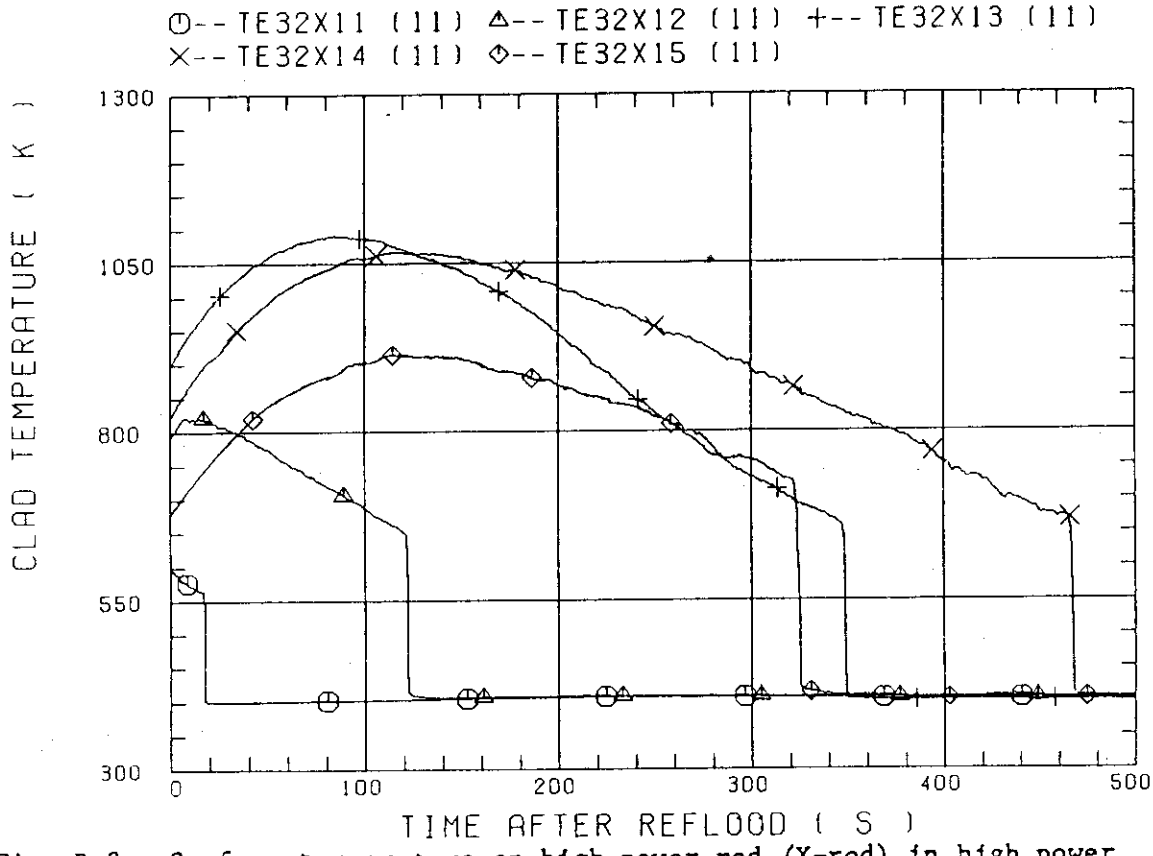

Fig. B-2 Surface temperature on high power rod (X-rod) in high power region (A region) (peak power rod)

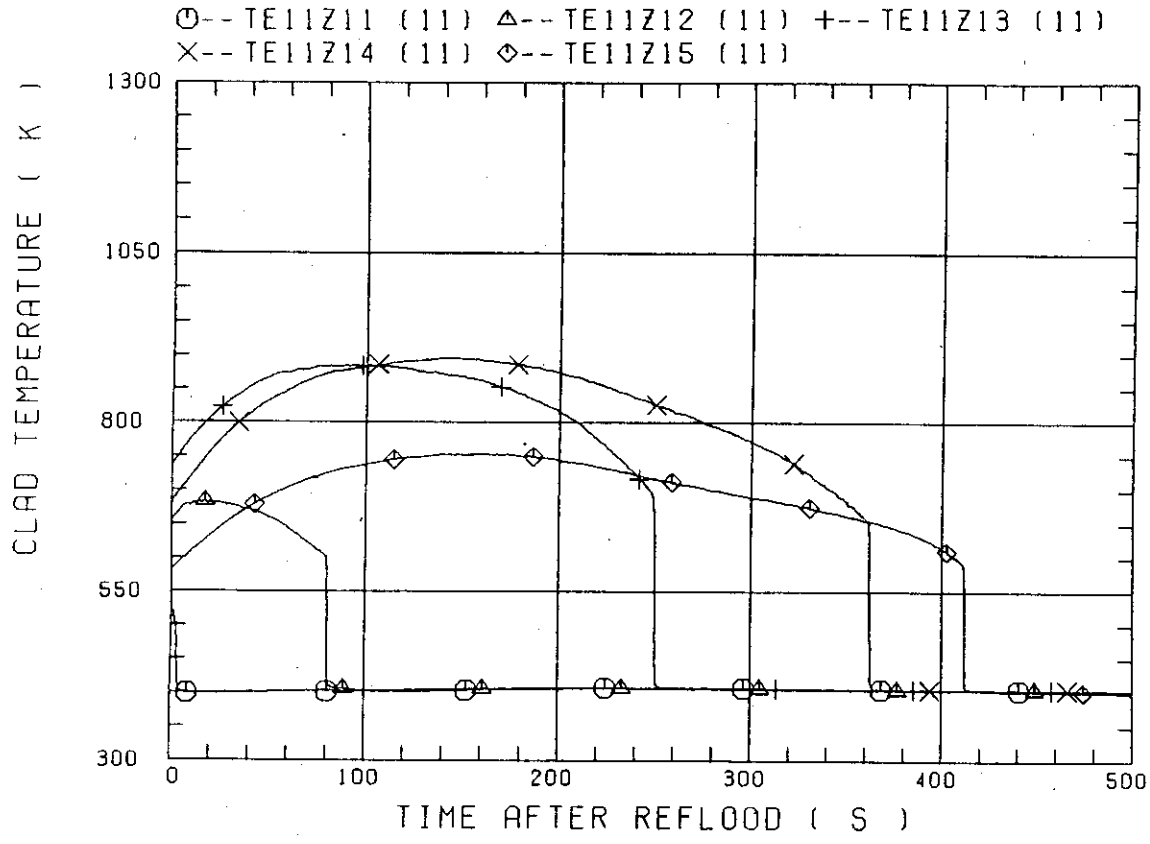

Fig. B-3 Surface temperature on low power rod (Z-rod) in low power region (C region) (lowest power rod)

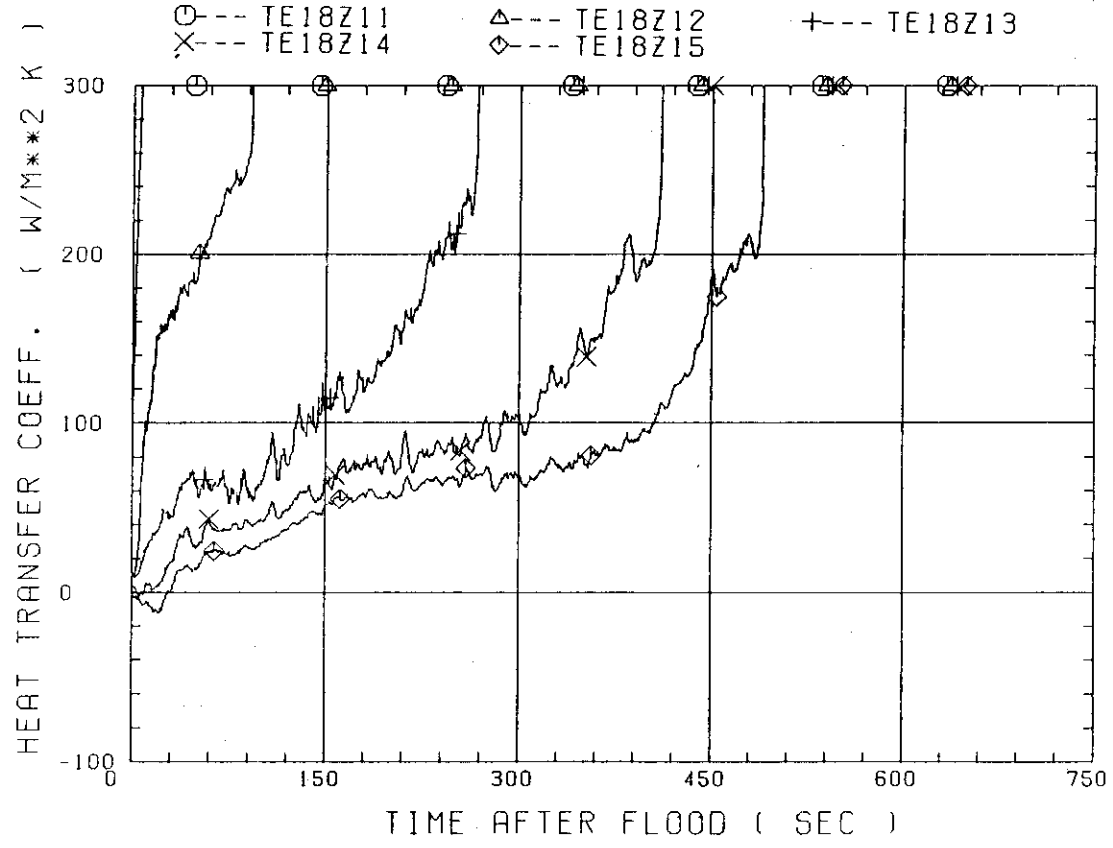

Fig. B-4 Heat transfer coefficient along a low power rod (Z-rod) in medium power region (B region) (average power rod)

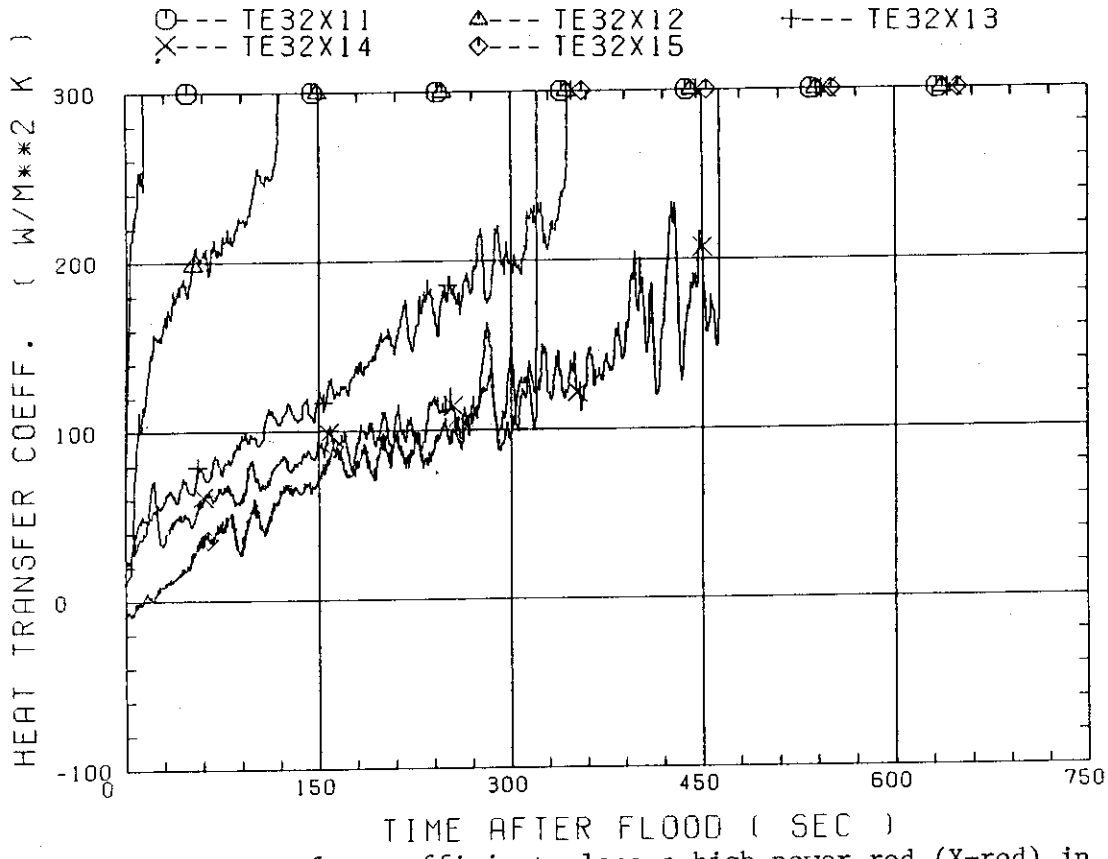

Fig. B-5 Heat transfer coefficient along a high power rod (X-rod) in high power region (A region) (peak power rod)

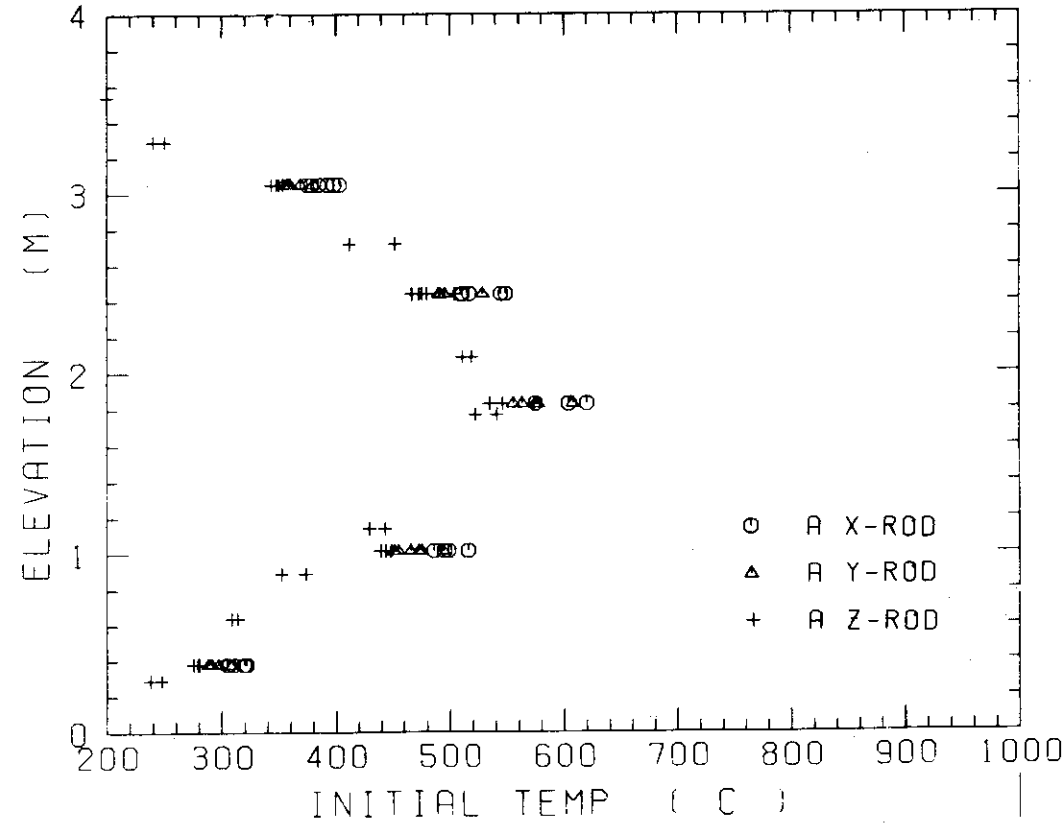

Fig. B-6 Initial rod surface temperature in high power region (A region)

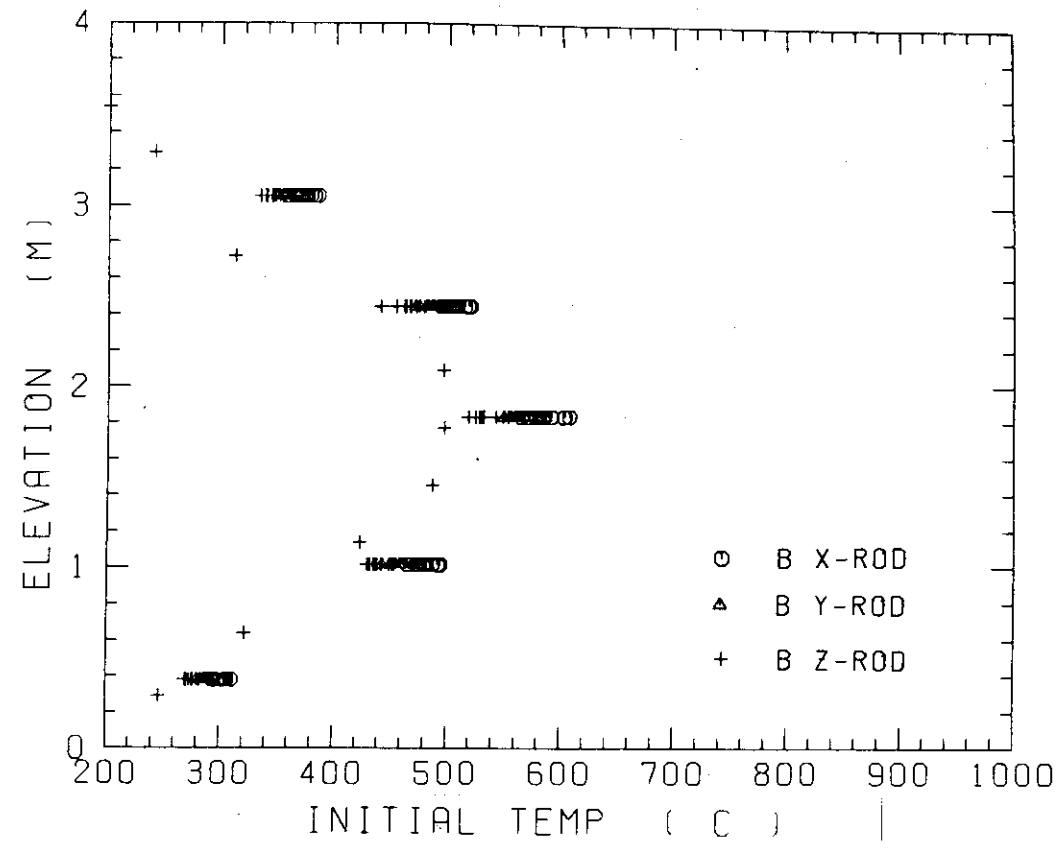

Fig. B-7 Initial rod surface temperature in medium power region (B region)

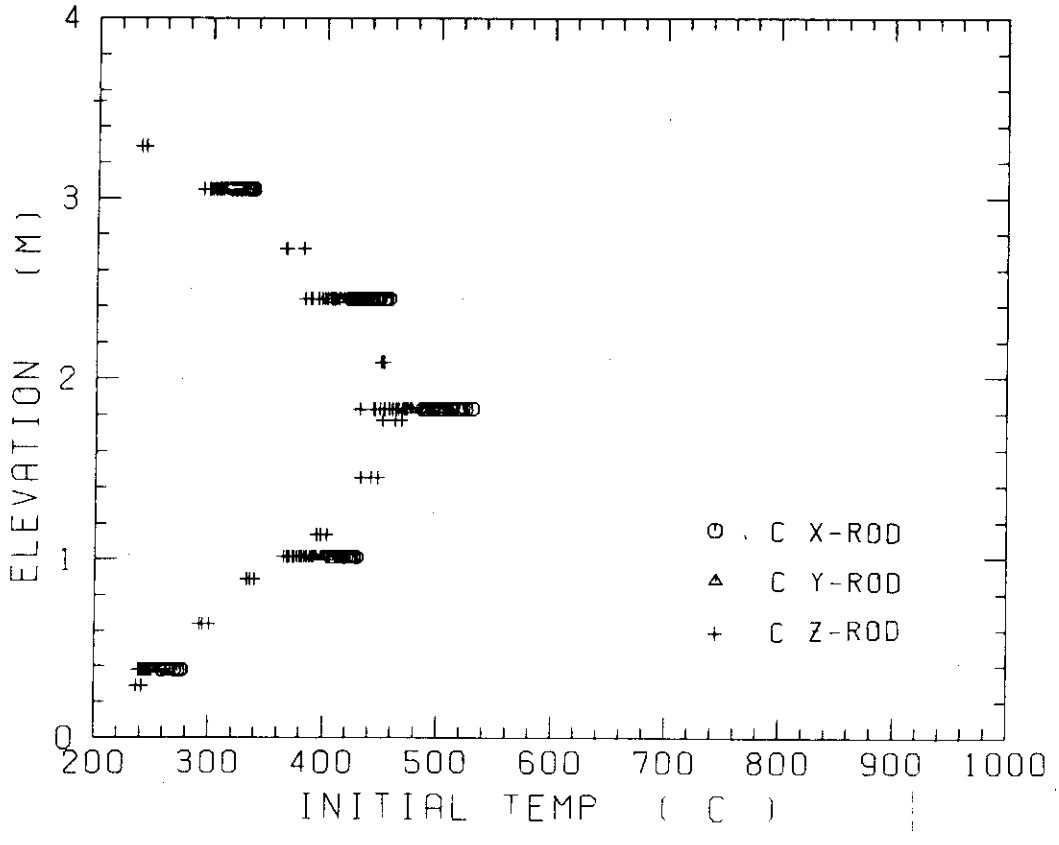

Fig. B-8 Inital rod surface temperature in low power region (C region)

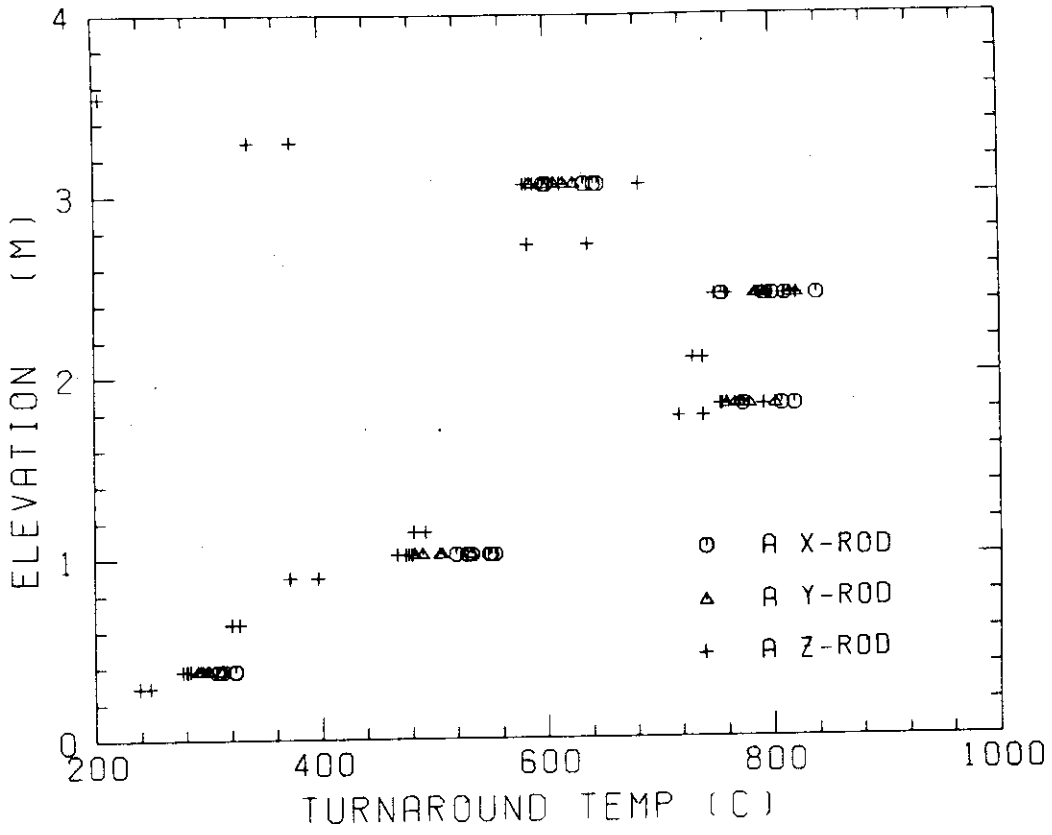

Fig. B-9 Turnaround temperature in high power region (A region)

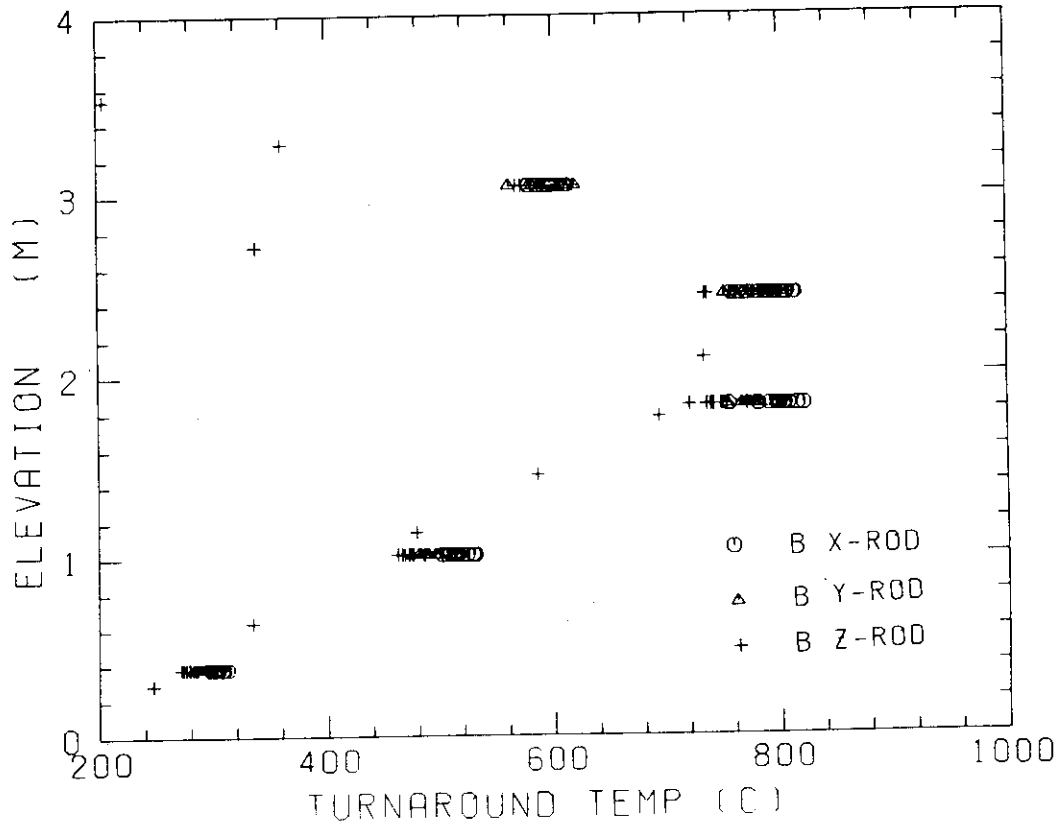

Fig. B-10 Turnaround temperature in medium power region (B region)

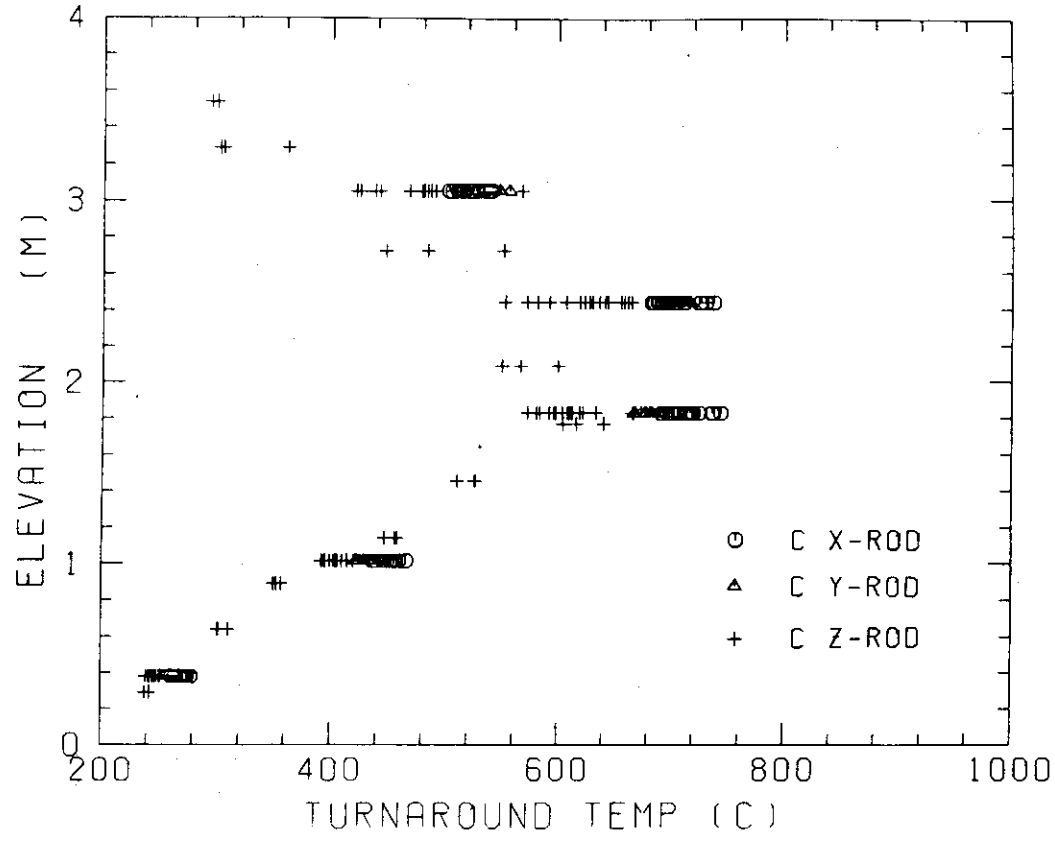

Fig. B-11 Turnaround temperature in low power region (C region)

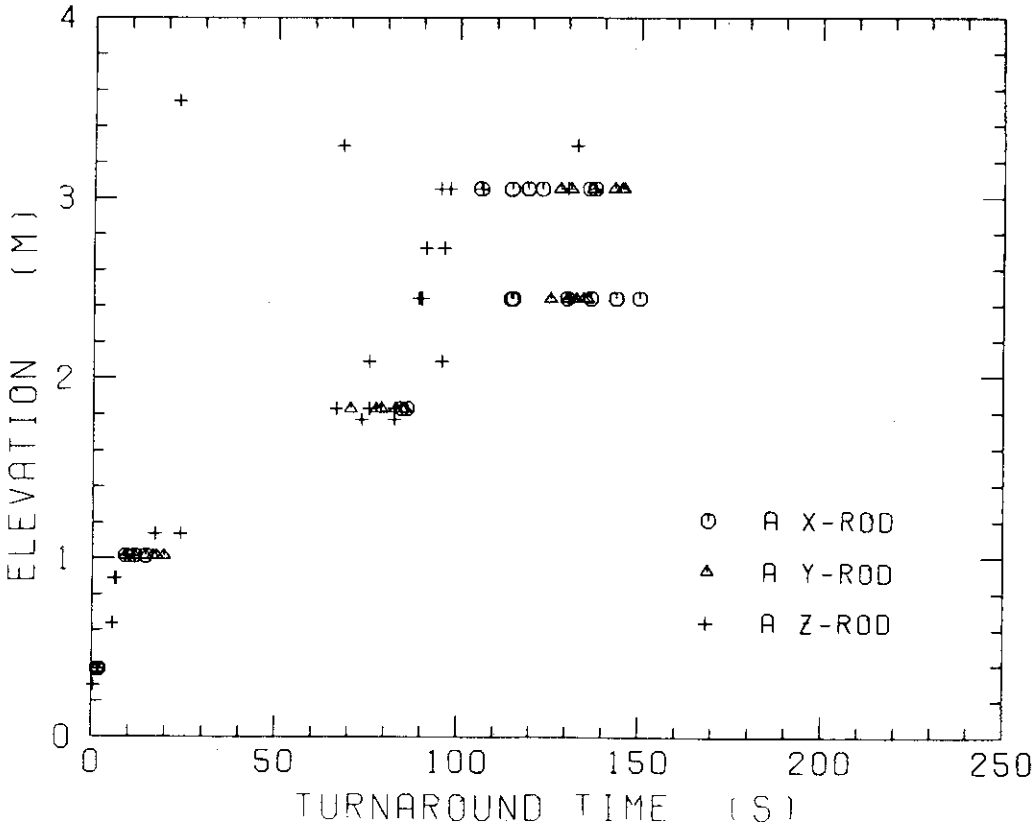

Fig. B-12 Turnaround time in high power region (A region)

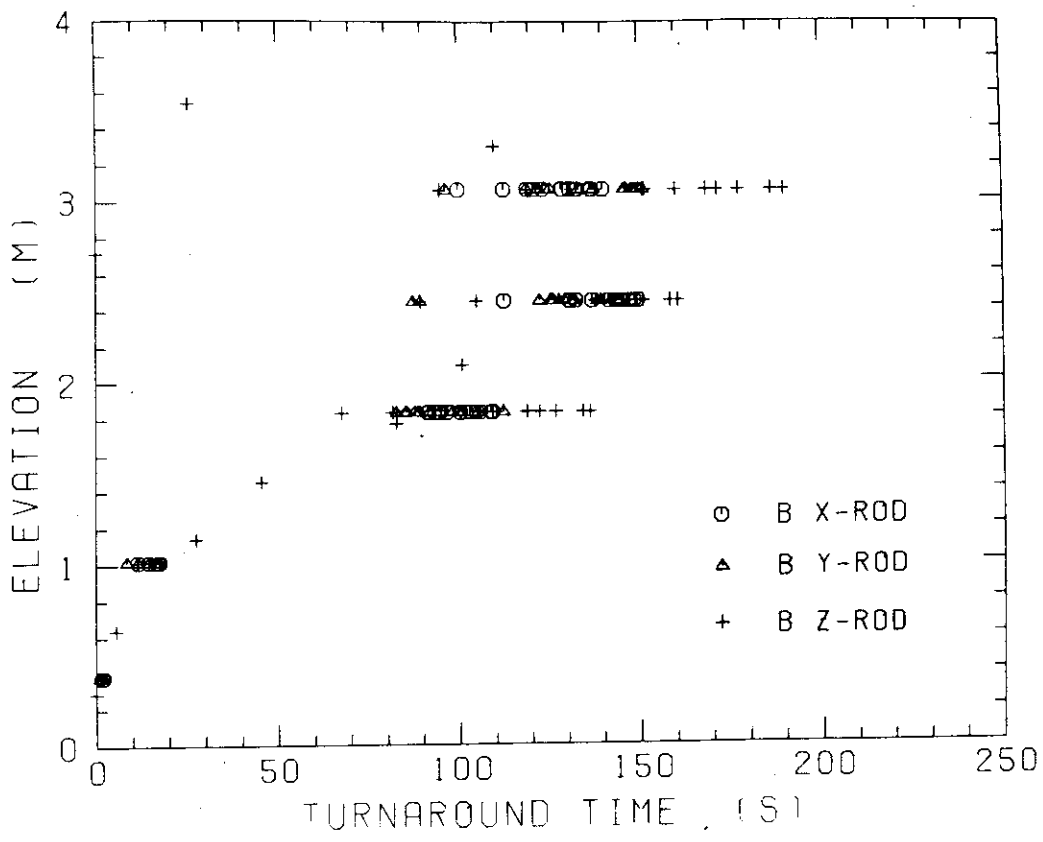

Fig. B-13 Turnaround time in medium power region (B region)

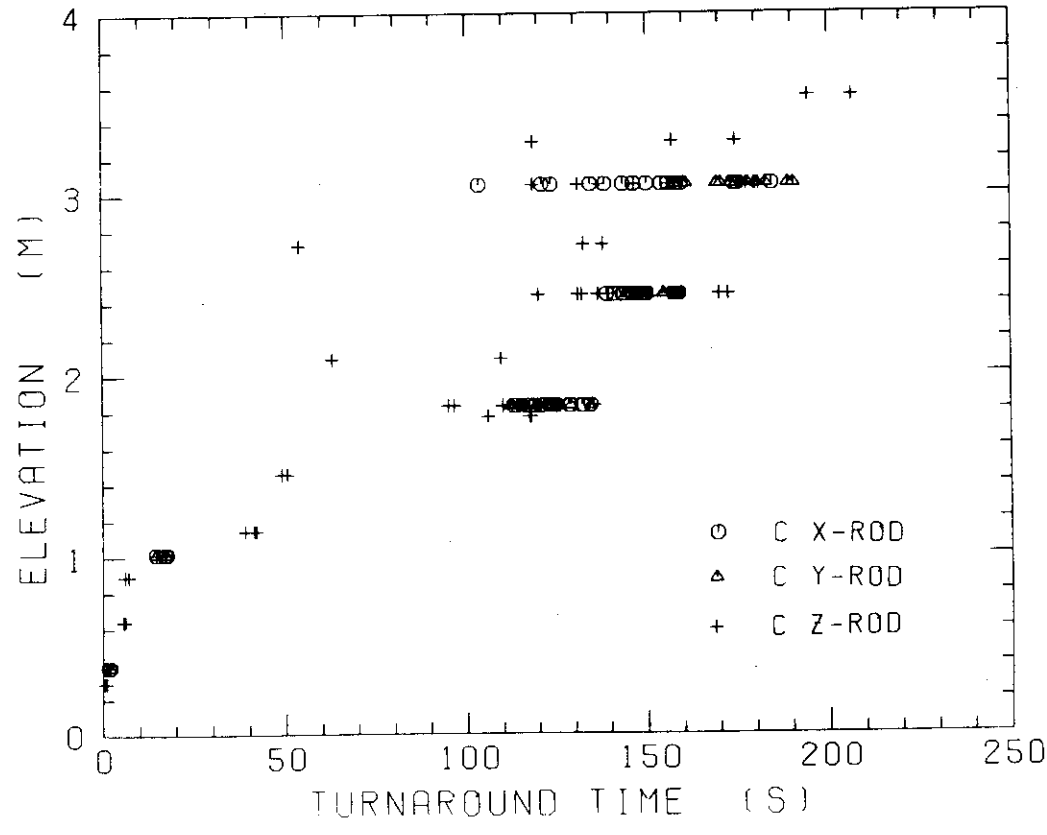

Fig. B-14 Turnaround time in low power region (C region)

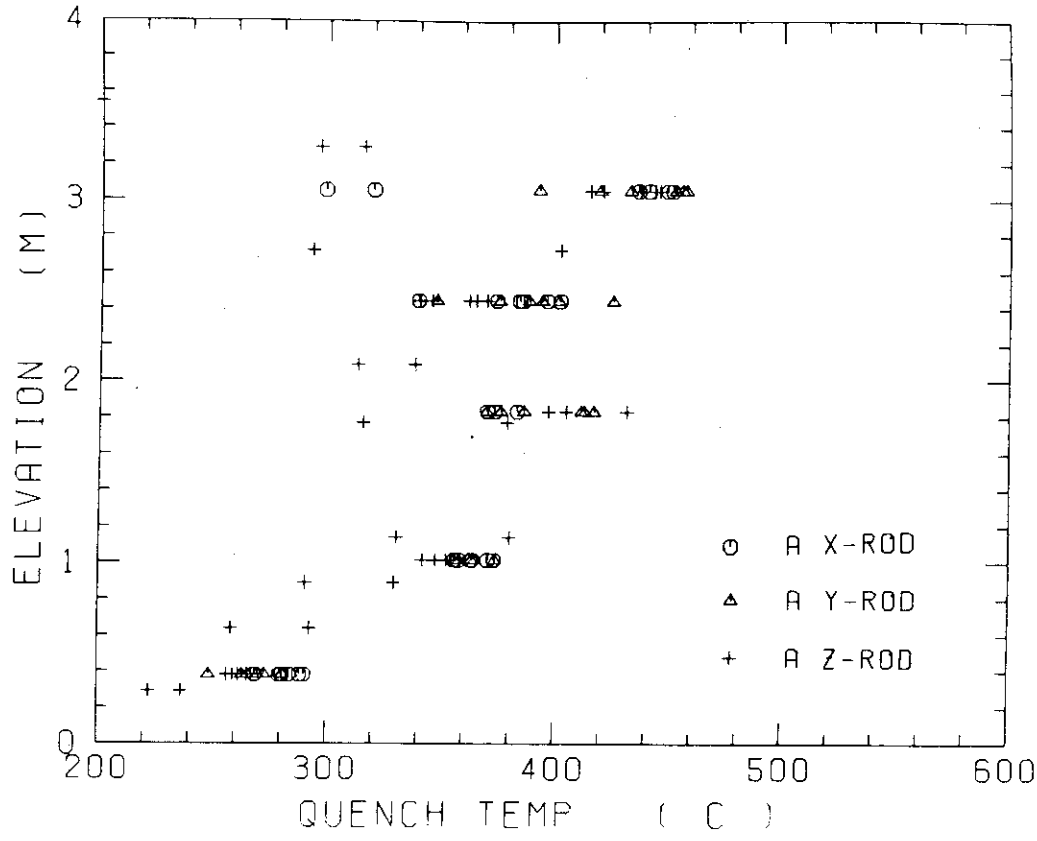

Fig. B-15 Quench temperature in high power region (A region)

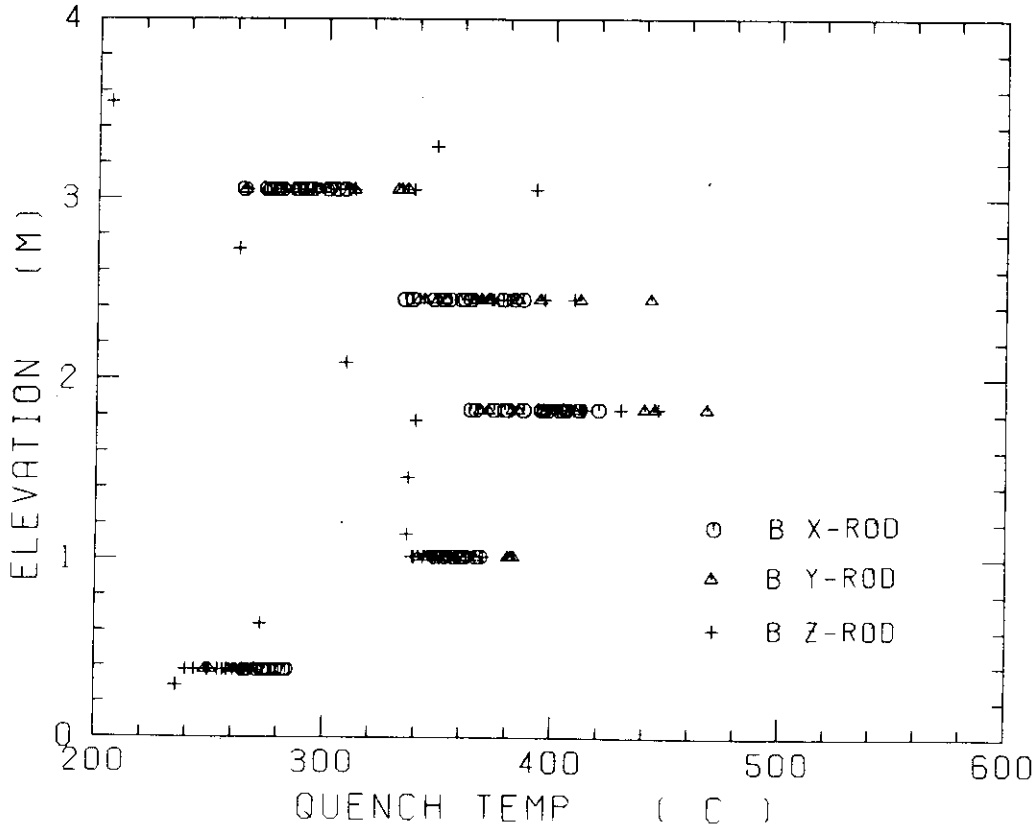

Fig. B-16 Quench temperature in medium power region (B region)

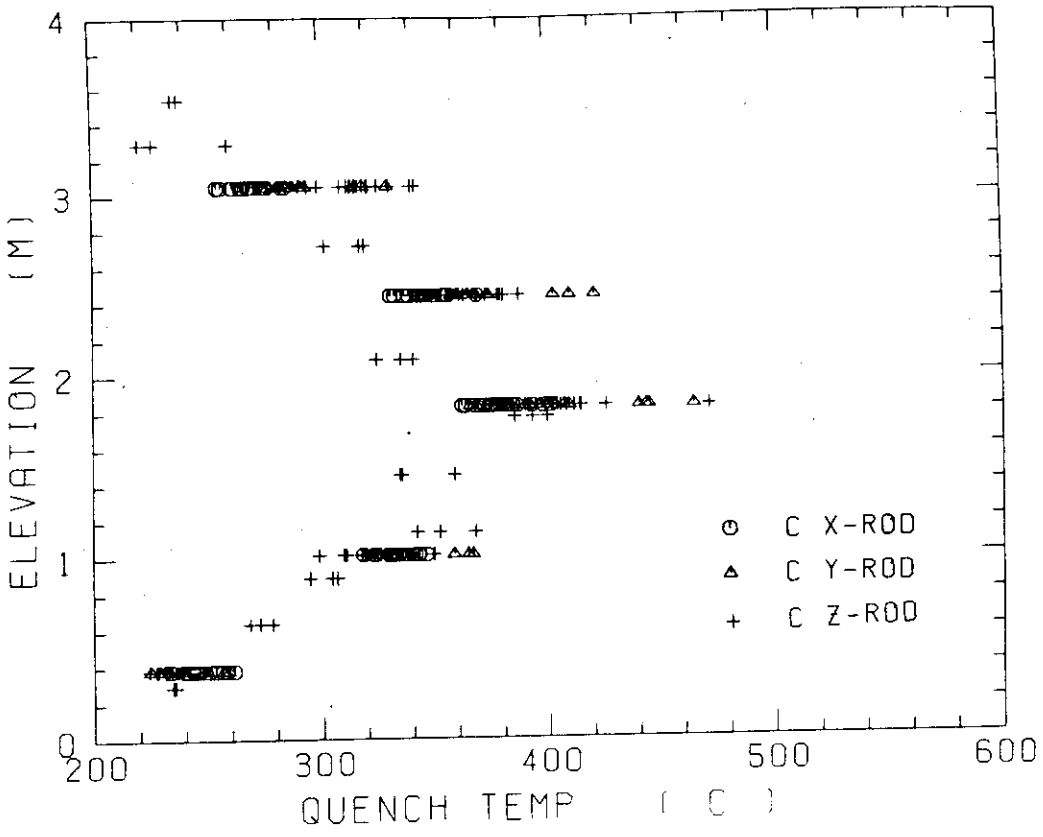

Fig. B-17 Quench temperature in low power region (C region)

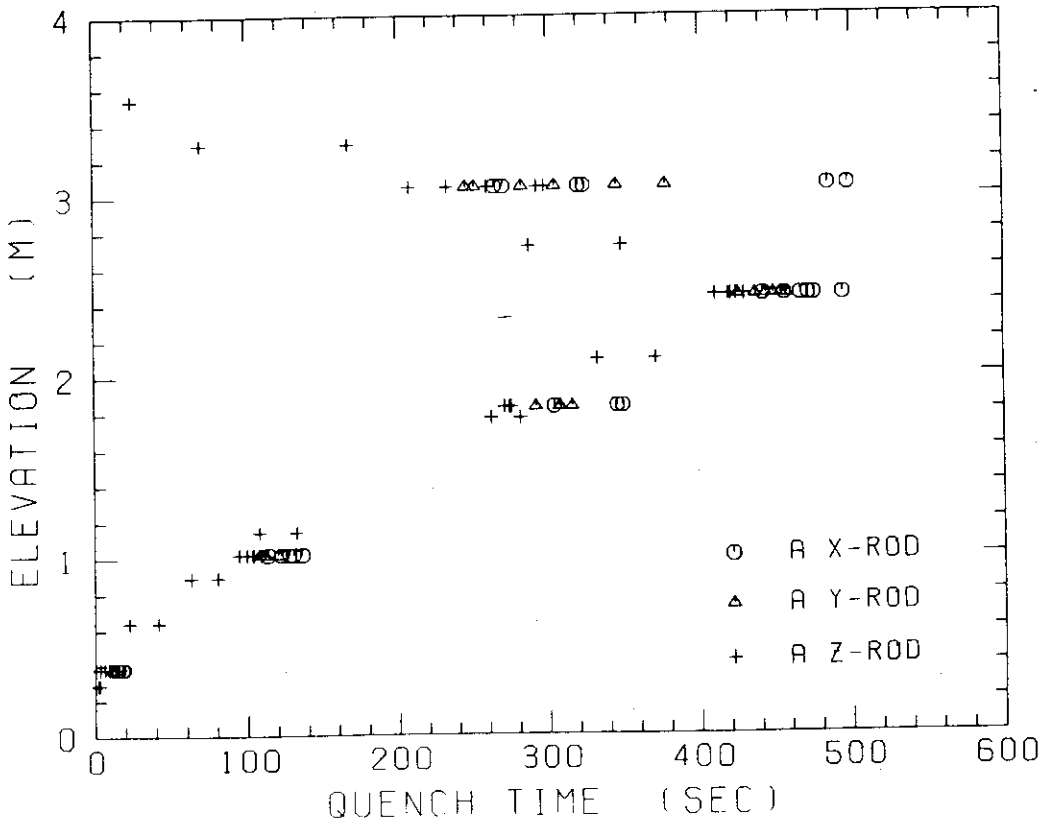

Fig. B-18 Quench time in high power region (A region)

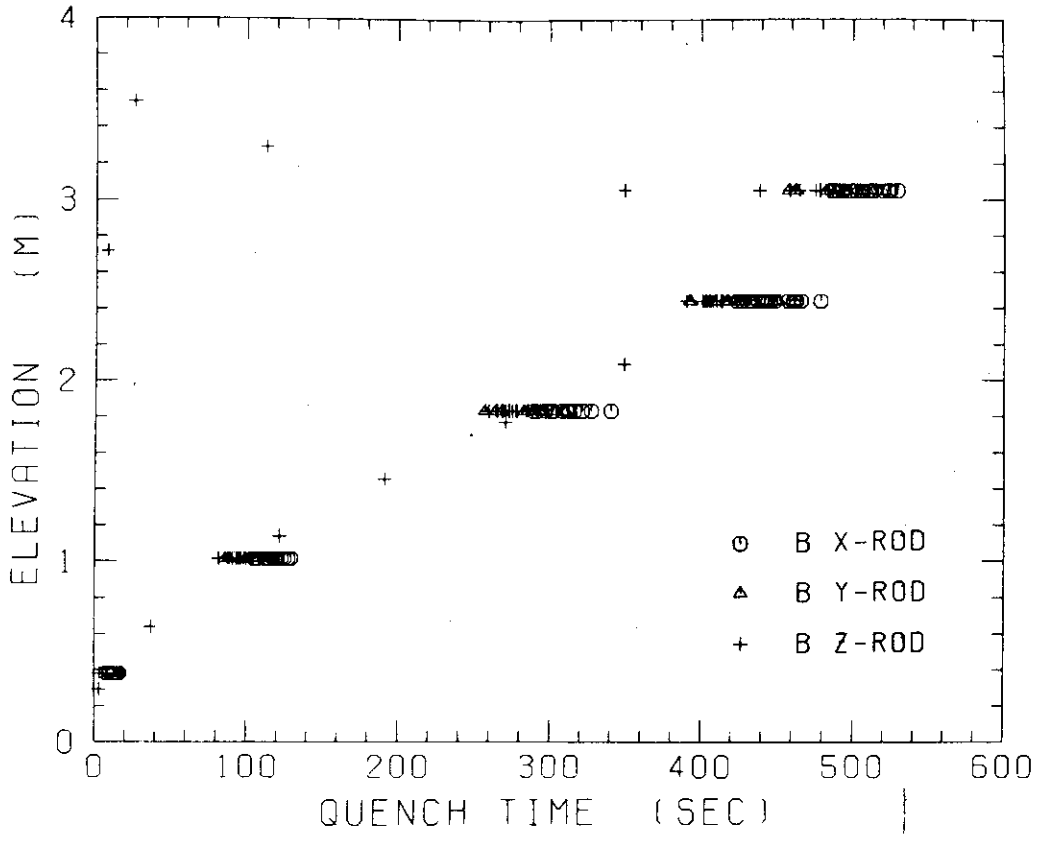

Fig. B-19 Quench time in medium power region (B region)

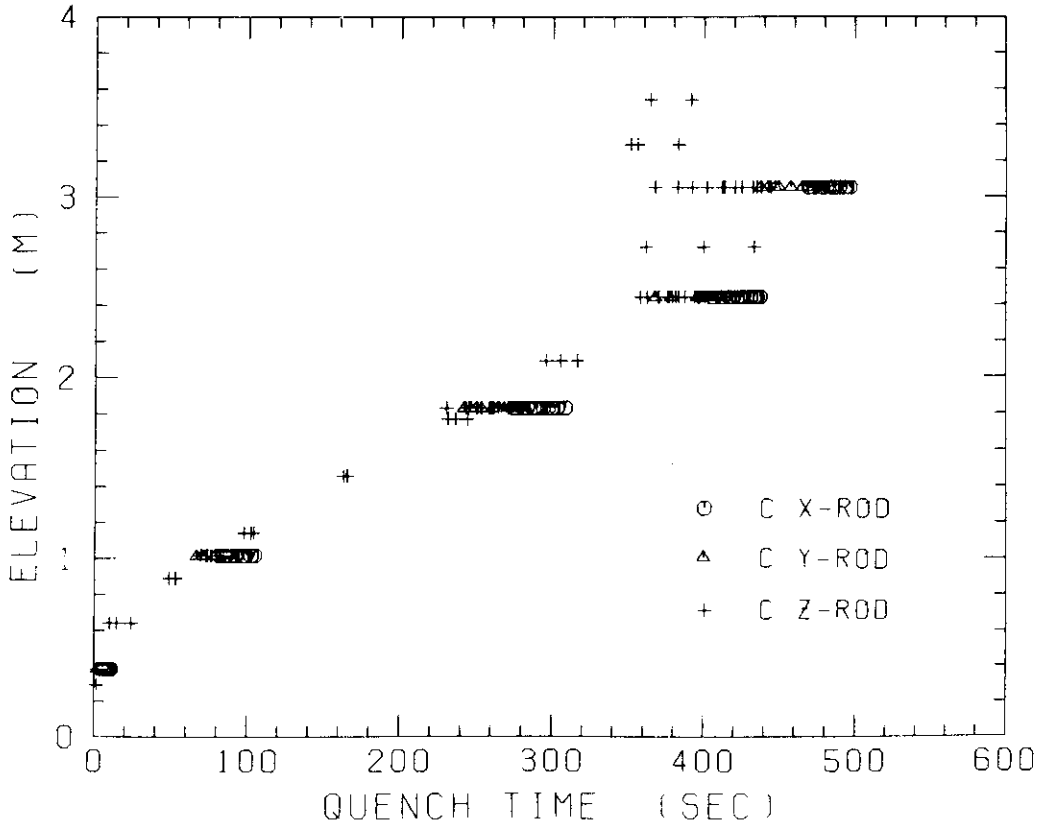

Fig. B-20 Quench time in low power region (C region)

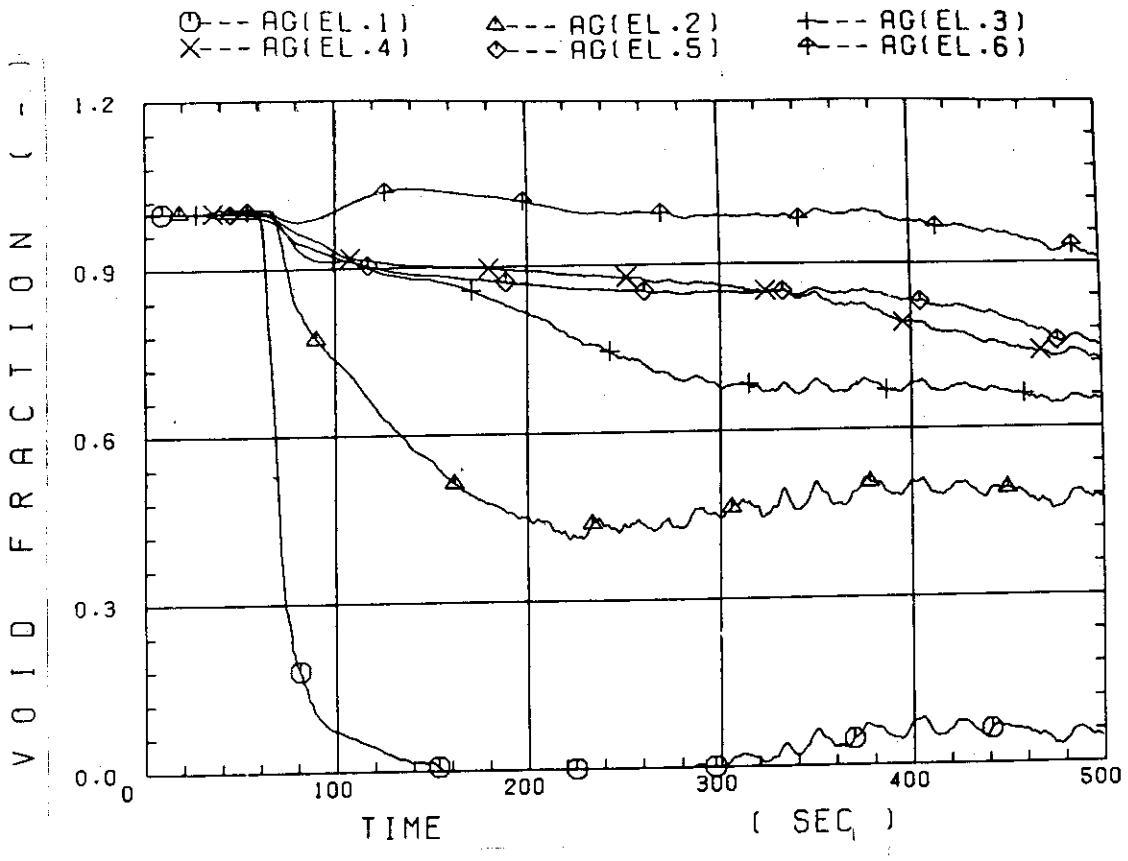

Fig. B-21 Void fraction in core

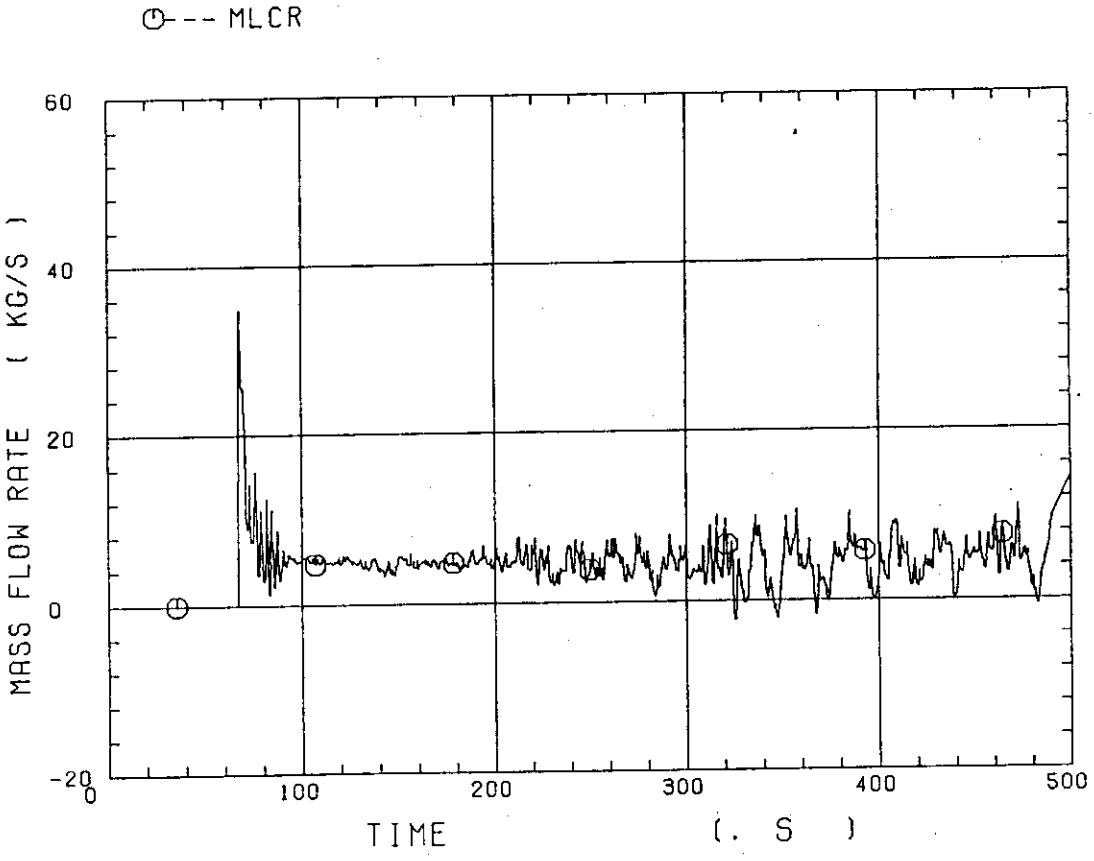

Fig. B-22 Evaluated core inlet mass flow rate

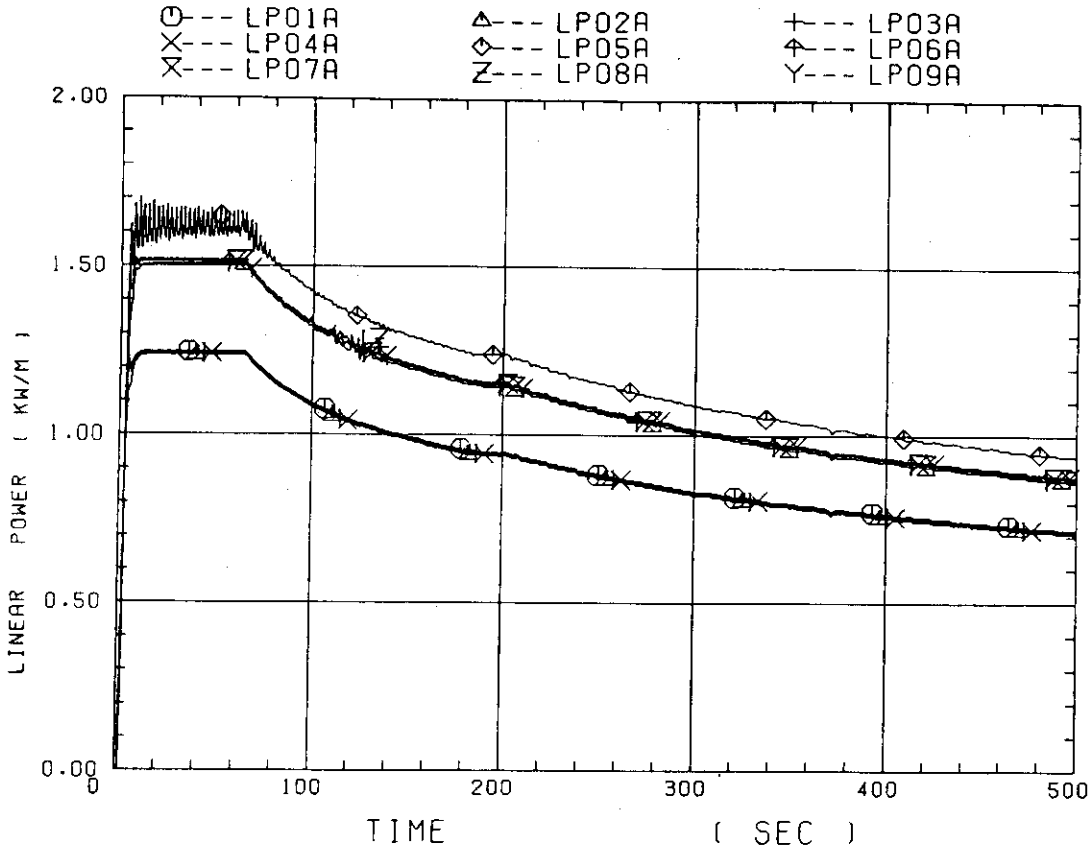

Fig. B-23 Average linear power of heater rod in each power unit zone

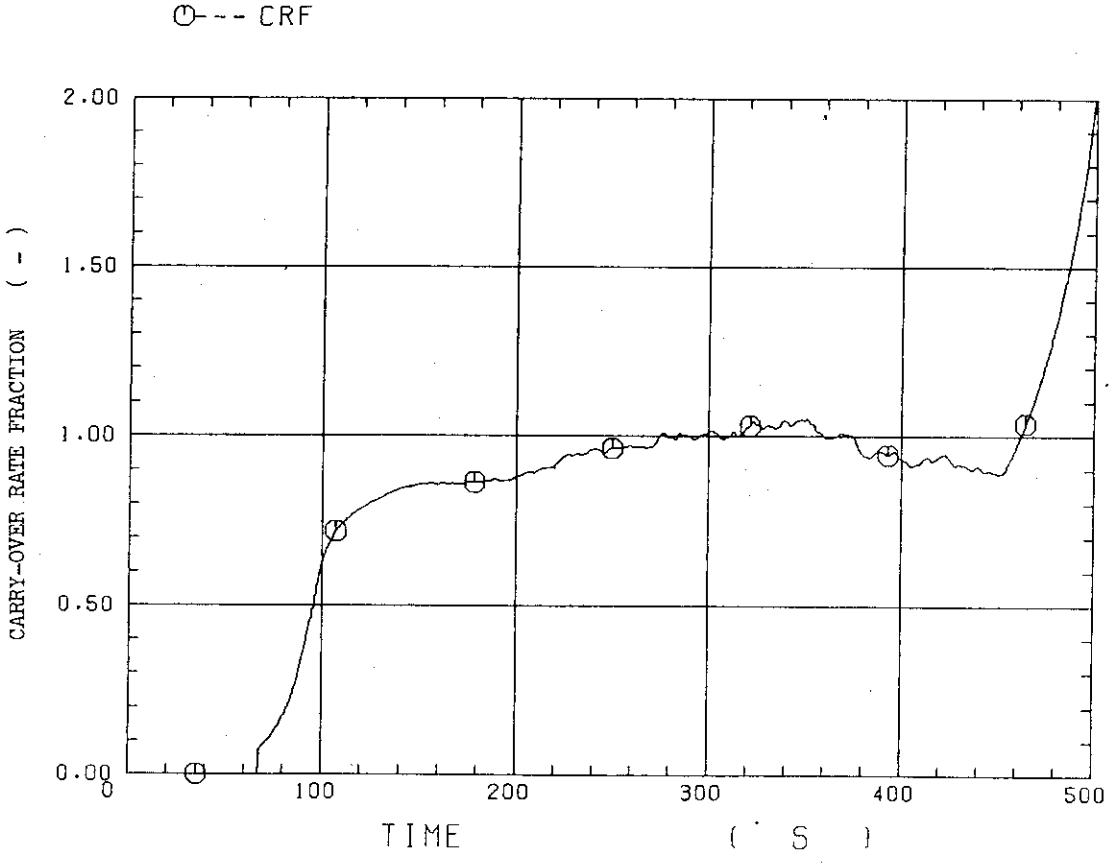

Fig. B-24 Carry-over rate fraction

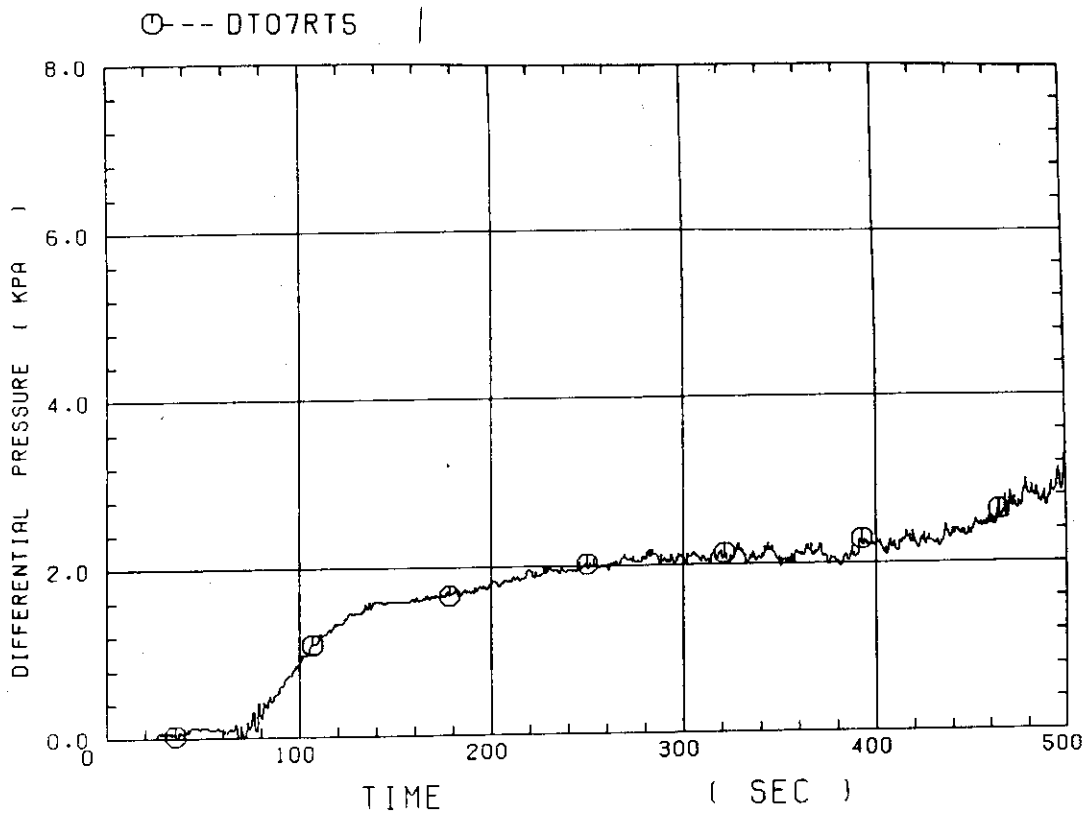

Fig. B-25 Differential pressure through upper plenum

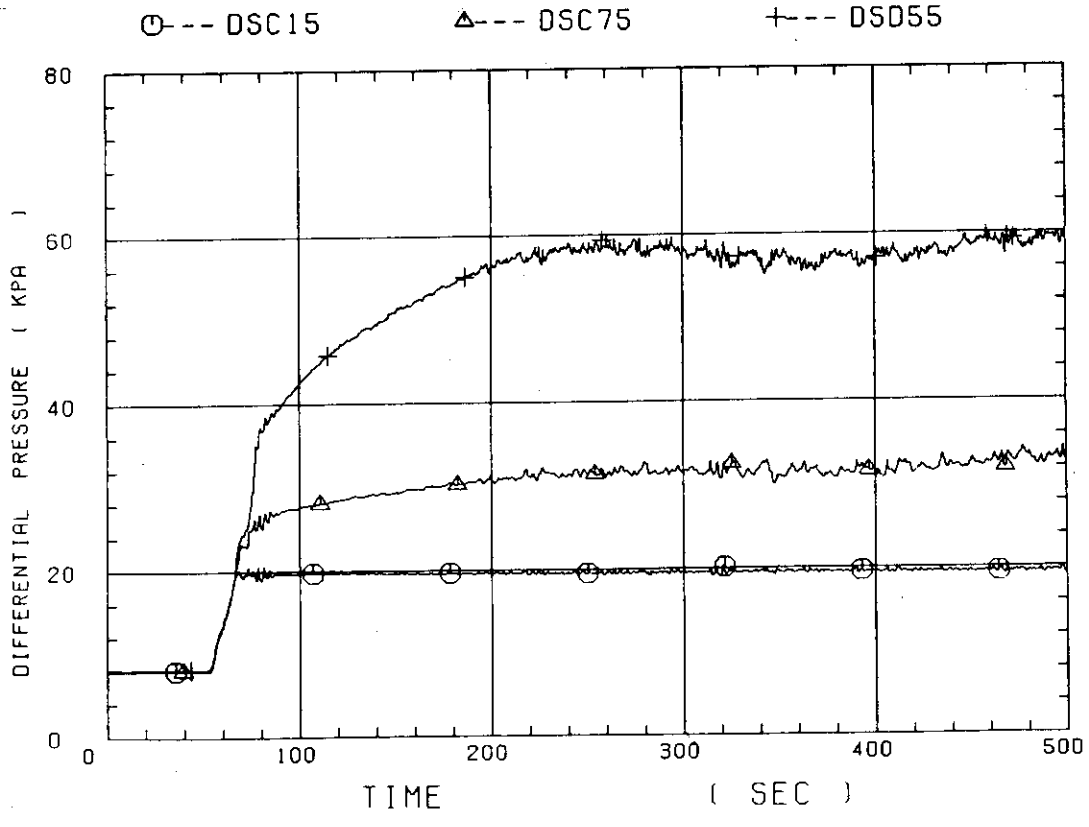

Fig. B-26 Differential pressure through downcomer, core, and lower plenum

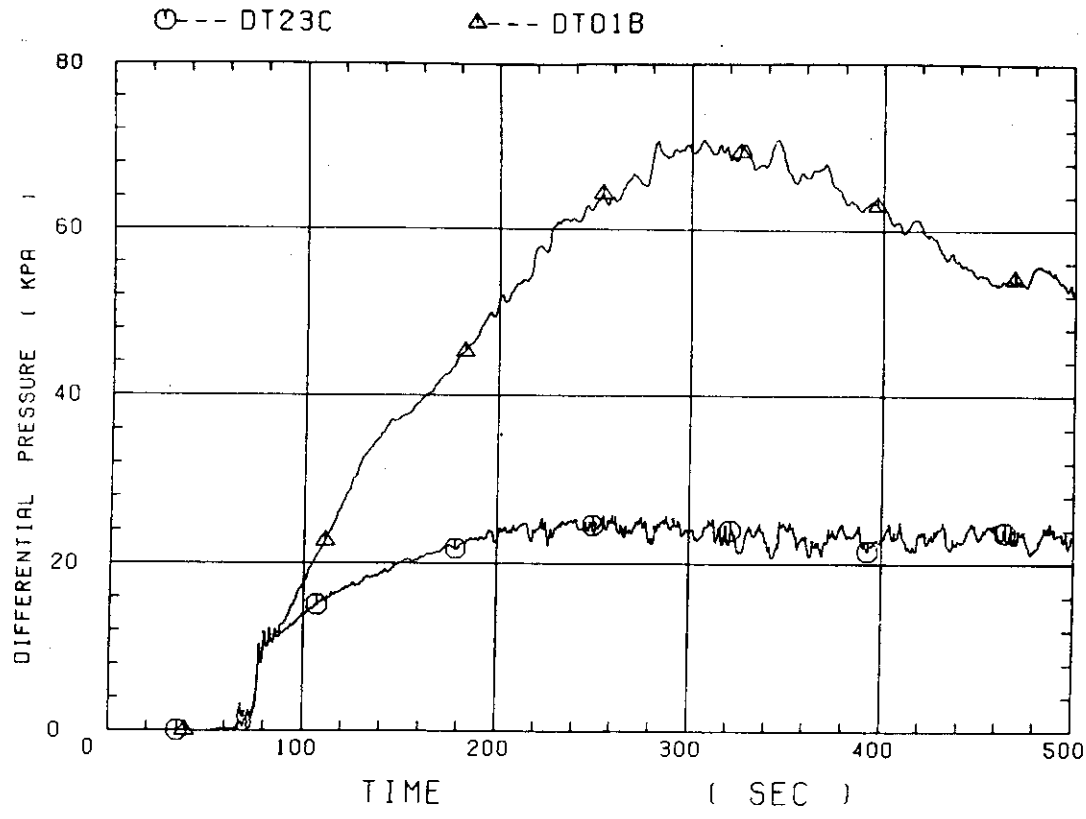

Fig. B-27 Differential pressure through intact and broken loops

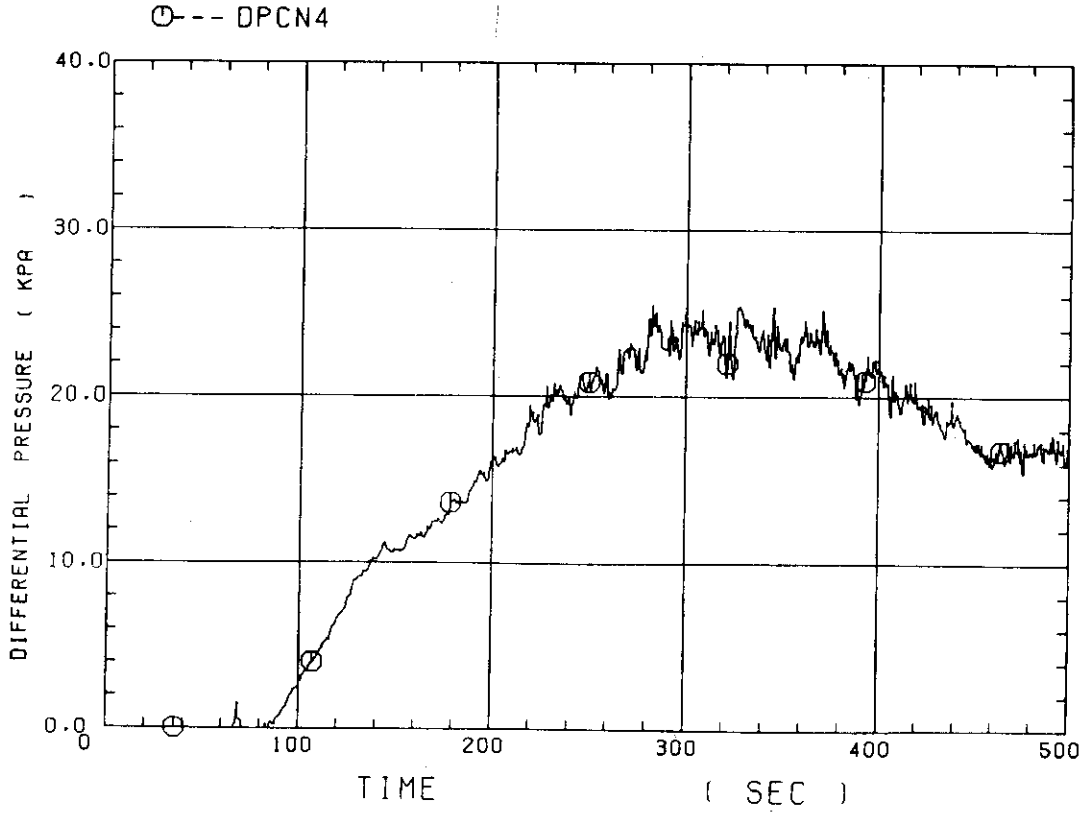

Fig. B-28 Differential pressure through broken cold leg nozzle

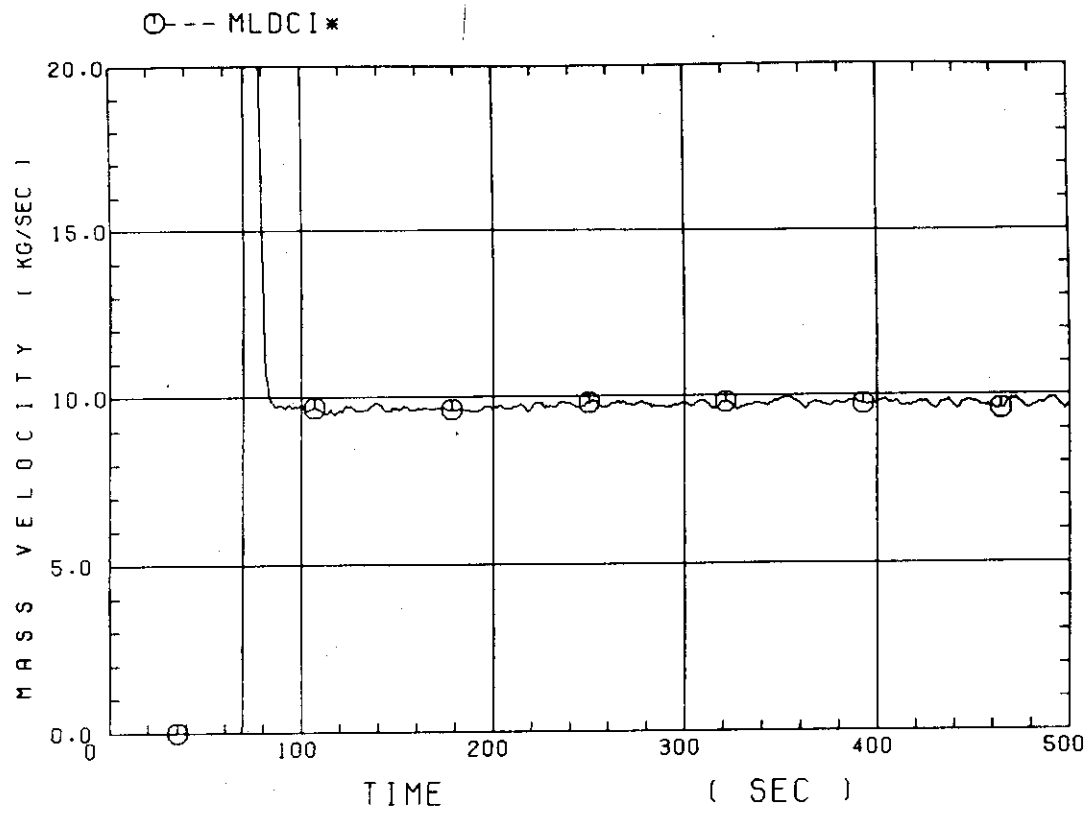

Fig. B-29 Total water mass flow rate from intact loops to downcomer

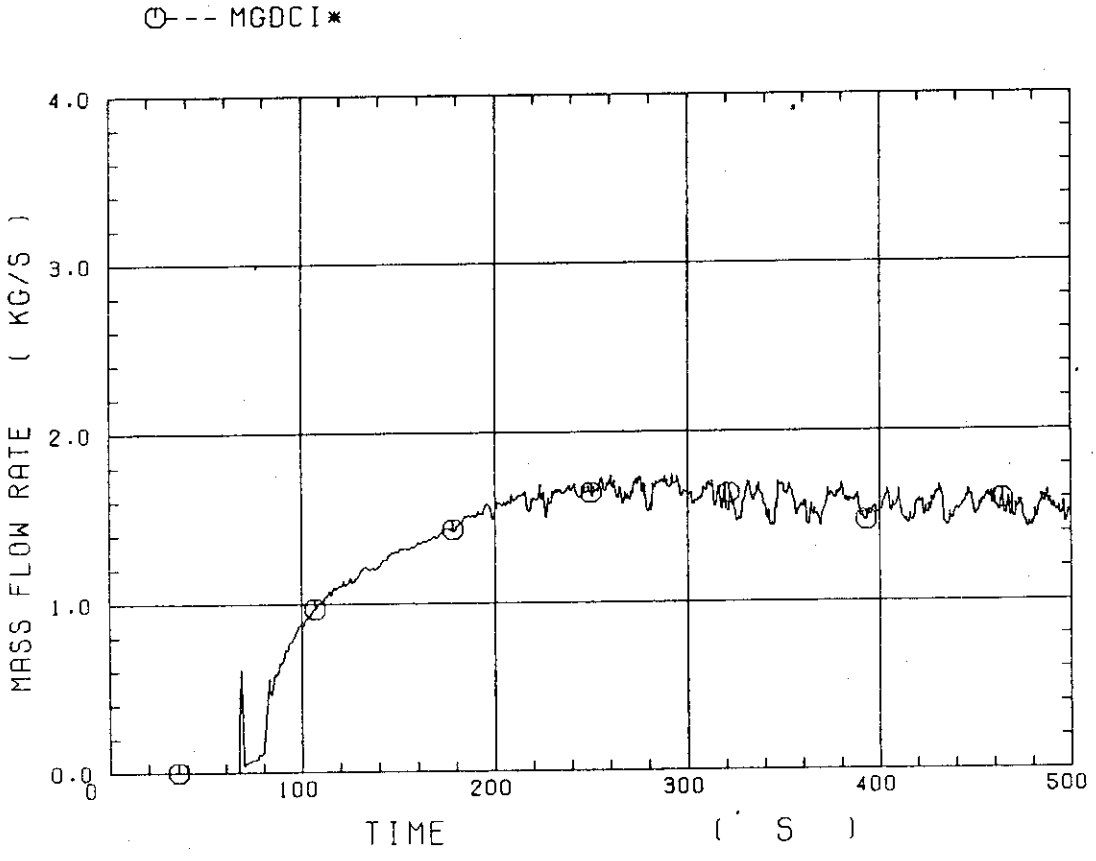

Fig. B-30 Total steam mass flow rate from intact loops to downcomer

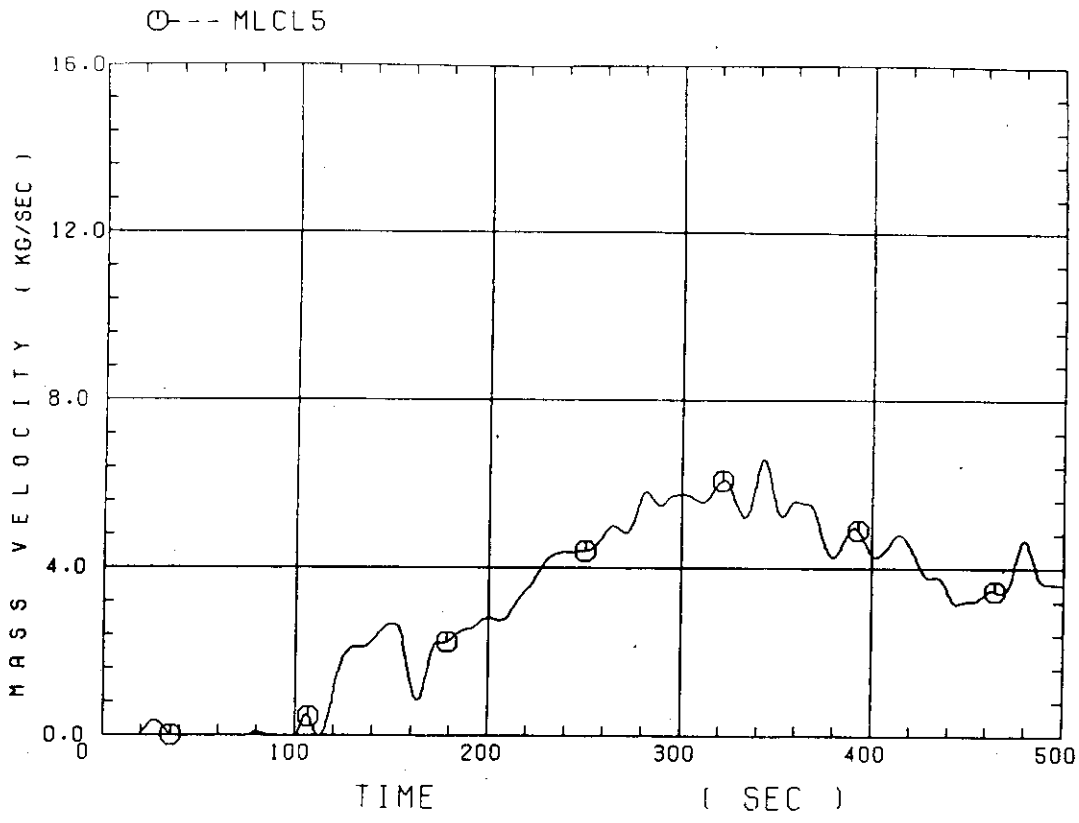

Fig. B-31 Water mass flow rate through broken cold leg nozzle

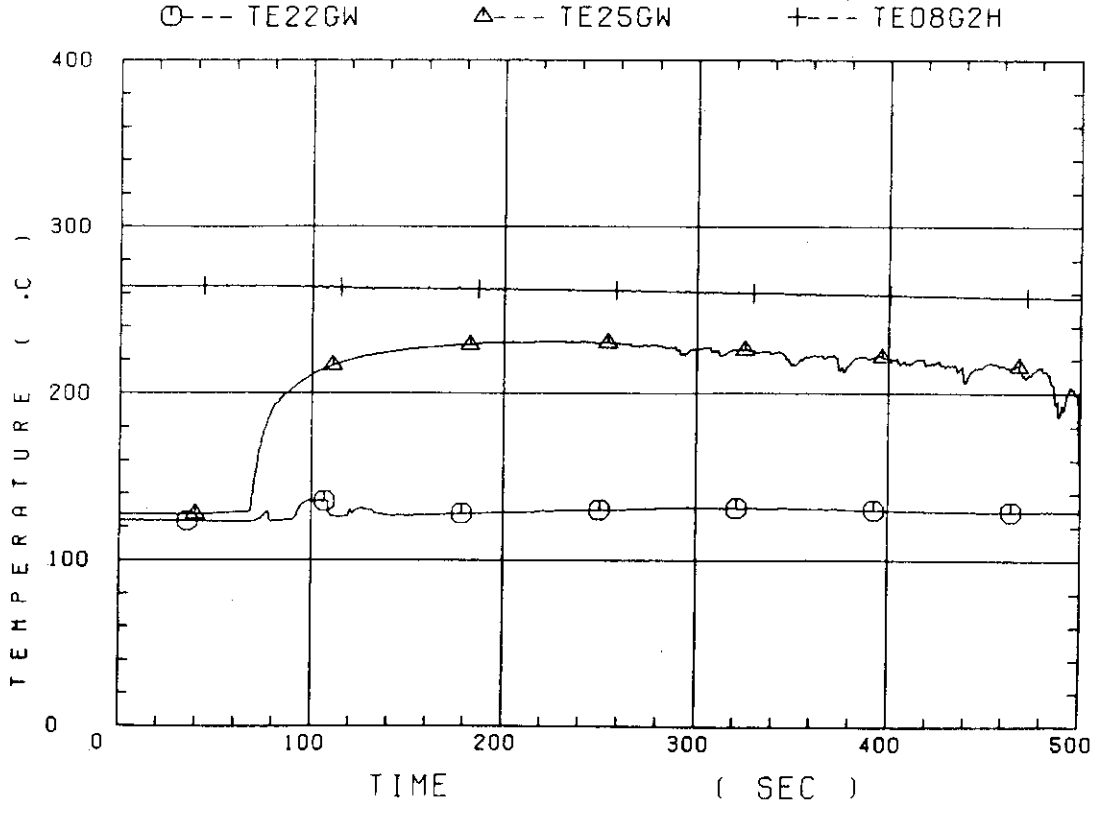

Fig. B-32 Fluid temperature in inlet plenum, outlet plenum, and secondary of steam generator 1

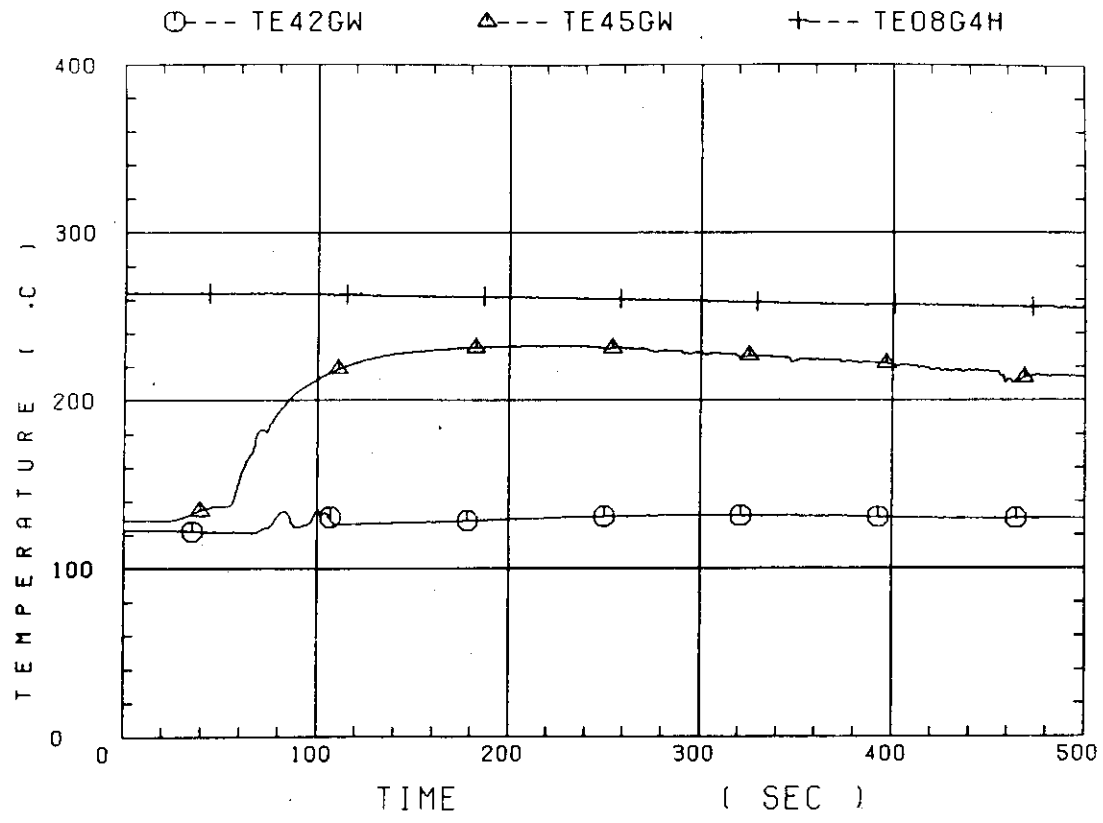

Fig. B-33 Fluid temperature in inlet plenum, outlet plenum, and secondary of steam generator 2

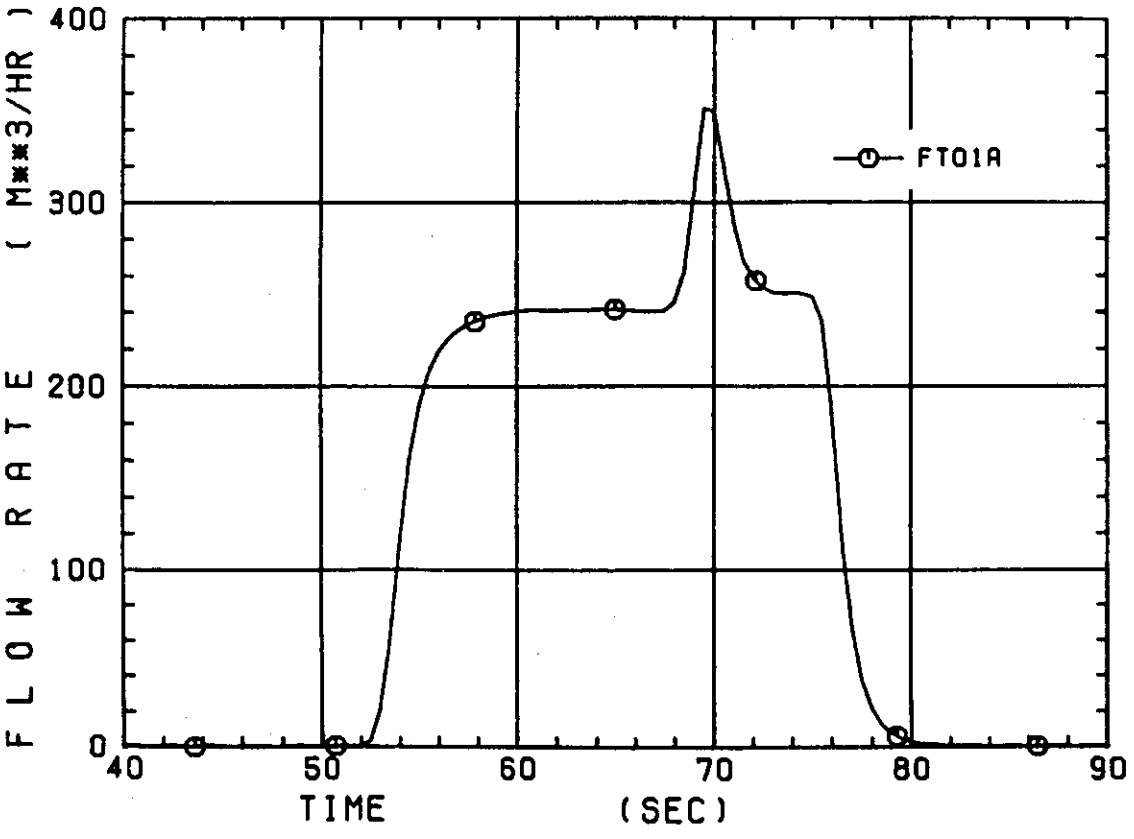

Fig. B-34 Total accumulator injection rate

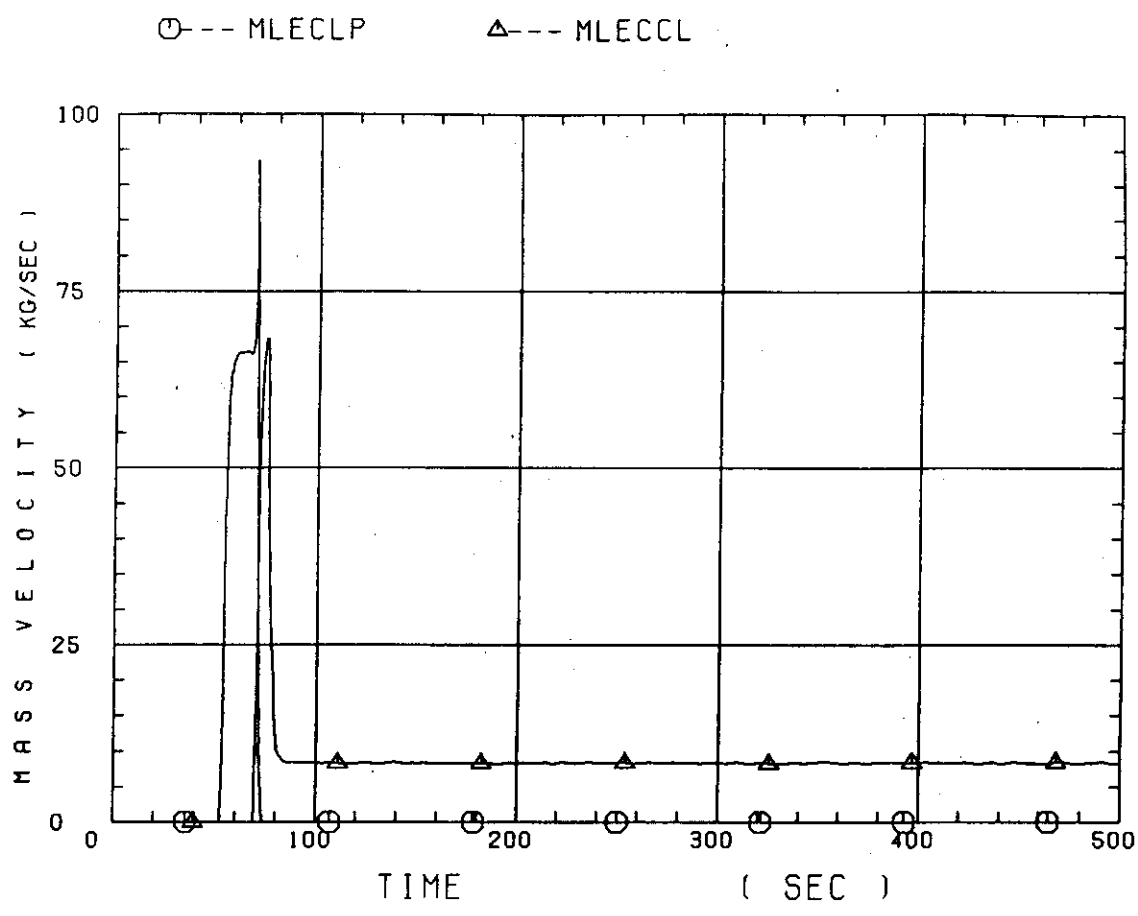

Fig. B-35 ECC water injection rates to lower plenum and to cold legs

Appendix C

Main results of the test C1-3

Table and Figure List

Table C-1 Summary of test conditions

1. TEST TYPE : TEST C1-3 (CCTF MAIN TEST NO.3)
2. TEST NUMBER : RUN 012 3. DATE : July 13, 1979
4. POWER : A: TOTAL: 9.35 MW; B:LINEAR: 1.4 KW/M
5. RELATIVE RADIAL POWER SHAPE :

   A: ZONE: A B C

   B: RATIO: 1.07 : 1.0 : 0.82
6. AXIAL POWER SHAPE : CHOPPED COSINE
7. PRESSURE (KG/CM^2A) :

   A: SYSTEM: 2.04, B: CONTAINMENT 2.05,

   C: STEAM GENERATOR SECONDARY: 50
8. TEMPERATURE (DEG.C) :

   A: DOWNCOMER WALLS 115, B: VESSEL INTERNALS 110

   C: PRIMARY PIPING WALLS 120, D: LOWER PLENUM LIQUID 106

   E: ECC LIQUID 38, F: STEAM GENERATOR SECONDARY 264

   G: CORE TEMPERATURE AT ECC INITIATION 502
9. ECC INJECTION TYPE: C

   A: COLD LEG, B: LOWER PLENUM, C: LOWER PLENUM + COLD LEG
10. PUMP K-FACTOR : ~15 (UNCERTAIN)
11. ECC FLOW RATES AND DURATION :

    A: ACCUMULATOR 252 M^3/HR FROM 0 TO 25 SECONDS

    B: LPCI 30.8 M^3/HR FROM 25 TO 809 SECONDS

    C: ECC INJECTION TO LOWER PLENUM : FROM 0 TO 15 SECONDS

    (VALVE OPENING AND CLOSING TIMES ARE INCLUDED IN THE INJECTION DURATION)
12. INITIAL WATER LEVEL IN LOWER PLENUM : 0.85 M.
13. POWER CONTROL : ANS x 1.2 + ACTINIDE (30 SEC AFTER SCRAM)
14. EXPECTED BOCREC TIME FROM ECC INITIATION 12 SEC
15. EXPECTED PEAK TEMPERATURE AT BOCREC 600 C

Table C-2 Chronology of events

Event	TIME (sec)
Test C1-3 initiated (Heater rods power on) (Data recording initiated)	0.0
Accumulator injection initiated	52
Power decay initiated (Beginning of core recovery)	65
Accumulator injection switched from lower plenum to cold leg	67
Accumulator injection ended and LPCI injection initiated	77
All heater rods quenched	571
Power off	648
LPCI injection ended	861
Test C1-3 ended (Data recording ended)	1073

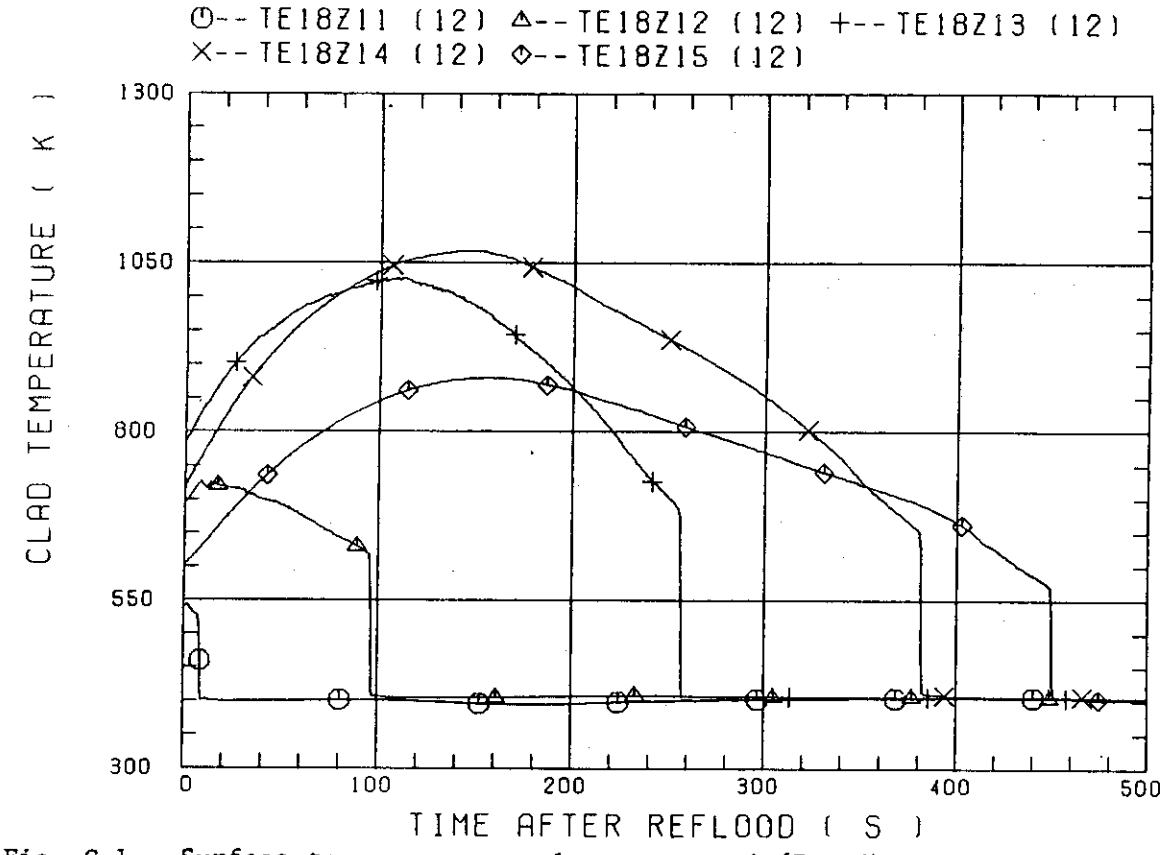

Fig. C-1 Surface temperature on low power rod (Z-rod) in medium power region (B region) (average power rod)

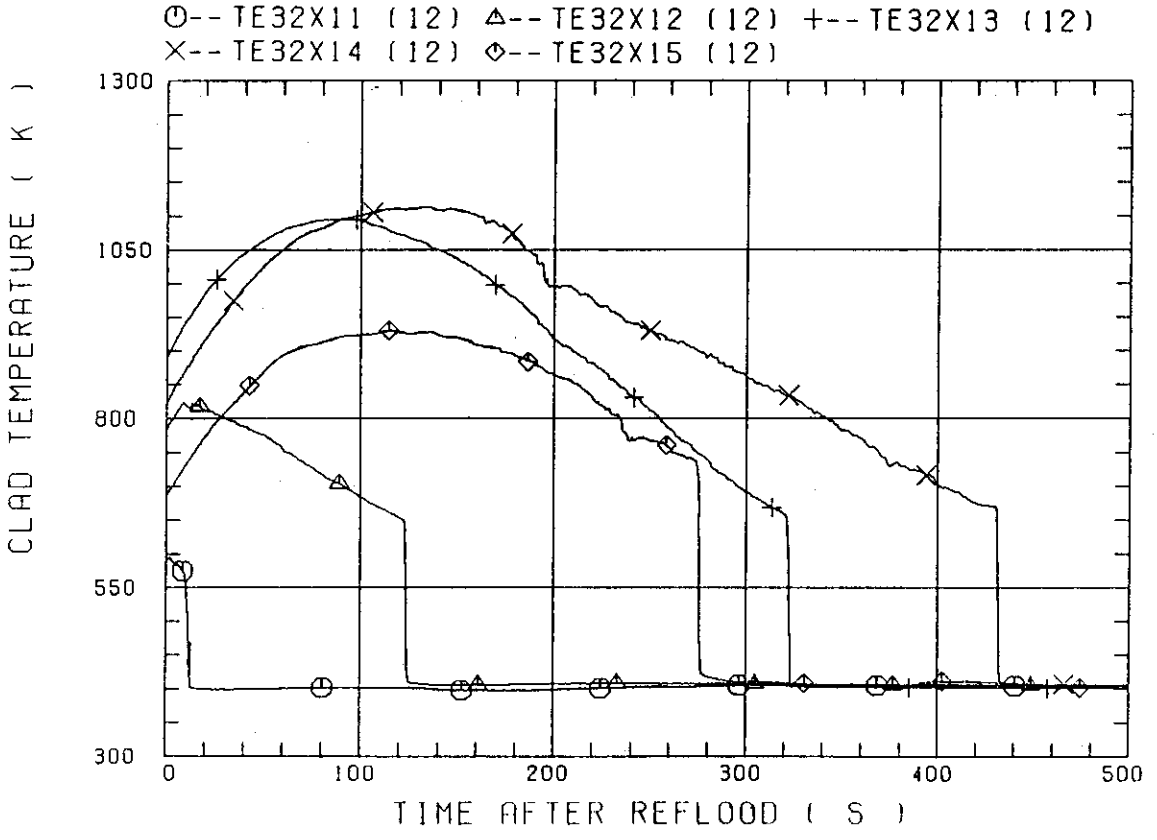

Fig. C-2 Surface temperature on high power rod (X-rod) in high power region (A region) (peak power rod)

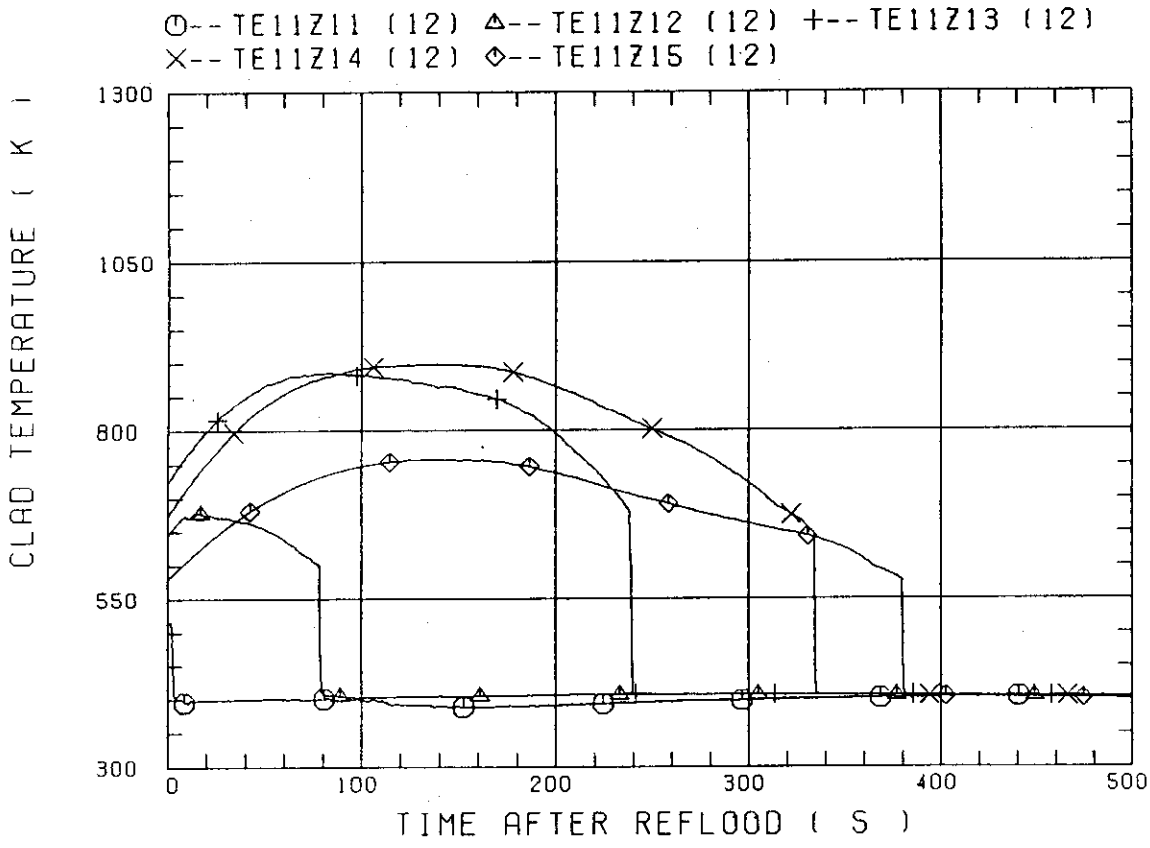

Fig. C-3 **Surface temperature on low power rod (Z-rod) in low power region (C region) (lowest power rod)**

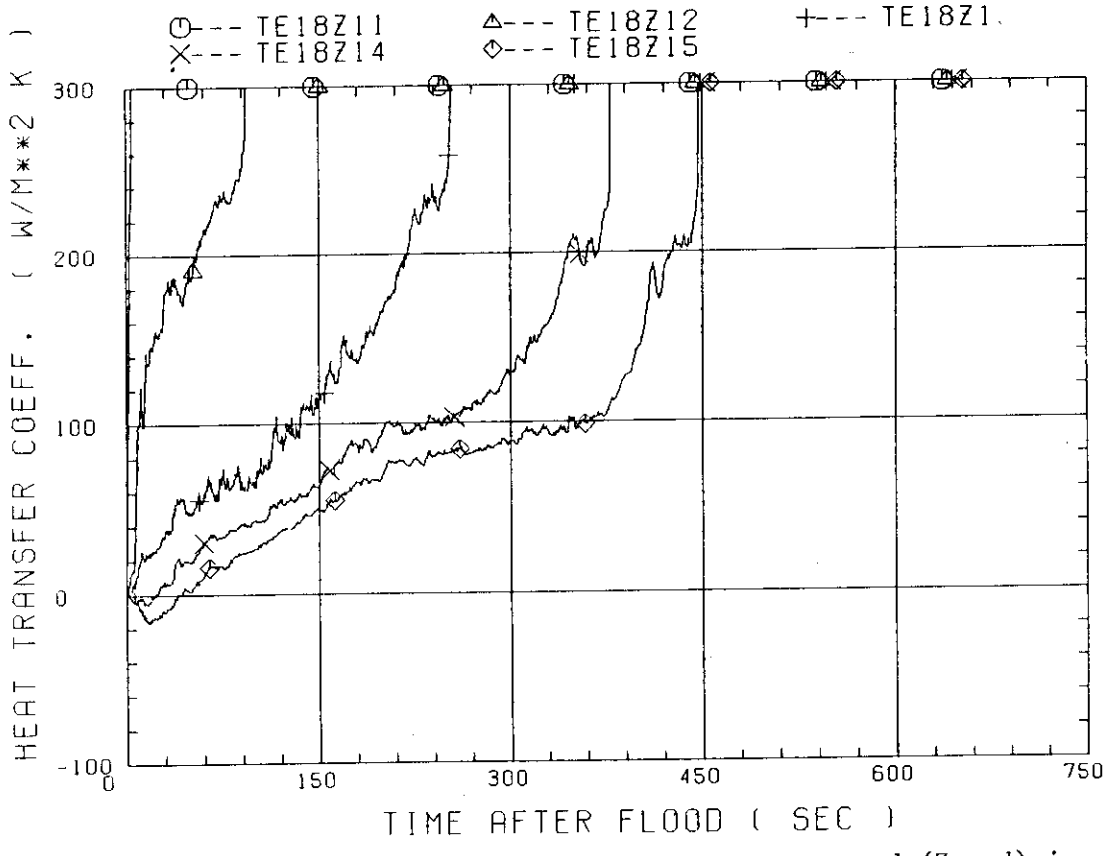

Fig. C-4 Heat transfer coefficient along a low power rod (Z-rod) in medium power region (B region) (average power rod)

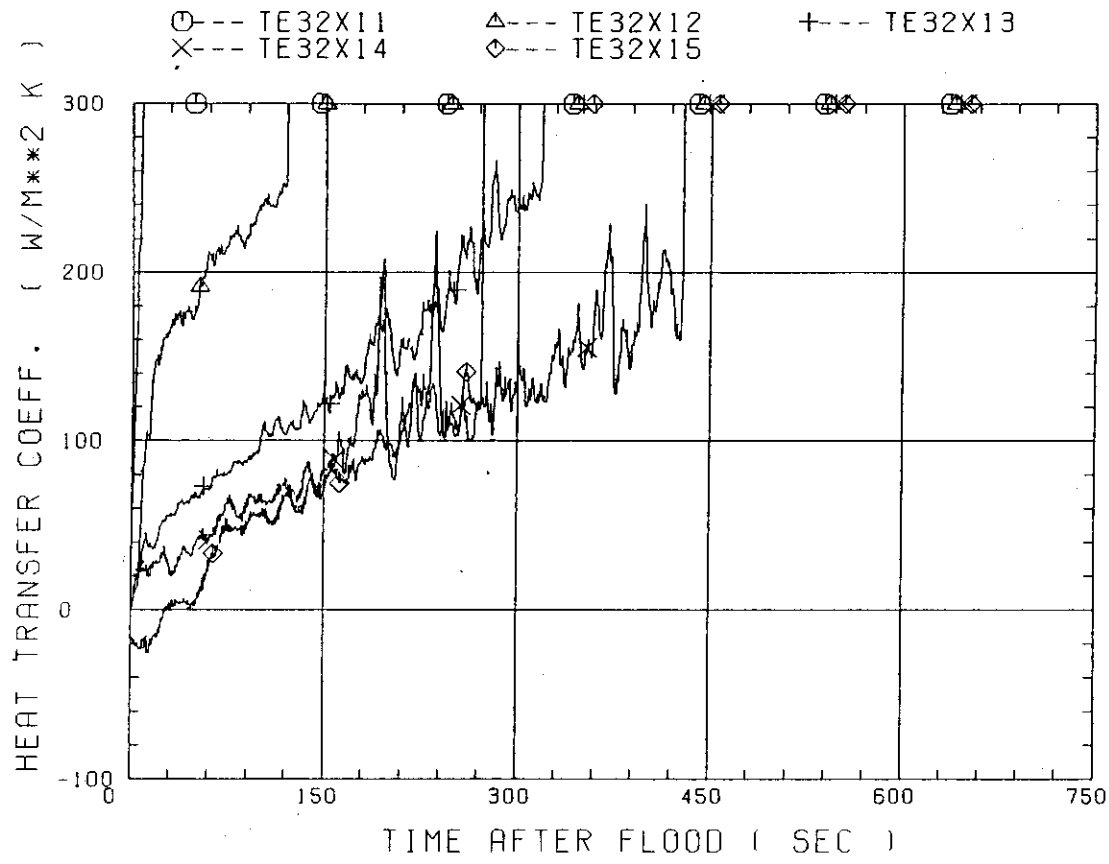

Fig. C-5 Heat transfer coefficient along a high power rod (X-rod) in high power region (A region) (peak power rod)

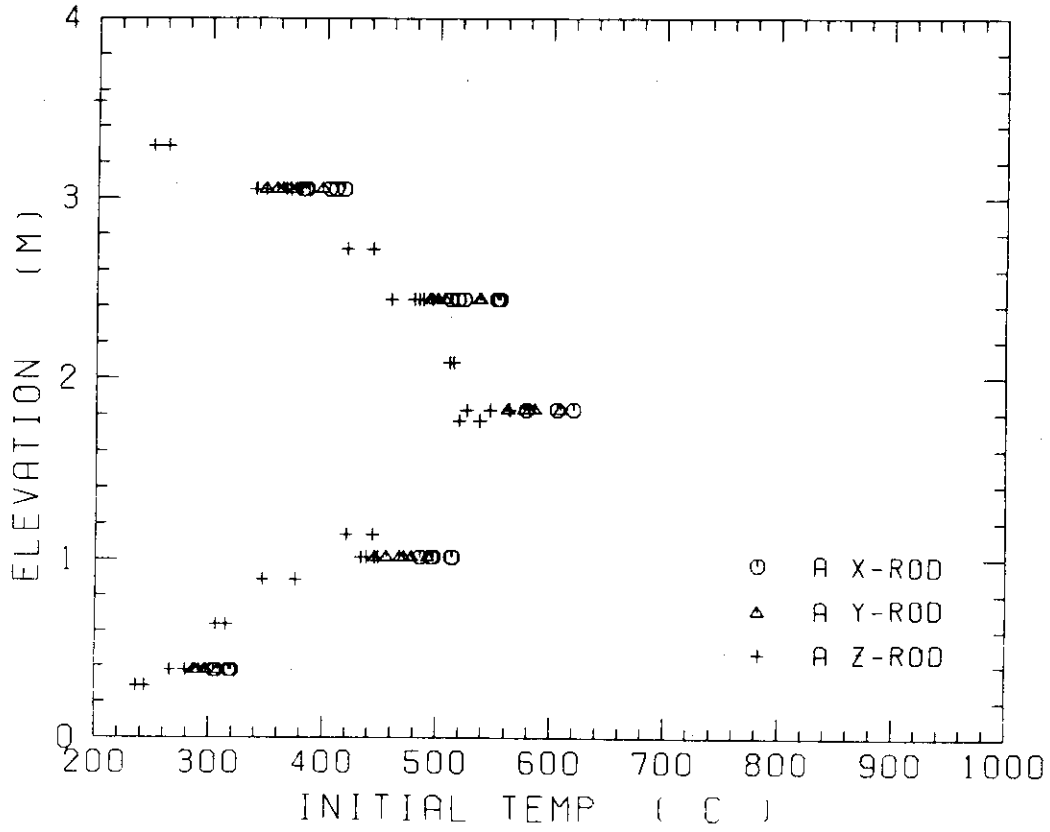

Fig. C-6 Initial rod surface temperature in high power region (A region)

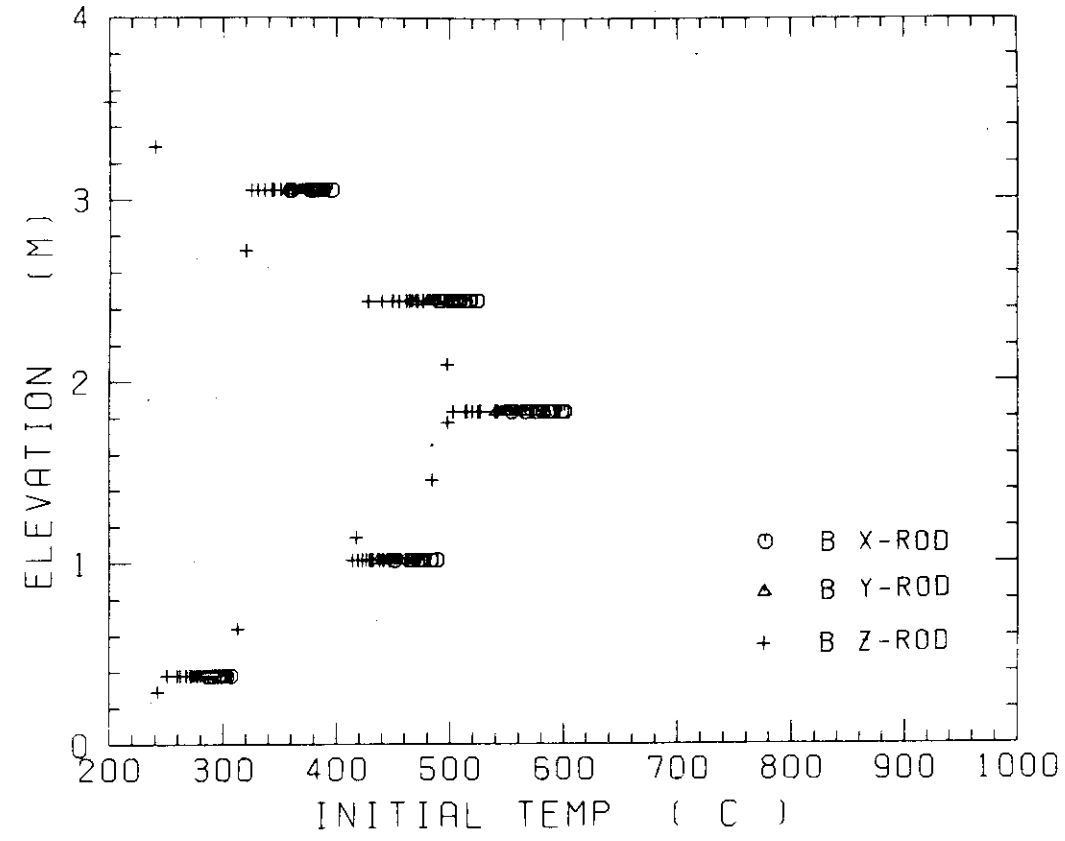

Fig. C-7 Initial rod surface temperature in medium power region (B region)

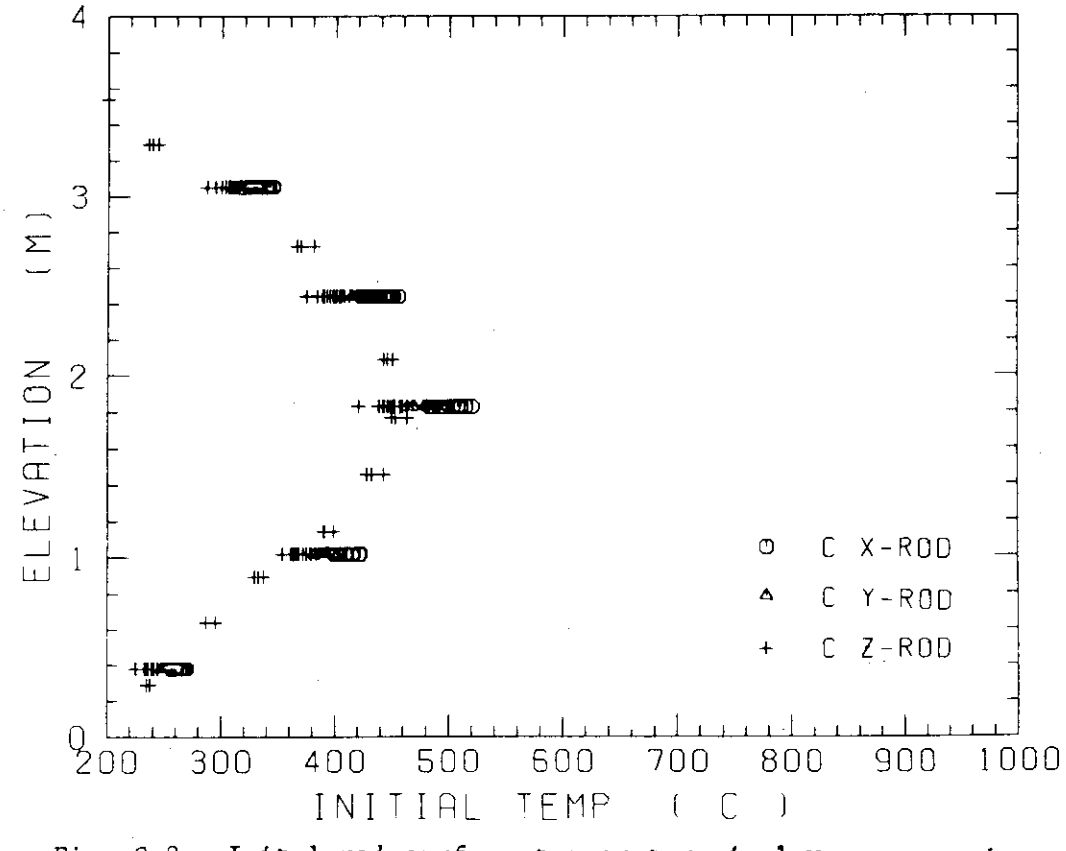

Fig. C-8 Inital rod surface temperature in low power region (C region)

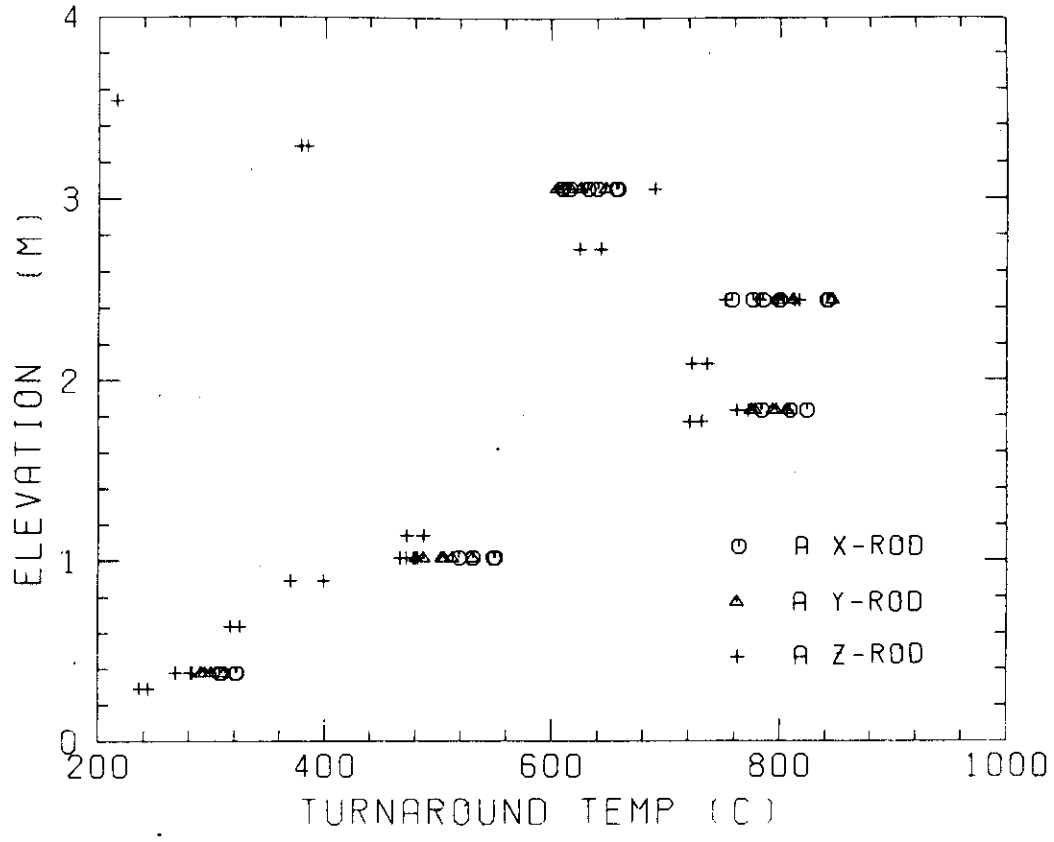

Fig. C-9 Turnaround temperature in high power region (A region)

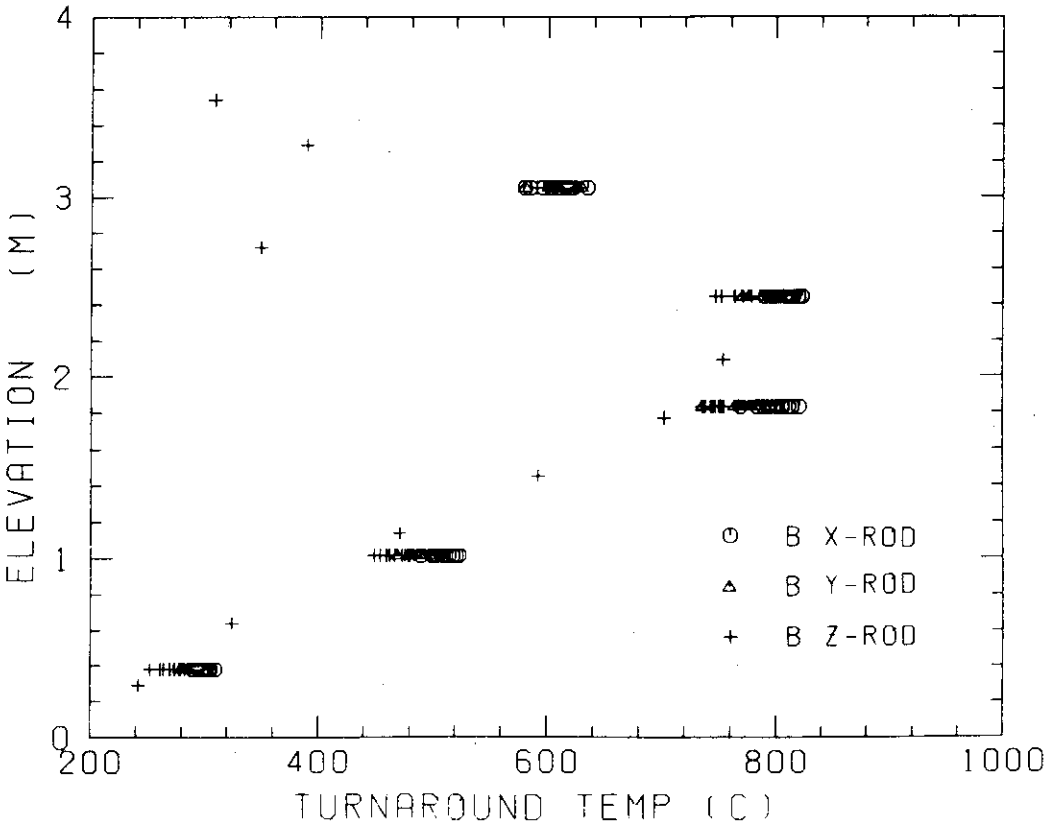

Fig. C-10 Turnaround temperature in medium power region (B region)

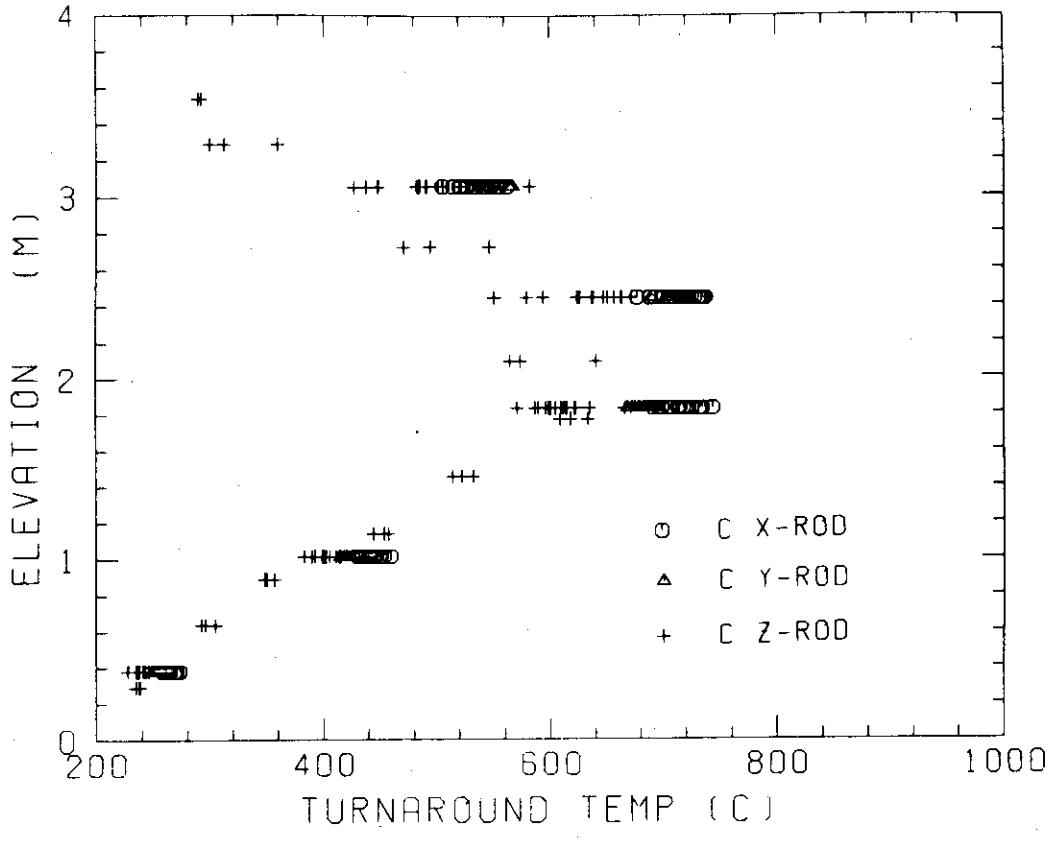

Fig. C-11 Turnaround temperature in low power region (C region)

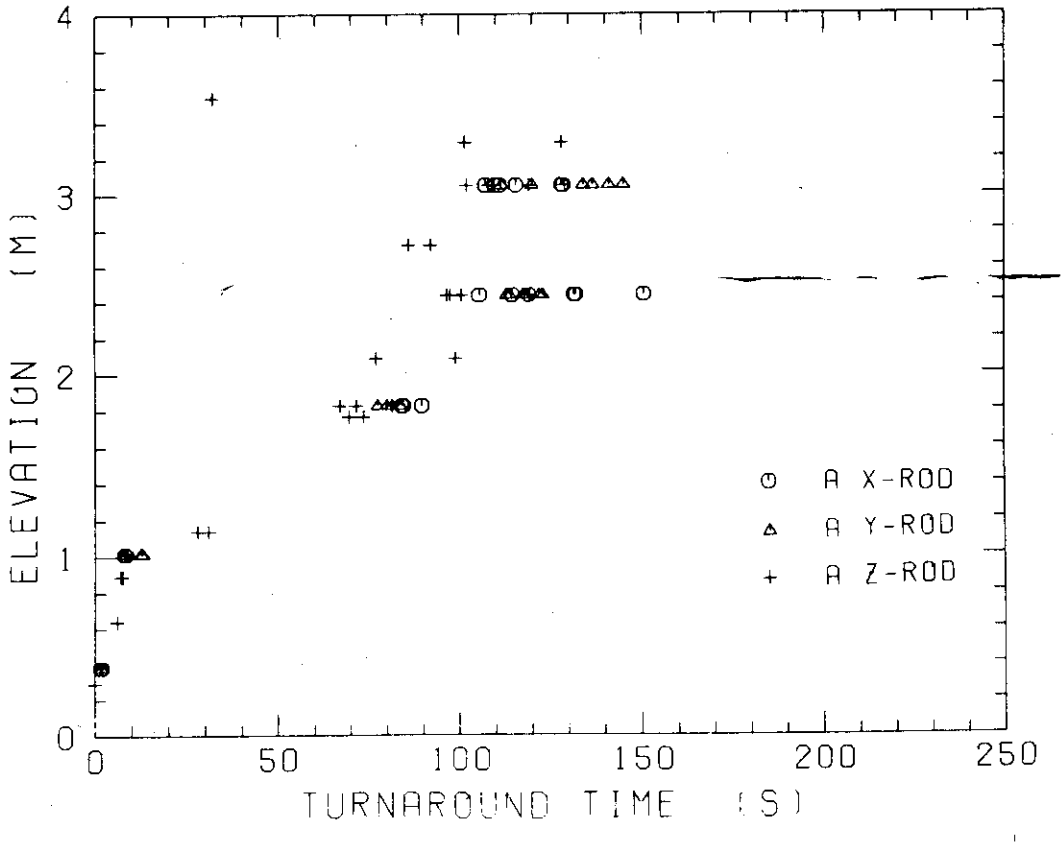

Fig. C-12 Turnaround time in high power region (A region)

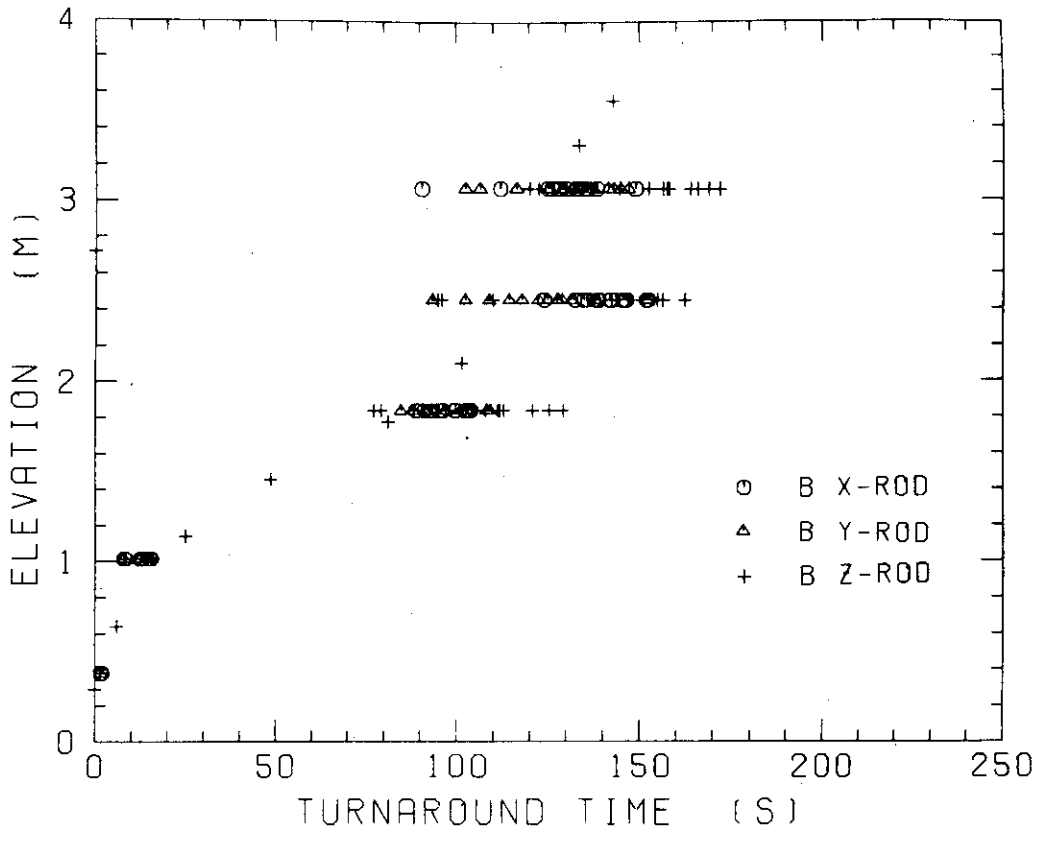

Fig. C-13 Turnaround time in medium power region (B region)

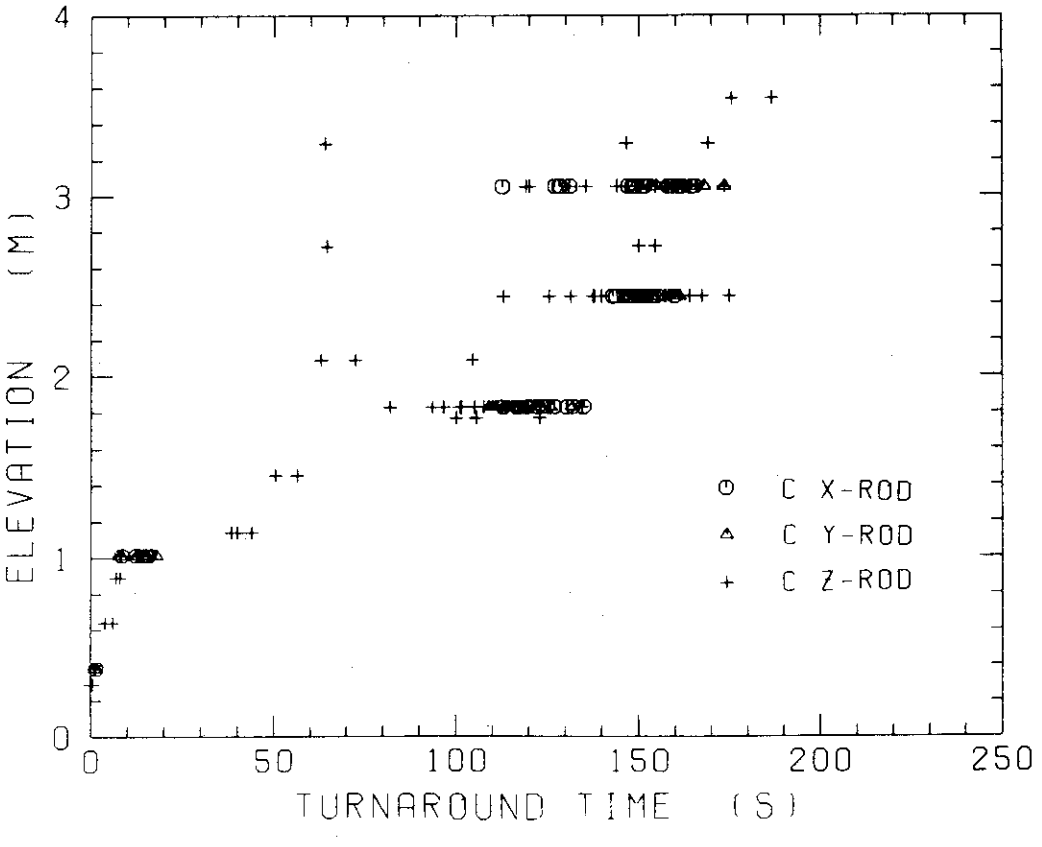

Fig. C-14 Turnaround time in low power region (C region)

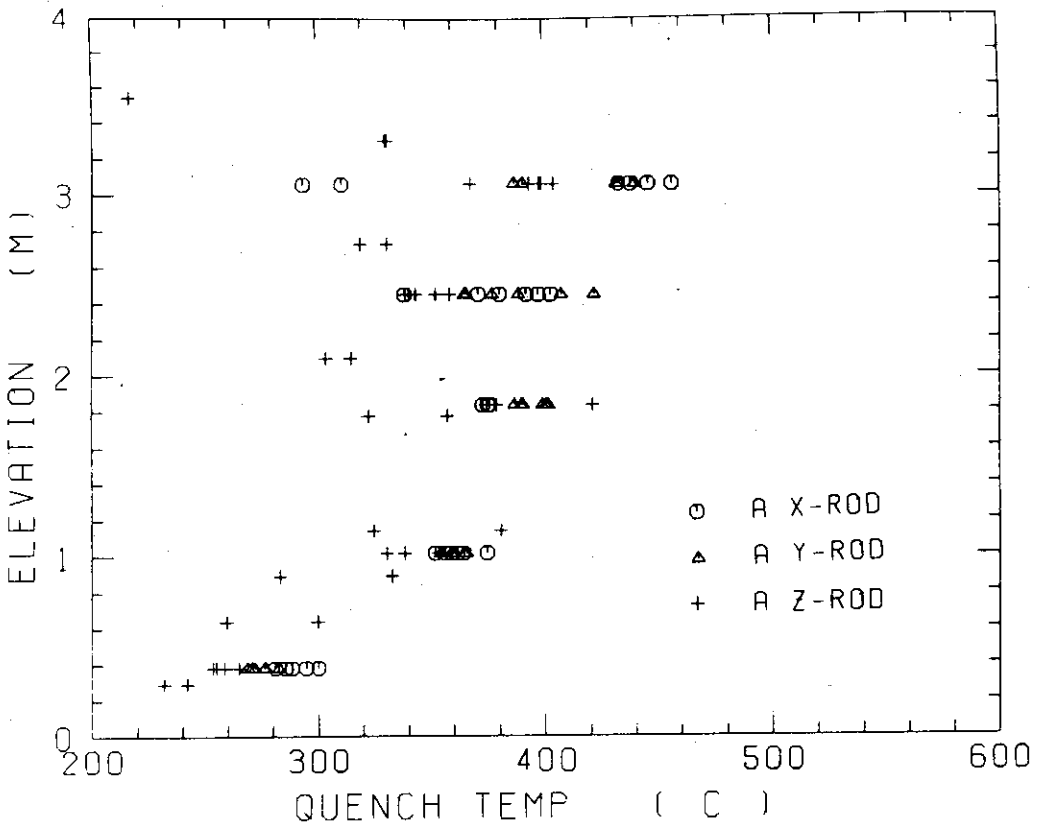

Fig. C-15 Quench temperature in high power region (A region)

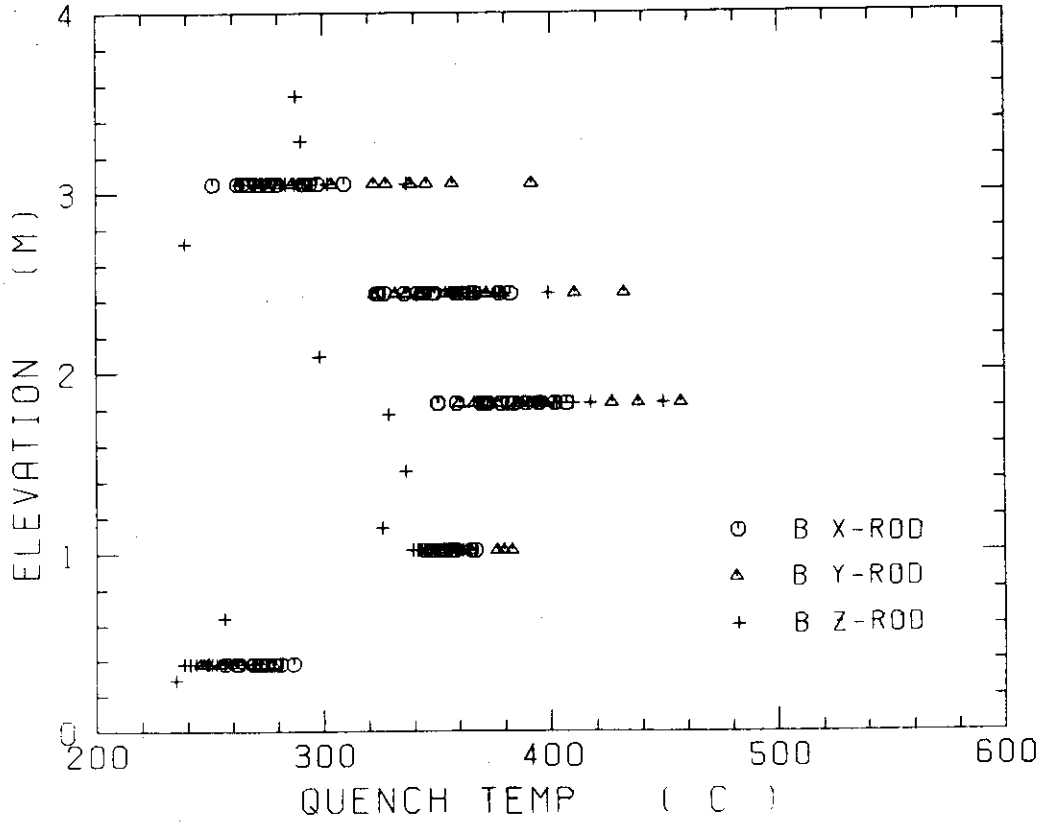

Fig. C-16 Quench temperature in medium power region (B region)

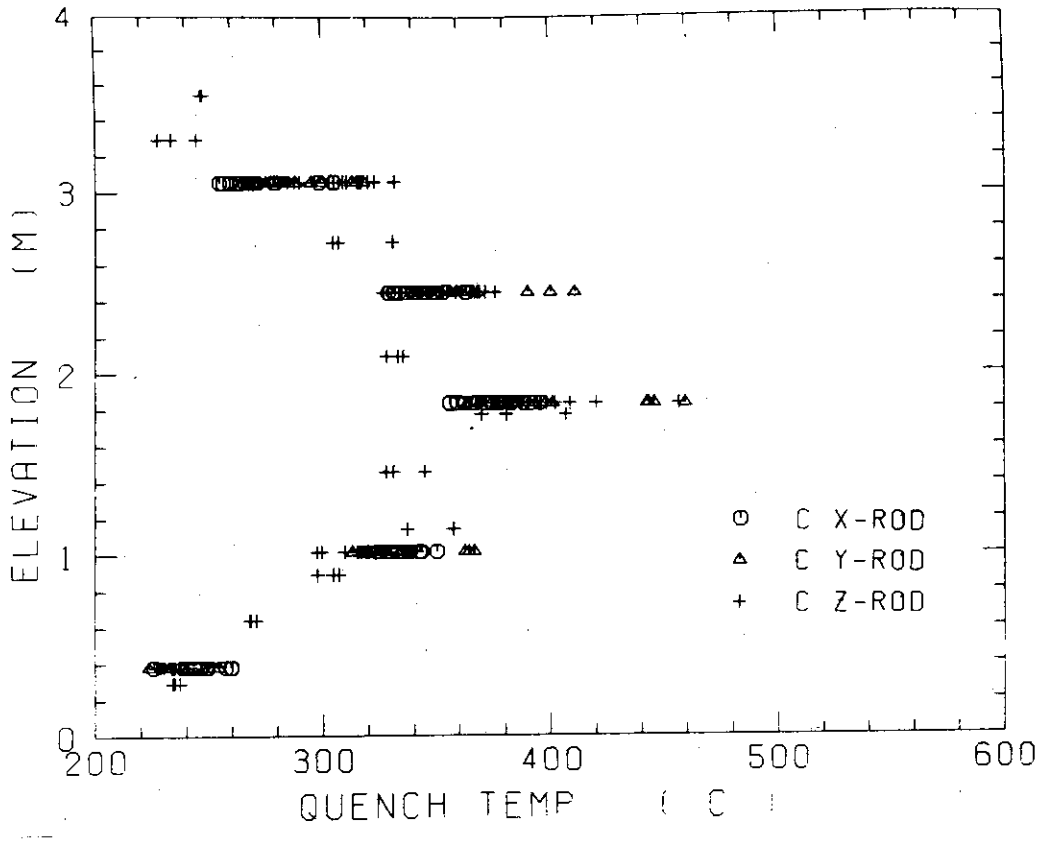

Fig. C-17 Quench temperature in low power region (C region)

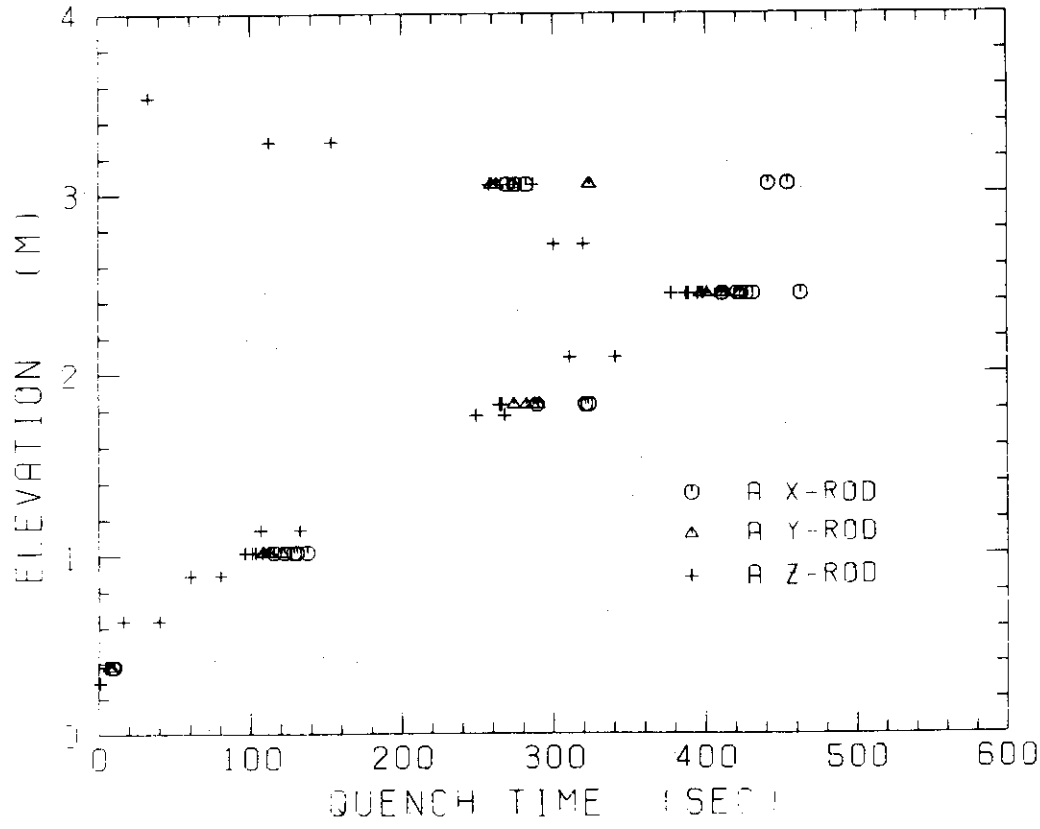

Fig. C-18 Quench time in high power region (A region)

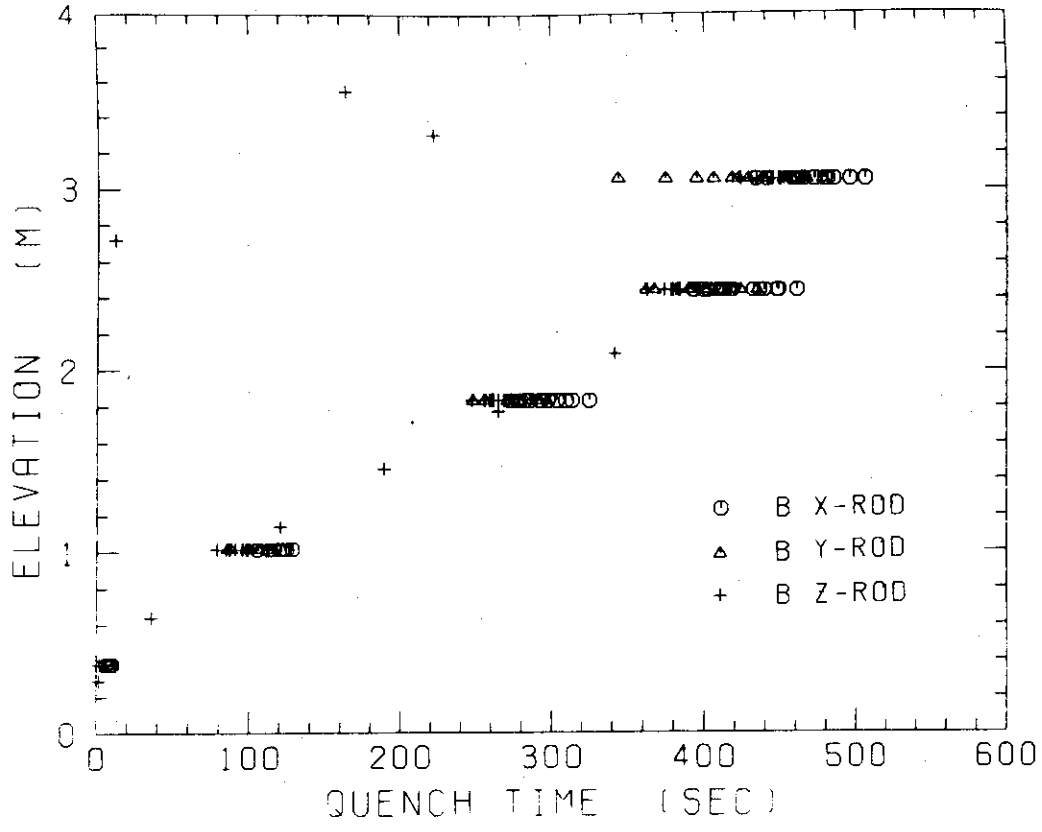

Fig. C-19 Quench time in medium power region (B region)

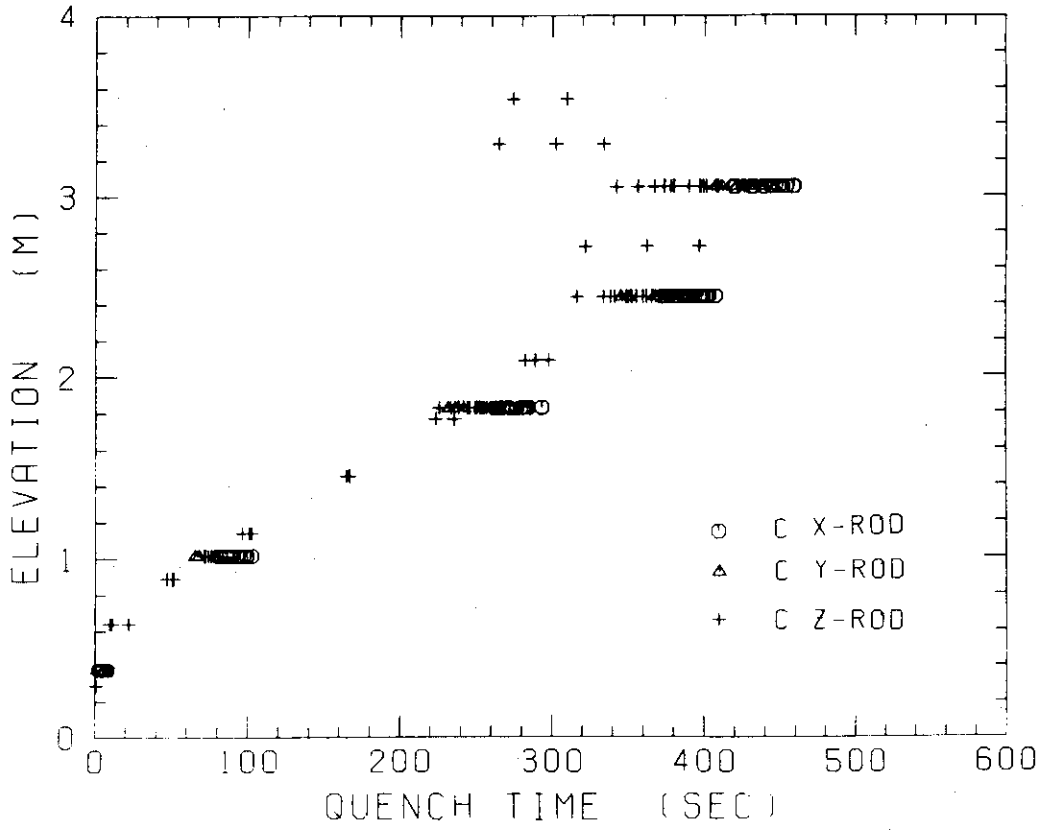

Fig. C-20 Quench time in low power region (C region)

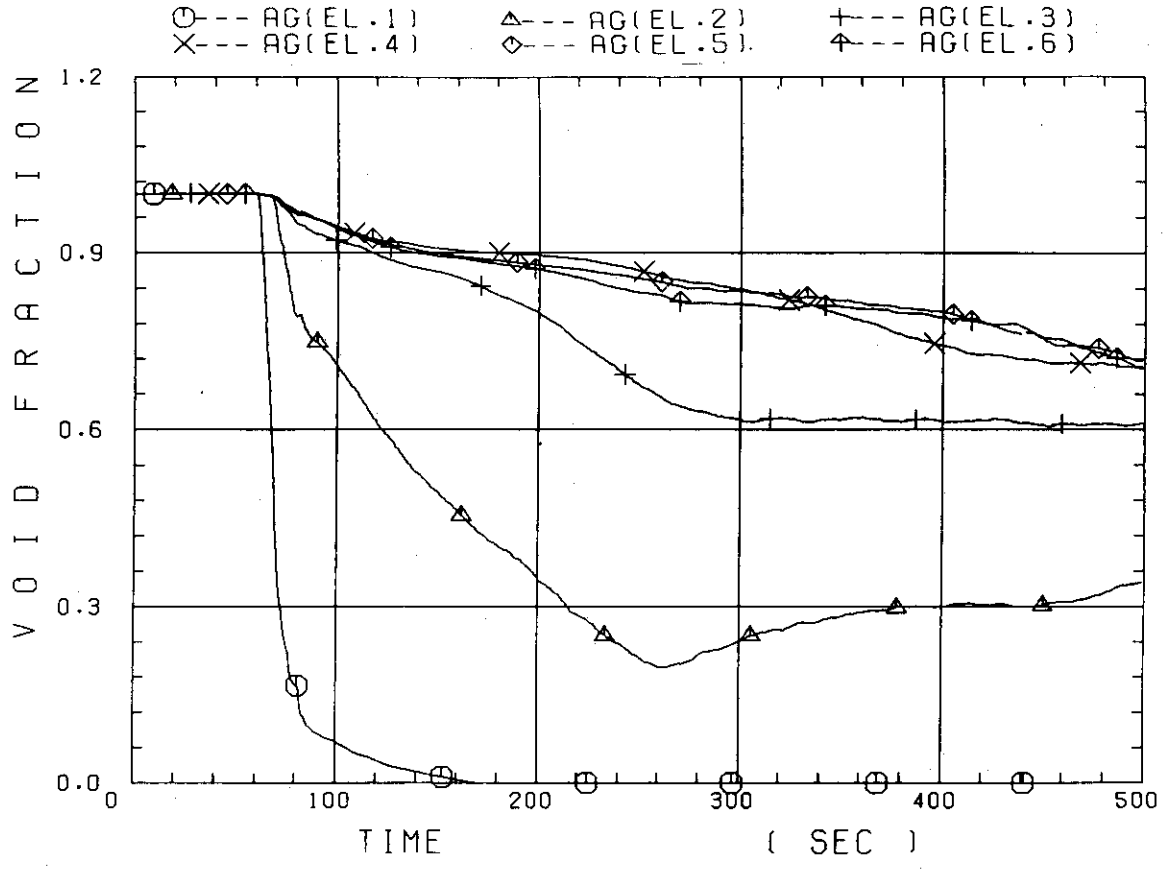

Fig. C-21 Void fraction in core

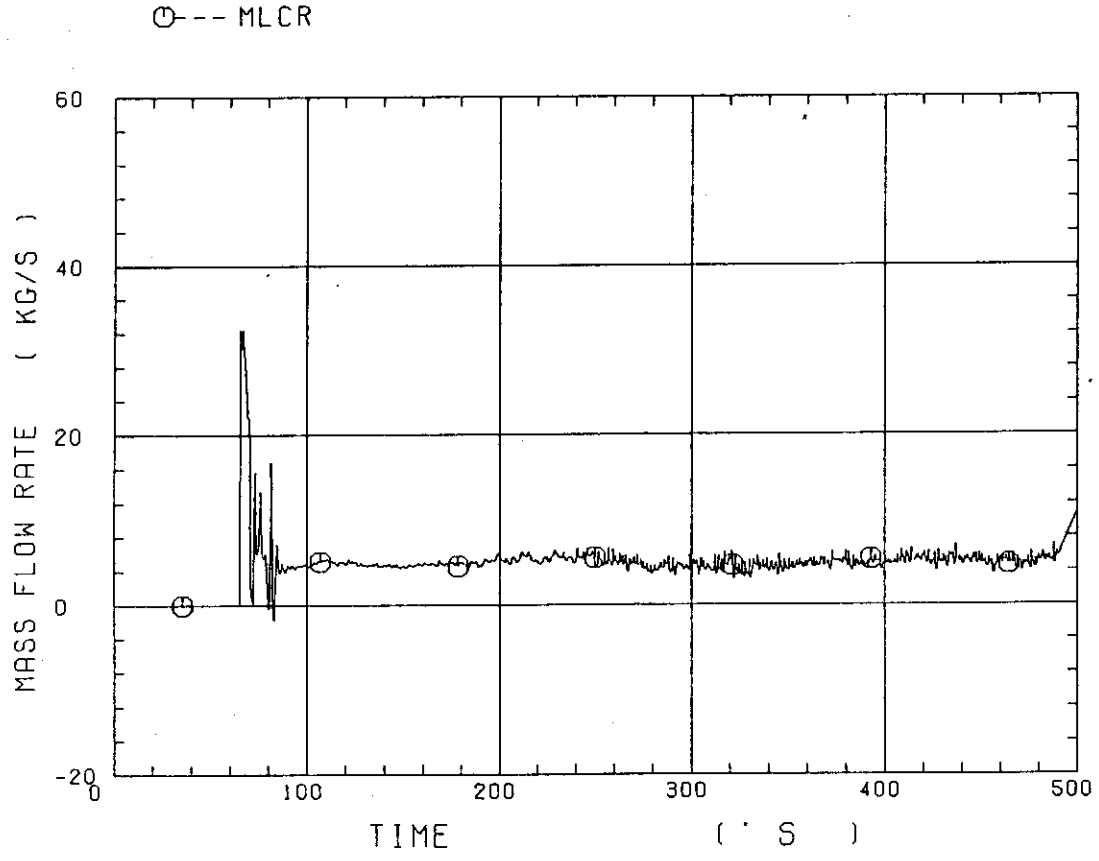

Fig. C-22 Core inlet mass flow rate

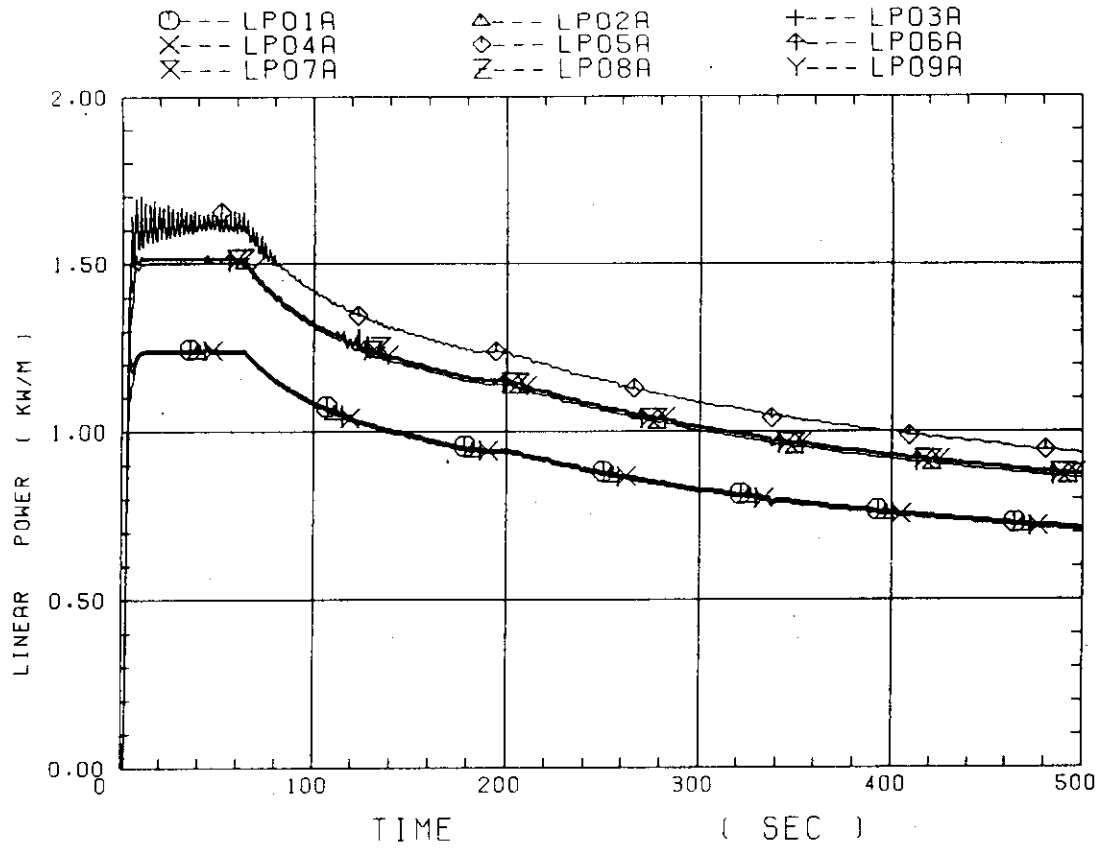

Fig. C-23 Average linear power of heater rod in each power unit zone

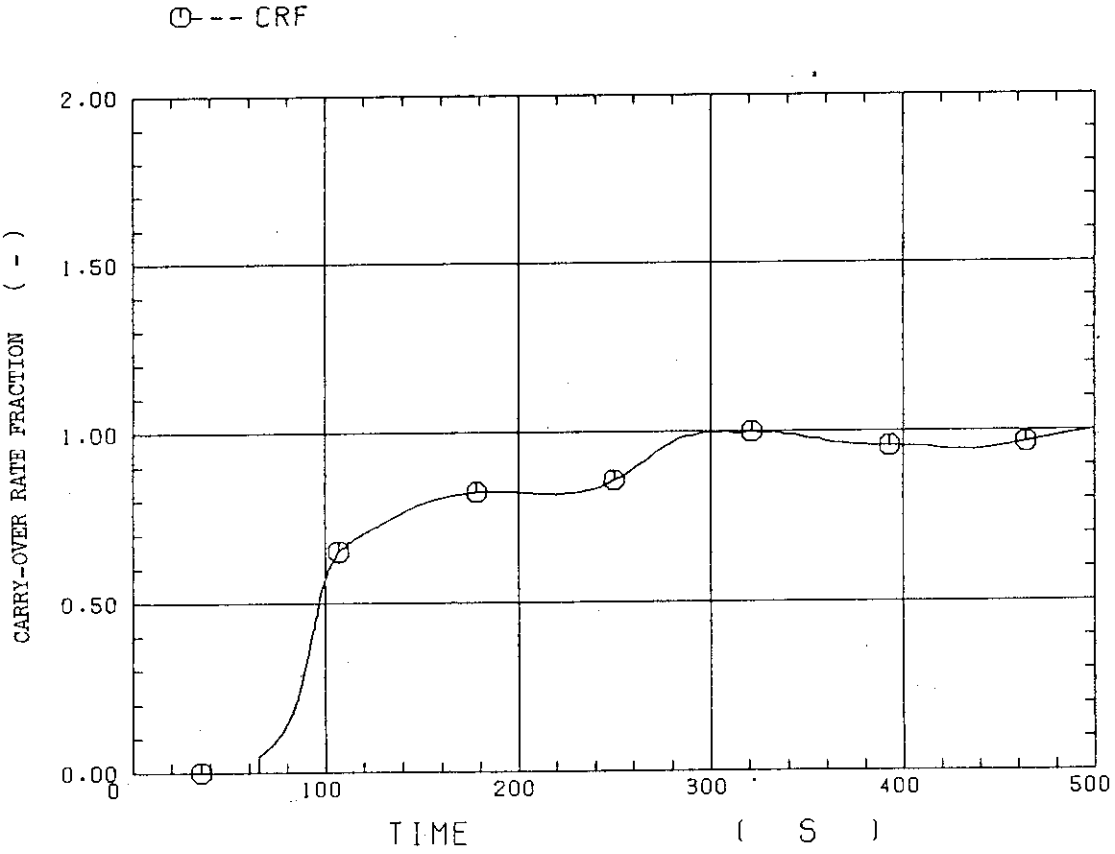

Fig. C-24 Carry-over rate fraction

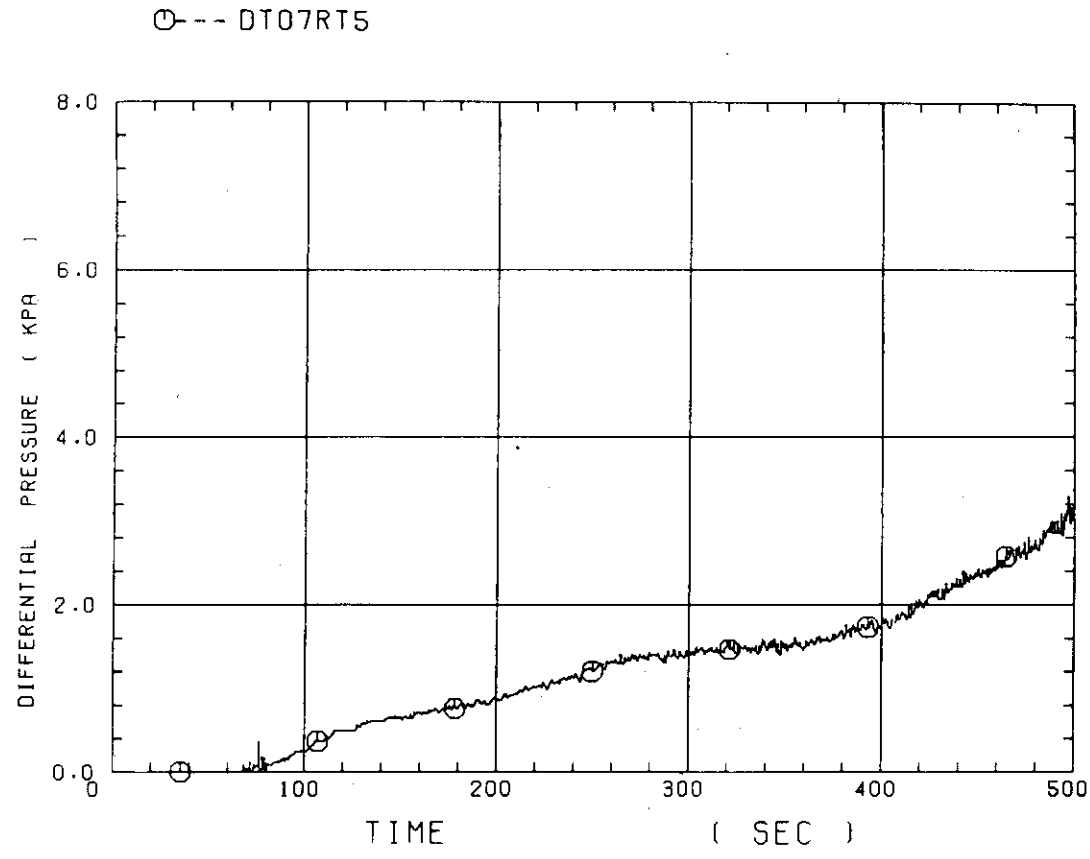

Fig. C-25 Differential pressure through upper plenum

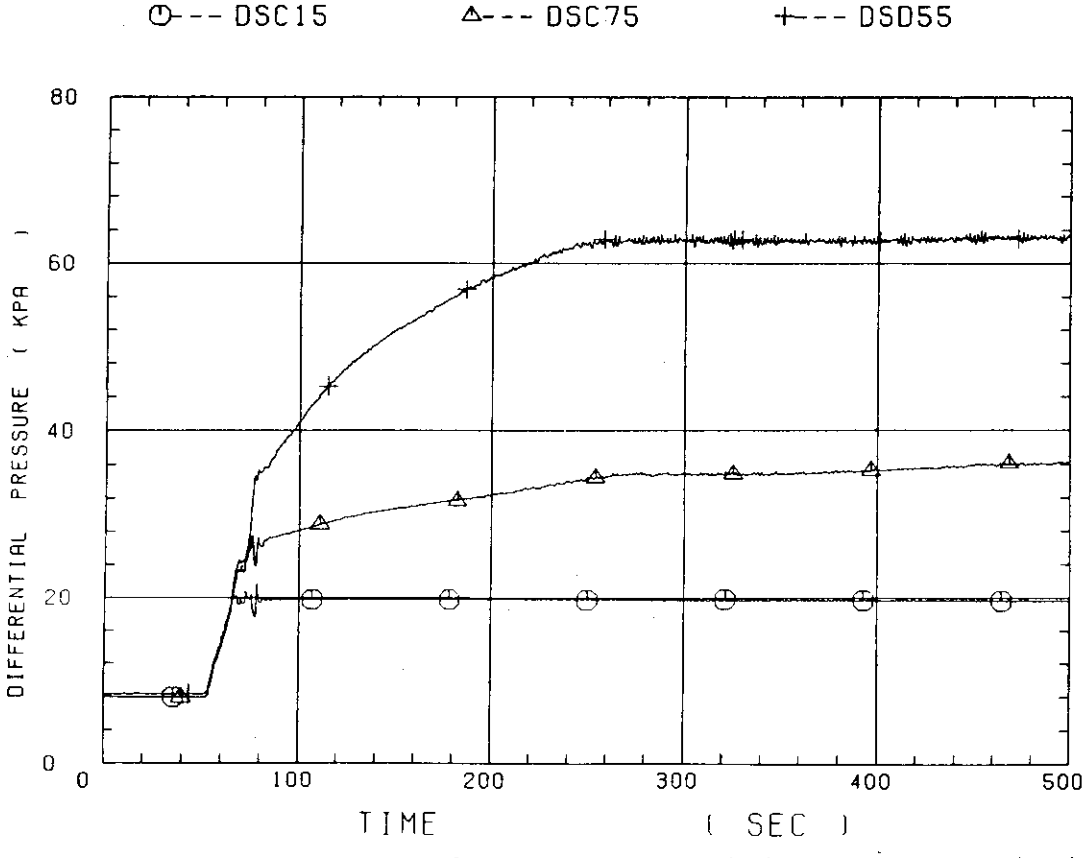

Fig. C-26 Differential pressure through downcomer, core, and lower plenum

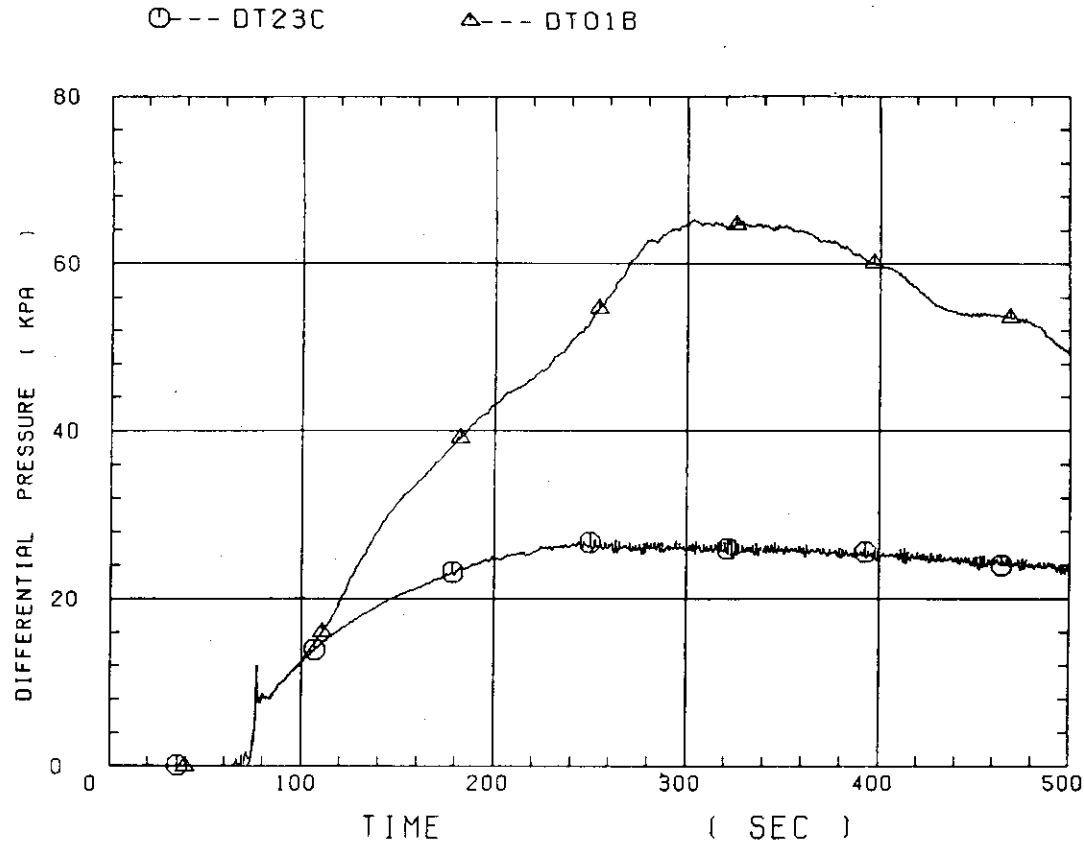

Fig. C-27 Differential pressure through intact and broken loops

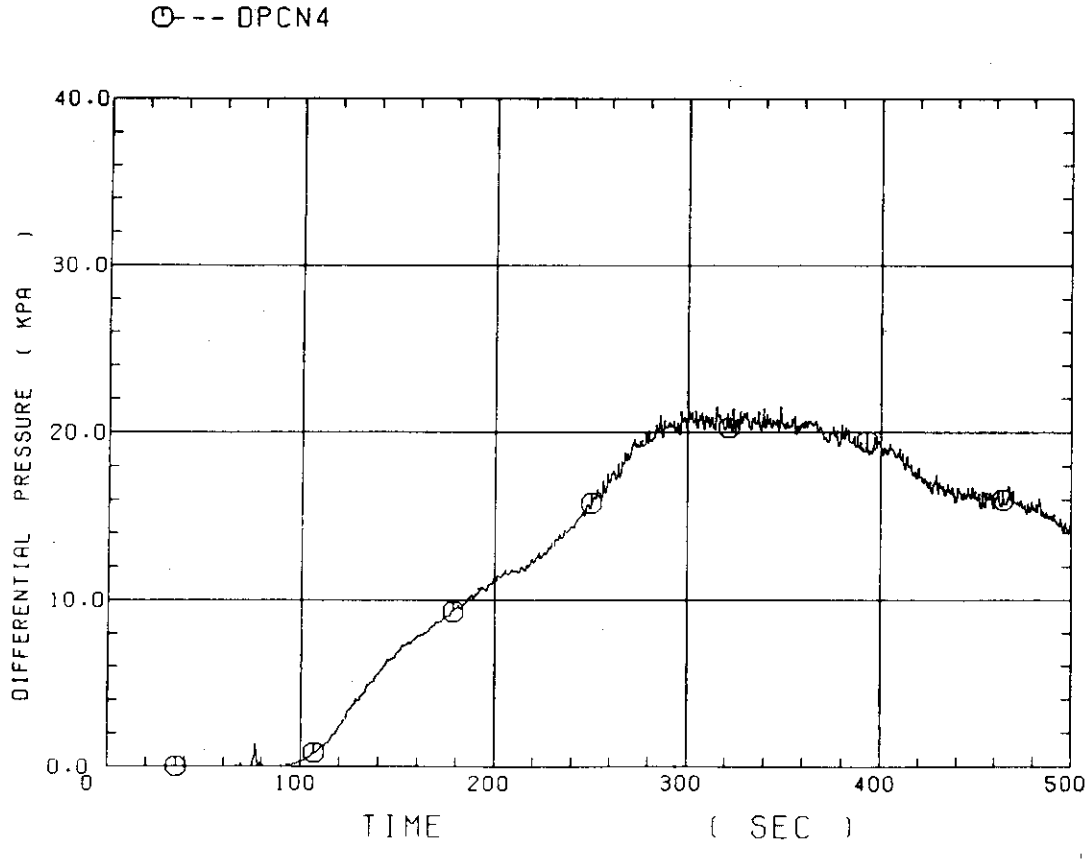

Fig. C-28 Differential pressure through broken cold leg nozzle

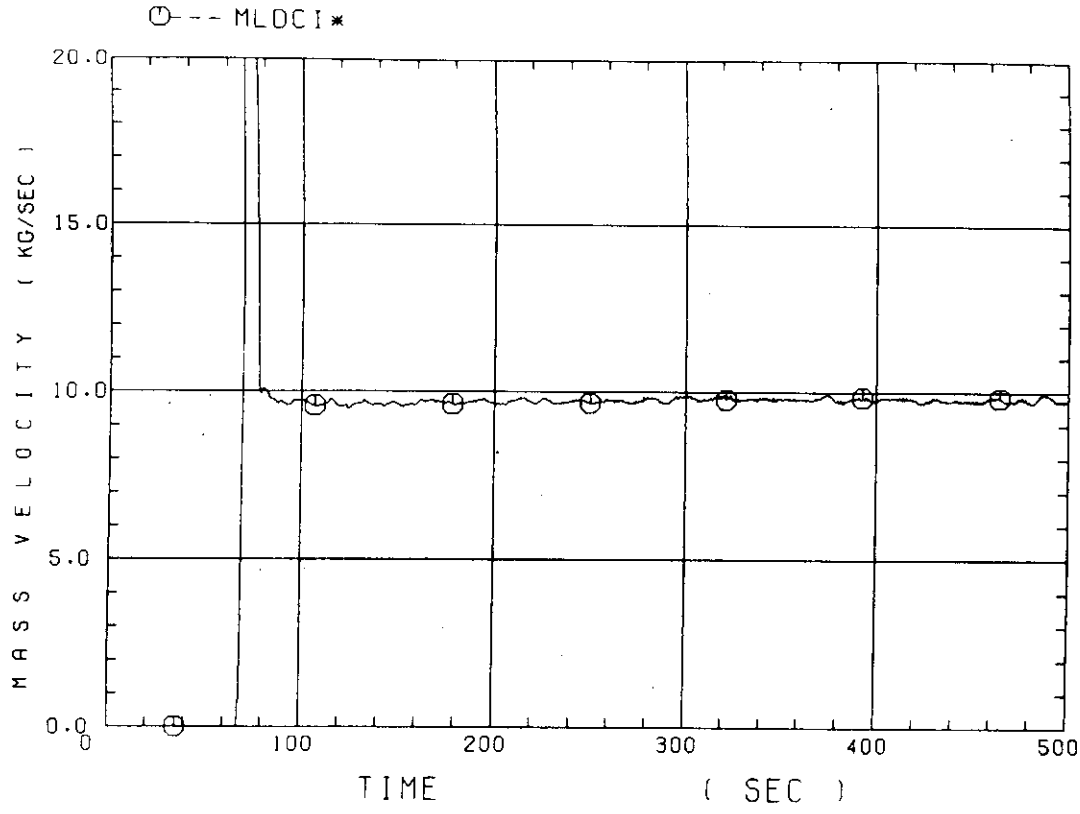

Fig. C-29 Total water mass flow rate from intact loops to downcomer

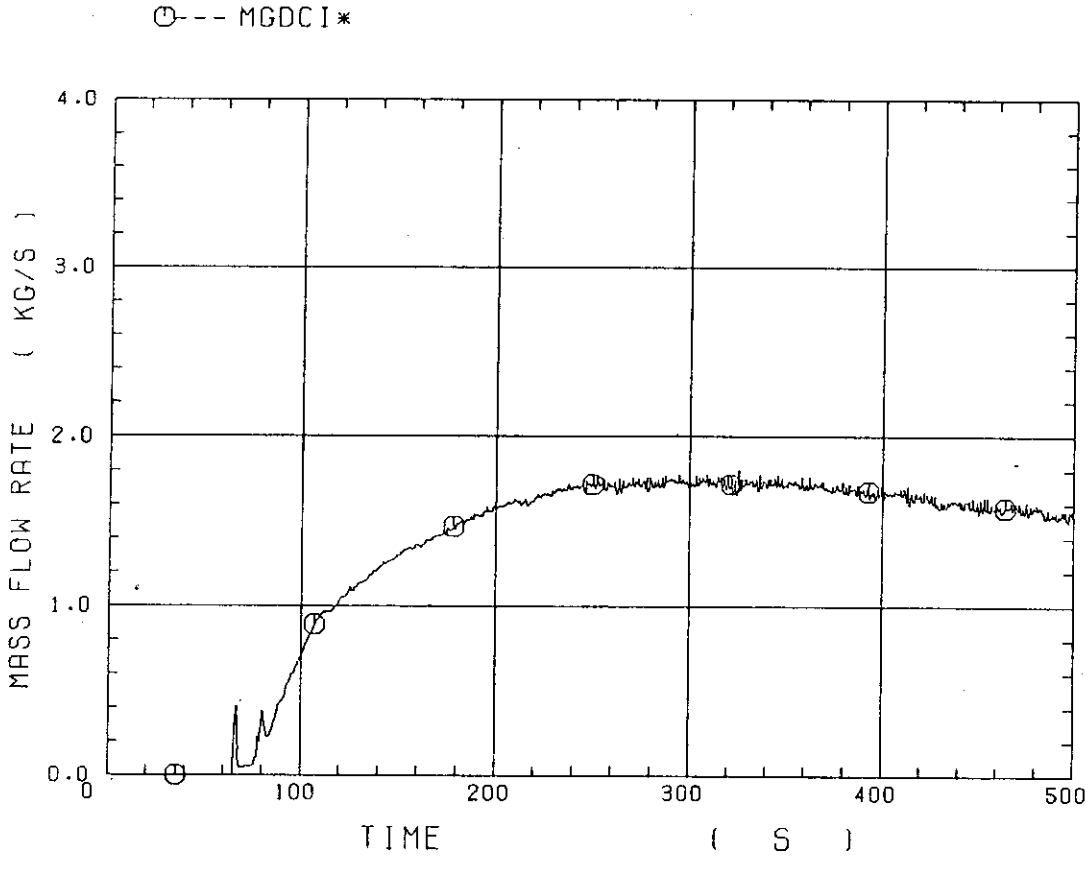

Fig. C-30 Total steam mass flow rate from intact loops to downcomer

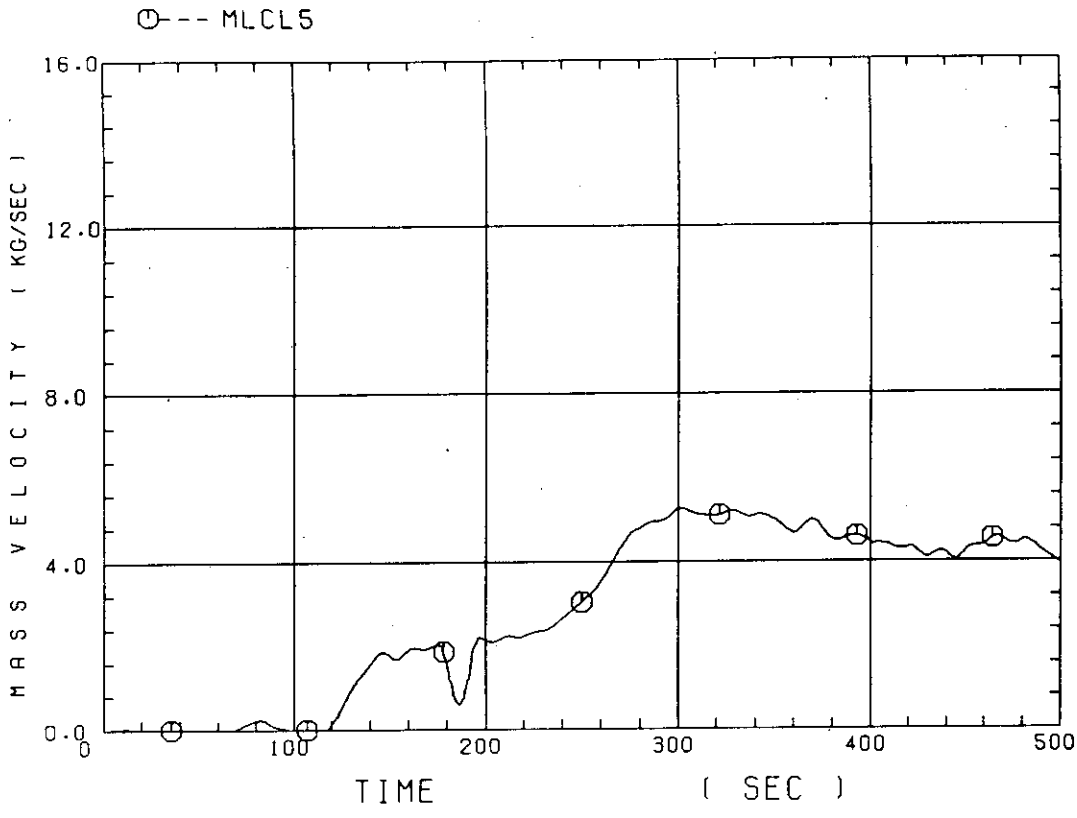

Fig. C-31 Water mass flow rate through broken cold leg nozzle

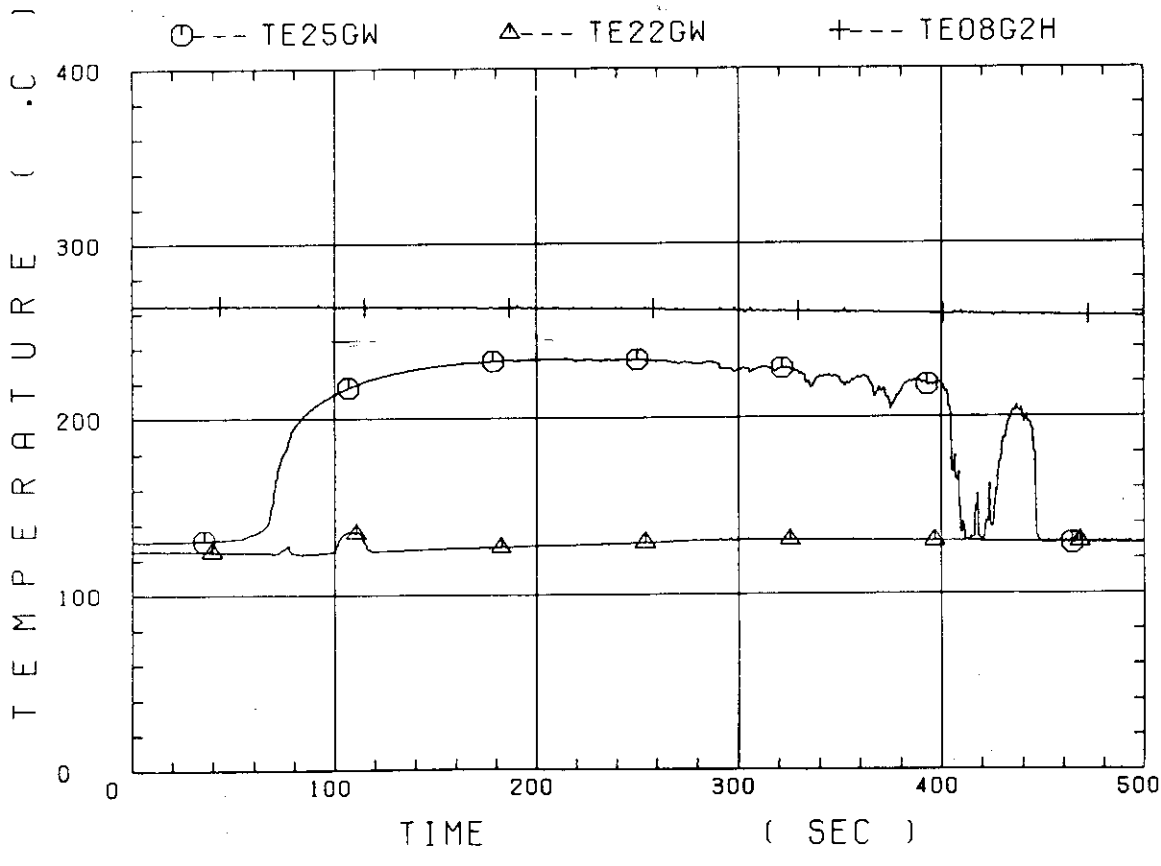

Fig. C-32 Fluid temperature in inlet plenum, outlet plenum, and secondary of steam generator 1

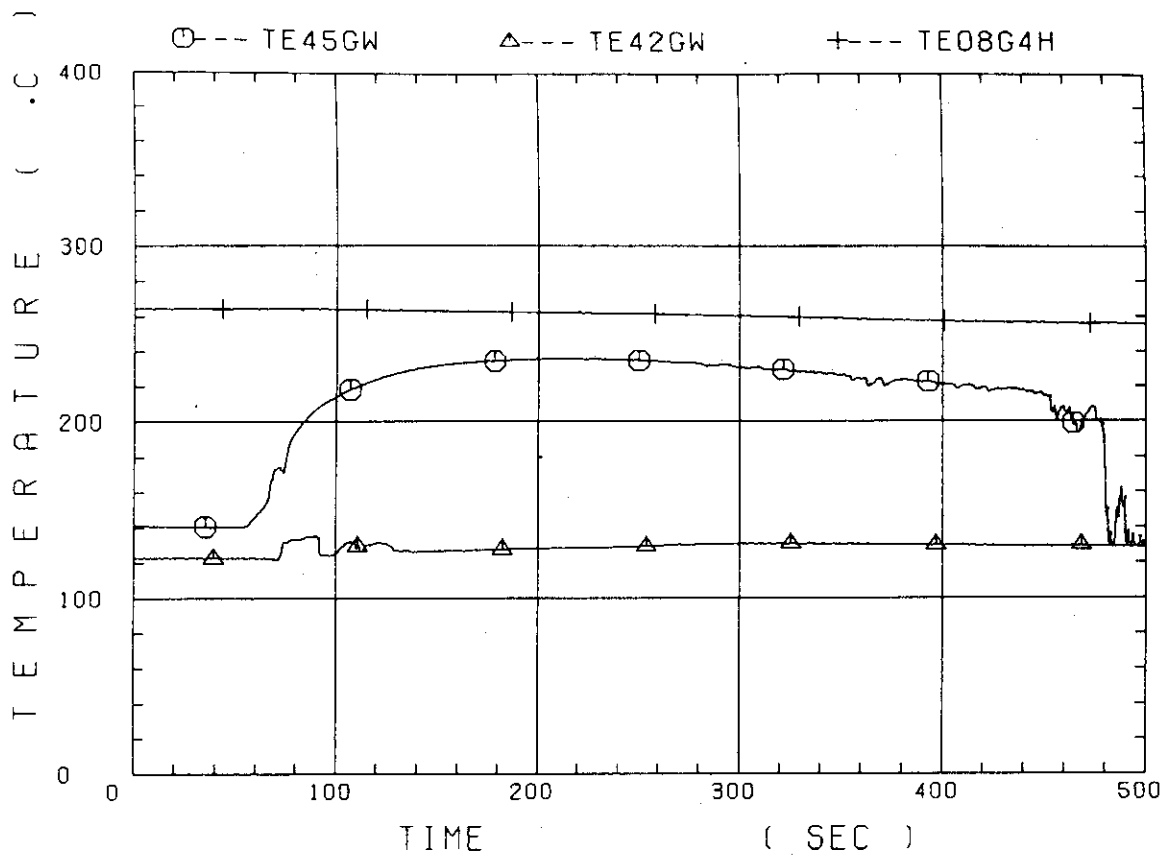

Fig. C-33 Fluid temperature in inlet plenum, outlet plenum, and secondary of steam generator 2

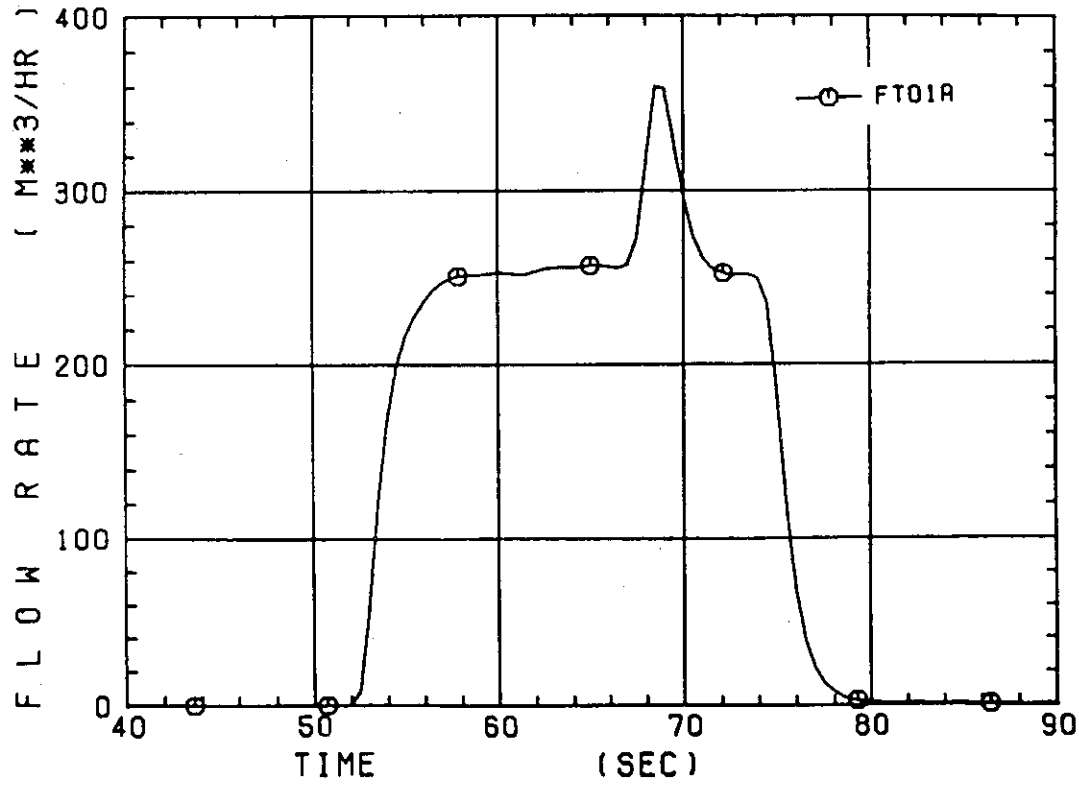

Fig. C-34 Total accumulator injection rate

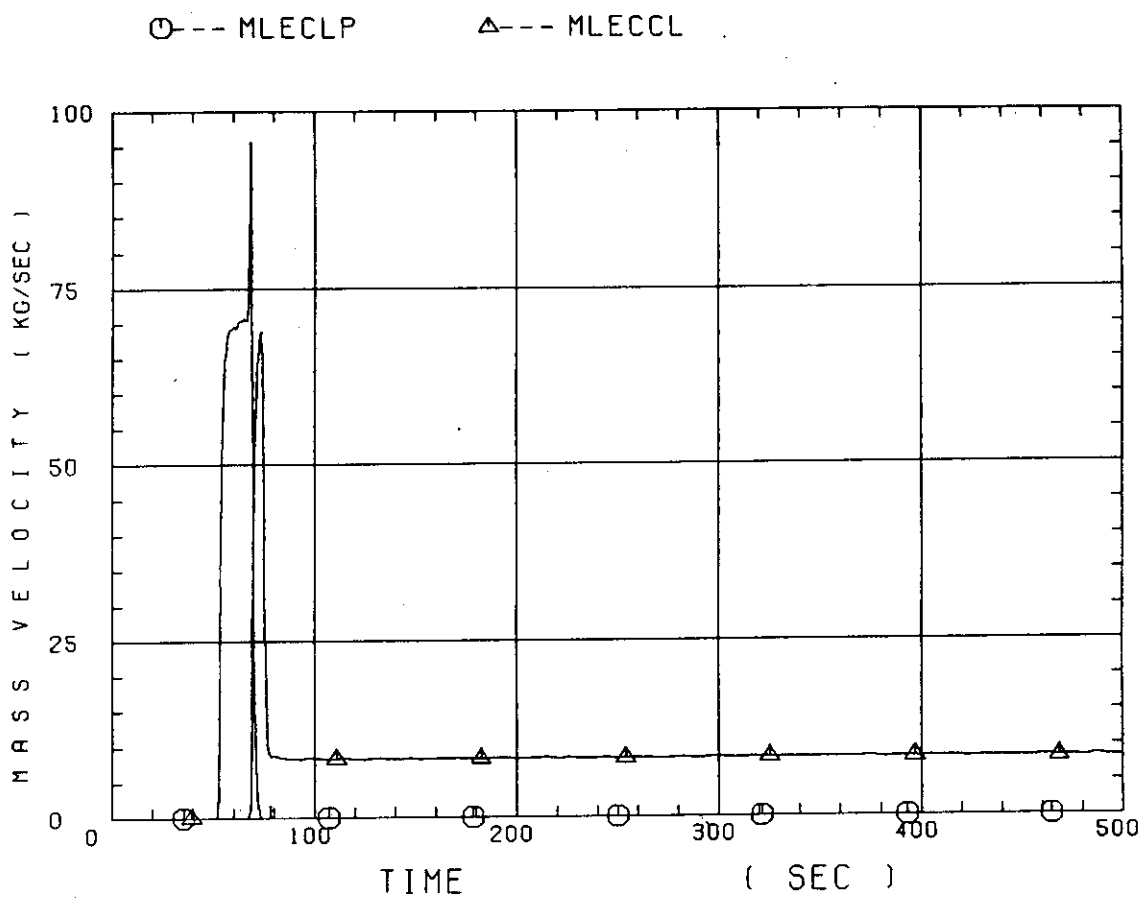

Fig. C-35 ECC water injection rates to lower plenum and to cold legs

Appendix D

Evaluation of core flooding mass flow rate

Figure list

The reflood phenomena is a relatively slow transient and is assumed to be a steady state condition. In a steady state condition, based on the mass balance relations of the system, the core flooding mass flow rates $\dot{m}_F$s can be written as follows:

By using the data measured at the downstream of the core inlet, $\dot{m}_F$ is derived as,

$$\dot{m}_F = \dot{m}_C + \dot{m}_U + \dot{m}_B + \Sigma\, \dot{m}_I \quad , \tag{1}$$

where $\dot{m}_C$ and $\dot{m}_U$ are the mass accumulation rates in the core and the upper plenum respectively. The $\dot{m}_B$ and $\dot{m}_I$ are the mass flow rates in the broken loop and the intact loop, respectively.

By using the data measured at the upstream of the core inlet, $\dot{m}_F$ is derived as,

$$\dot{m}_F = \Sigma\, \dot{m}_{DL} - \dot{m}_D - \dot{m}_O + \dot{m}_{ECC/LP} \quad , \tag{2}$$

where $\dot{m}_{DL}$, $\dot{m}_O$ and $\dot{m}_{ECC/LP}$ are the mass flow rates of the water flowing into and overflowing from the downcomer and the mass flow rate of the ECC water injected into the lower plenum, respectively.

The $\dot{m}_I$s AND $\dot{m}_B$ can be obtained from the pressure drops at the pump simulators with orifices by assuming the K-factor of the orifice is constant or from the data of Pitot tubes. The values of $\dot{m}_C$, $\dot{m}_D$ and $\dot{m}_U$ can be evaluated with the differential pressure ΔP_C, ΔP_D and ΔP_U, respectively, as follows:

$$\dot{m}_n = d(\Delta P_n S_n/g)/dt \qquad (n : C, D, U) \quad , \tag{3}$$

where g is the gravitational acceleration and S_n is the crosssectional area. The value of $\dot{m}_O$ can be obtained from the liquid level X in the Containment tank 1 as,

$$m_O = d(X\rho_\ell S_o)/dt, \tag{4}$$

where ρ_ℓ is the liquid density and S_o is the cross sectional area of the containment tank.

The value of $\dot{m}_{DL}$ is obtained from the following mass and energy

balance relations at each ECC port under the assumption of thermal equilibrium:

$$\dot{m}_{DV} + \dot{m}_{DL} = \dot{m}_{ECC} + \dot{m}_{I} \quad , \tag{5}$$

$$(\dot{m}_{DV} + \dot{m}_{DL})i = \dot{m}_{ECC}i_{ECC} + \dot{m}_{I}i_{I} \quad , \tag{6}$$

$$\text{if} \quad i_g \geq i \geq i_\ell \quad , \quad (\dot{m}_{DV} + \dot{m}_{LD})i = \dot{m}_{DV}i_g + \dot{m}_{DL}i_\ell$$

$$\text{if} \quad i > i_g \quad , \quad \dot{m}_{DL} = 0 \quad , \tag{7}$$

$$\text{if} \quad i < i_\ell \quad , \quad \dot{m}_{DV} = 0 \quad ,$$

where i is enthalpy of fluid and i_ℓ and i_g are enthalpies of liquid and steam at the saturation temperature, respectively.

The fluid temperatures can be measured with thermocouples immersed in the fluid and the enthalpies i_I, i_{ECC} can be estimated.

Mass balance calculations were performed with Eqs. (1) and (2), since it was found that the water entering the steam generator was completely evaporated. In the differentiation, higher frequency components of the data tends to be amplified more. Therefore, in the differentiation of the differential pressure data, the smoothing procedure was used to suppress the high frequency components of the data. Figure C-1 shows the flooding mass flow rates, $\dot{m}_F$s, calculated from Eqs. (1) and (2) by averaging data in 20 seconds.

The calculated core flooding rate with Eqs. (1) and (2) for the superheated and the saturated downcomer wall tests are shown in Figs. D-1 and D-2, respectively. The integrated $\dot{m}_F$s are shown in Figs. D-3 and D-4.

In the Acc injection period, the calculated values $\dot{m}_F$s, are significantly different from each other. This discrepancy may be caused by inaccuracy of the mass flow rate injected into the system and by the unaccounting of the storage of water in the cold leg pipe. The former might be introduced from the slow time response (time constant 1 second) and the change of the gas volume in the injection line. In this period,

especially before the steam generation from the core became noticable, the mass flow rate, $\dot{m}_F$, calculated with Eq. (1) is reasonable, since the calculation needs the increasing rates of the masses in the core and the upper plenum and their accuracy is enough for our estimation.

In the LPCI injection period, the calculated $\dot{m}_F$s are slightly different each other in the superheated downcomer wall test. The discrepancy can be caused by the disregard of the bypass flow from the upper plenum or of the water accumulation in the hot leg piping and the inlet plenum of the steam generator in the calculation with Eq. (1). On one hand, the discrepancy can be caused by the disregard of the steam generation on the superheated downcomer wall in the calculation with Eq. (2). It was estimated that the error of 0.25 kg/s on predicted $\dot{m}_F$ was caused by the disregard of the steam generation in the downcomer through the comparisons between the superheated and the saturated downcomer wall test results. In the LPCI injection period except for the early period, the mass flow rate calculated with Eq. (2) is considered to be reasonable, because the error from ECC injection rate measurement is negligible under quasi-steady condition and the error from the steam generation in the downcomer is small, too.

In order to obtain the best estimate core flooding rate, the calculation was performed with Eq. (1) using corrected values of the loop mass flow rates, $\dot{m}_I$s and $\dot{m}_B$. The correction was made by multiplying $\dot{m}_I$s and $\dot{m}_B$ by a factor which yields identical $\dot{m}_F$s in the calculations with Eqs. (1) and (2). The core flooding rate evaluated by the method is shewn in Figs. B-22 and C-22. The error of these core flooding rate is estimated to be about 15 % at most.

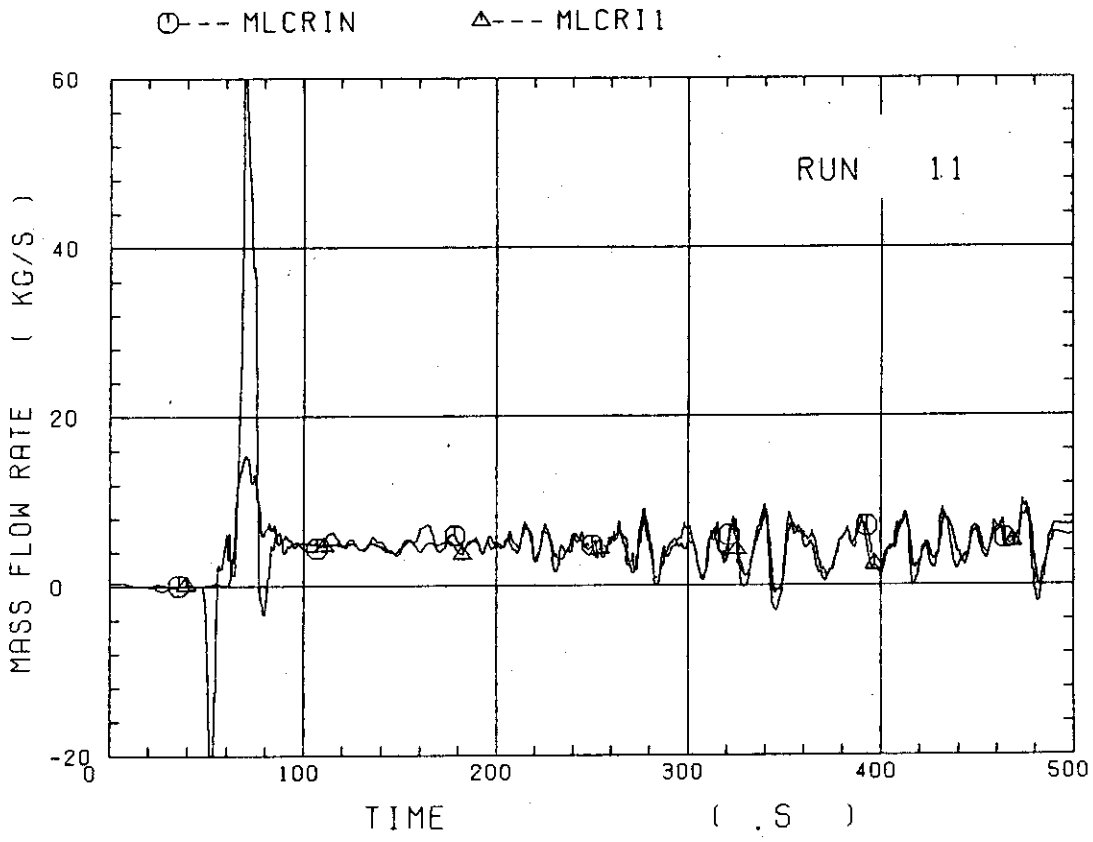

Figure D-1. Core flooding rate evaluated with Eqs. (1) or (2) for the superheated downcomer wall test.

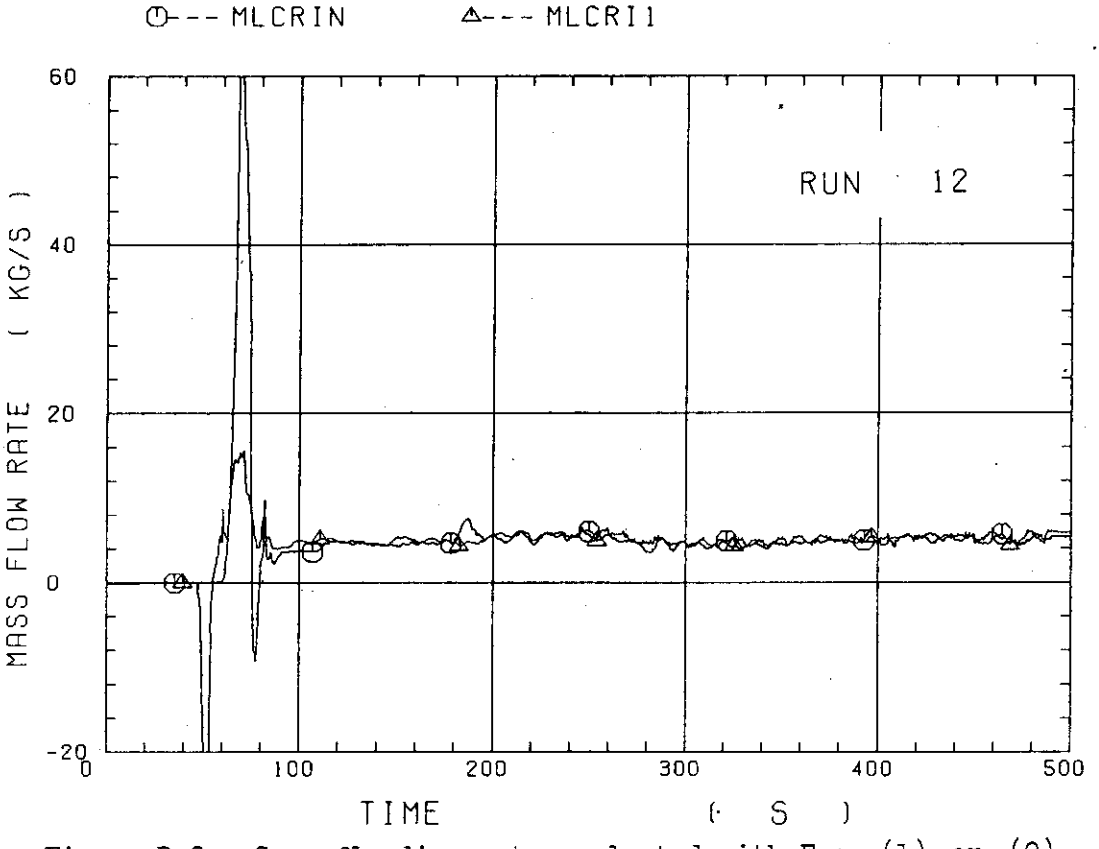

Figure D-2. Core flooding rate evaluated with Eqs. (1) or (2) for the saturated downcomer wall test.

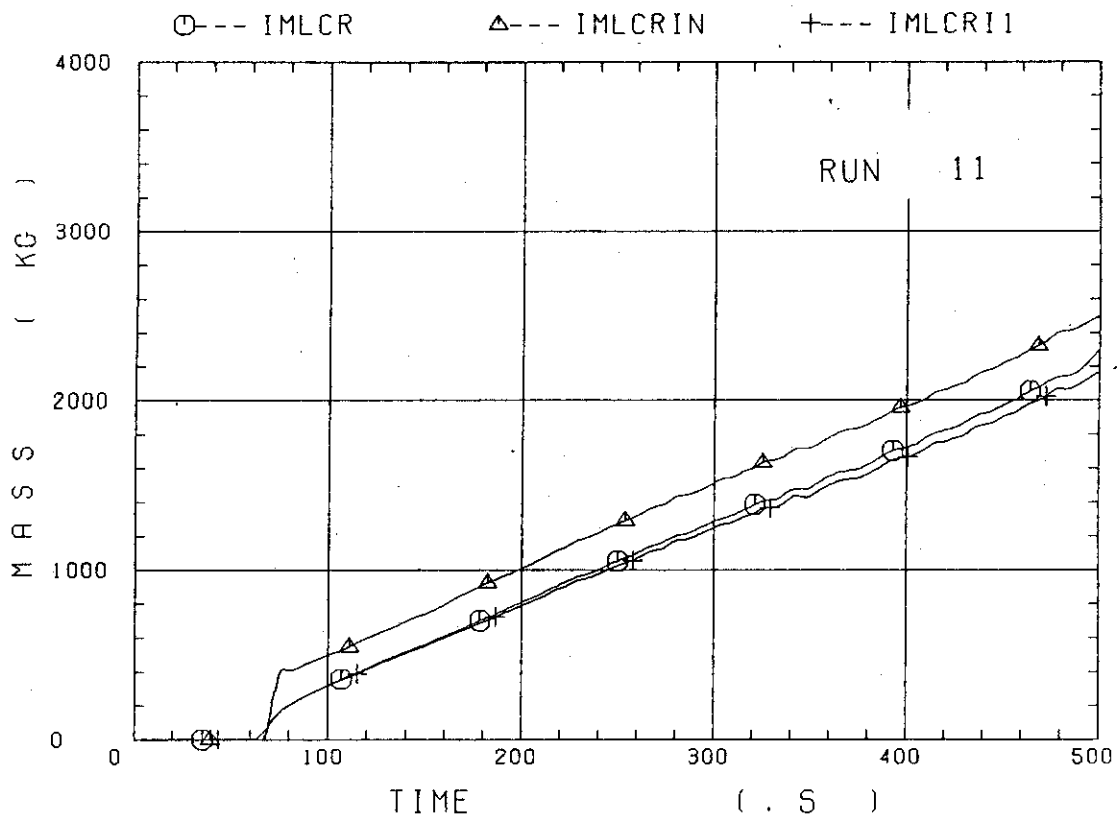

Figure D-3. Integrated $\dot{m}_F$s(core flooding rate with Eqs. (1), (2) or best estimate) for the superheated downcomer wall test.

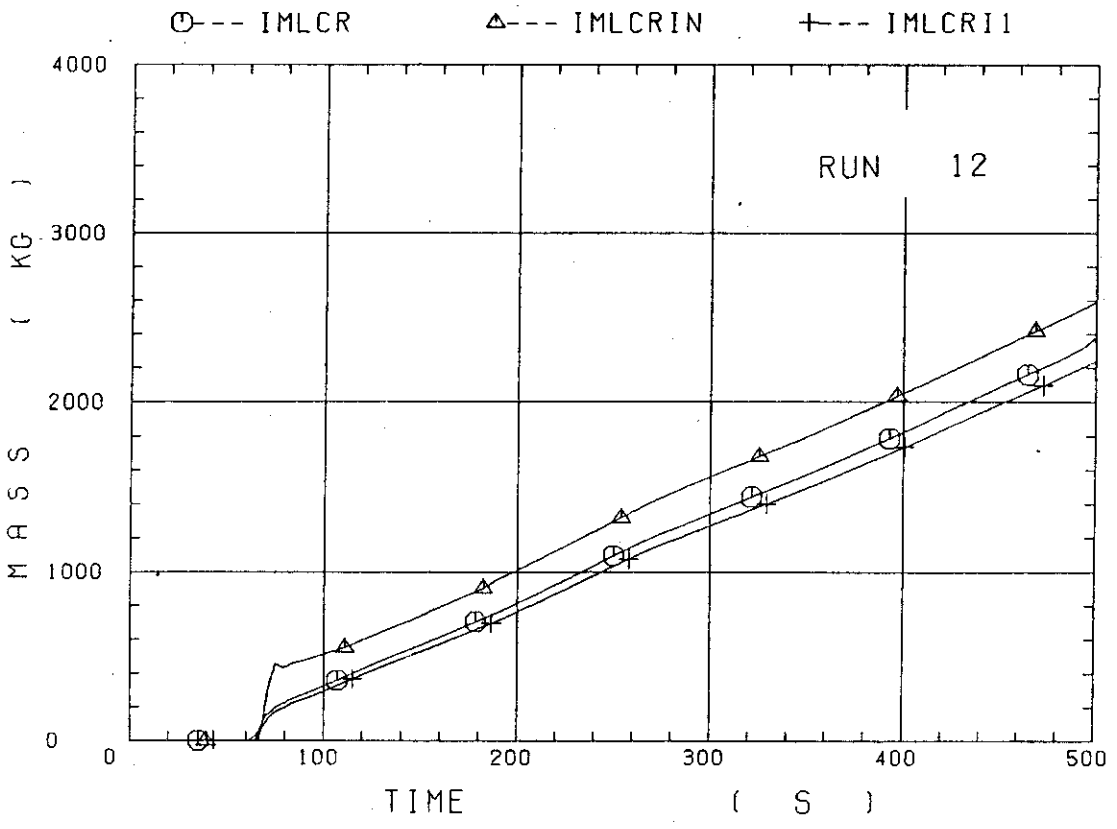

Figure D-4. Integrated $\dot{m}_F$s(core flooding rate with Eqs. (1),(2) or best estimate) for the saturated downcomer wall test.